THE UNIVERSITY OF CALGARY

PHYSICAL SEISMIC MODELLING OF PINNACLE REEFS

by

TINA Y.N. CHOW

A THESIS

SUBMITTED TO THE FACULTY OF GRADUATE STUDIES

IN PARTIAL FULFILLMENT OF THE REQUIREMENTS FOR THE

DEGREE OF MASTER OF SCIENCE

DEPARTMENT OF GEOLOGY AND GEOPHYSICS

CALGARY, ALBERTA

SEPTEMBER, 1989

ISBN 0-315-54197-0

FACULTY OF GRADUATE STUDIES

The undersigned certify that they have read, and recommend to the Faculty of Graduate Studies for acceptance, a thesis entitled "Physical Seismic Modelling of Pinnacle Reefs" submitted by Tina Y.N. Chow in partial fulfillment of the requirements for the degree of Master of Science.

D.C. Lawton

Supervisor, Dr. D.C. Lawton,
Department of Geology and Geophysics

R. James Brown

Dr. R.J. Brown,
Department of Geology and Geophysics

L.V. Hills

Dr. L.V. Hills,
Department of Geology and Geophysics

H. Laue

Dr. H. Laue, Department of Physics

Date: September 12, 1989

ABSTRACT

Reef models based on the morphologies of the Leduc Formation Golden Spike reef in central Alberta and a Keg River Formation pinnacle reef in the Shekilie Basin located in northwestern Alberta were studied using the methods of physical seismic modelling and normal-incidence raytrace modelling. The physical seismic modelling system at the University of Calgary was expanded as part of this study to accommodate three-dimensional (3-D) seismic acquisition geometries and was used extensively throughout this thesis.

The first part of this study involved the construction of a physical model based on the morphology of the Golden Spike reef mass. This model provided familiarization with the physical modelling system and with model construction using synthetic compounds. Comparison between numerical modelling and physical modelling was also carried out with these data. Significant sideswipe energy from outside the plane of the seismic lines was identified on the physical modelling data and dispersal of energy due to 3-D curvature of the reef was noted.

The second part of this thesis involved the examination of data from a model based on the morphology of a pinnacle reef in the Shekilie Basin. 3-D seismic survey acquisition parameters were reviewed to facilitate

the design of an efficient survey and to help with the interpretation of the final data. Bounds on the maximum unaliased dip for the case of draping interfaces were developed. The concept of a Fresnel zone was reviewed to help with the analysis of the physical modelling data. Reflection characteristics of the physically modelled data were analyzed and the effectiveness of the two-pass migration procedure to reduce the size of the Fresnel zone was addressed. Comparisons between physically modelled data and field data indicated very similar responses and led to the conclusion that the interpretation based on the field data was accurate.

Analysis of the numerical modelling data and comparisons with the physical modelling data led to the conclusion that normal-incidence raytrace modelling was not a suitable method for modelling effects associated with these small features.

ACKNOWLEDGEMENTS

This project was supported by a grant from the Petroleum Aid to Education Trust Fund. Computer contour maps of the Golden Spike reef were made available by Chevron Canada Resources Ltd. The 3-D field seismic dataset over the Shekilie pinnacle reef was generously provided by Canterra Energy Ltd. Western Geophysical Company of Canada granted time on the Crystal® workstation on which the intepretation of the Shekilie field seismic data was performed. Also, processing of the physically modelled datasets by Western Geophysical Company of Canada is gratefully acknowledged. Specifically, I would like to thank Ms. Christine St.Clair and Mr. Randy Gagnon, who processed the physically modelled data as well as Mr. Ron Schmid who provided assistance on the Crystal® workstation.

Many thanks to Dr. Scott Cheadle who guided me through the steps of the operation of the physical modelling system. Mr. Malcolm Bertram's contribution to the electronic components for the physical modelling tank, Mr. Eric Gallant's help in model construction, and assistance in the handling of the modelling material from Mr. Bob Fisher of the Enviromnental Design Workshop are all greatly appreciated.

I would like to express my gratitude to my supervisior

Dr. Don Lawton for his guidance and patience throughout this project. Advice and constructive criticisms from Dr. Jim Brown and Dr. Len Hills are also gratefully acknowledged.

TABLE OF CONTENTS

CHAPTER FIVE: CONCLUSIONS AND RECOMMENDATIONS

LIST OF TABLES

LIST OF FIGURES

Chapter One: Introduction

1.1 General Statement

Devonian-aged strata have been and are predicted to be major hydrocarbon producing reservoirs in Alberta, Canada (Podruski et al., 1988). Most of the Devonian-aged hydrocarbon reserves have been discovered in large reefal build-ups. As most of the large reef structures have probably already been discovered, present exploration efforts are concentrated on smaller pinnacle reefs which have very subtle seismic characteristics and therefore are more difficult to delineate. Since 1965, the two-dimensional (2-D) common mid-point (CMP) method of seismic acquisition has been widely employed to locate potential reef structures. However, the small size and steeply dipping margins of pinnacle reefs produce weak reflections which frequently come from out of the plane of the conventional 2-D seismic section. These "sideswipe" reflections are difficult to interpret reliably and for this reason 2-D seismic surveys may be of limited value. Recently, three-dimensional (3-D) seismic surveys have become a popular method to improve the delineation of these targets.

Complex seismic reflections are often associated with structural and stratigraphic anomalies. May and Hron

(1978) have shown that in many examples, even for rather simple structures, the geometries of seismic reflections cannot be anticipated without the aid of numerical modelling. The ability of numerical methods to predict correctly the complex relationships among the many variables controlling wave propagation is limited by the validity of the assumptions of the algorithms used and the available computing capacity. However, in the physical modelling method, the complete interaction between a known model and a controlled source is directly recorded in the laboratory. Thus, physical modelling can provide a clear representation of the seismic response from a given model. In this research project, both numerical modelling and physical seismic modelling studies were conducted to gain insight into the seismic response of reefs.

1.2 Purpose of Study

Using the physical seismic modelling system at the University of Calgary, seismic responses from two selected Devonian reef models were studied. The reef models are based on the morphologies of the Leduc Formation Golden Spike reef located in south-central Alberta (Figure 1.1), and a Keg River Member pinnacle reef in the Shekilie Basin situated in northwestern Alberta (Figure 1.2). The two reefs are very different in terms of their sizes and

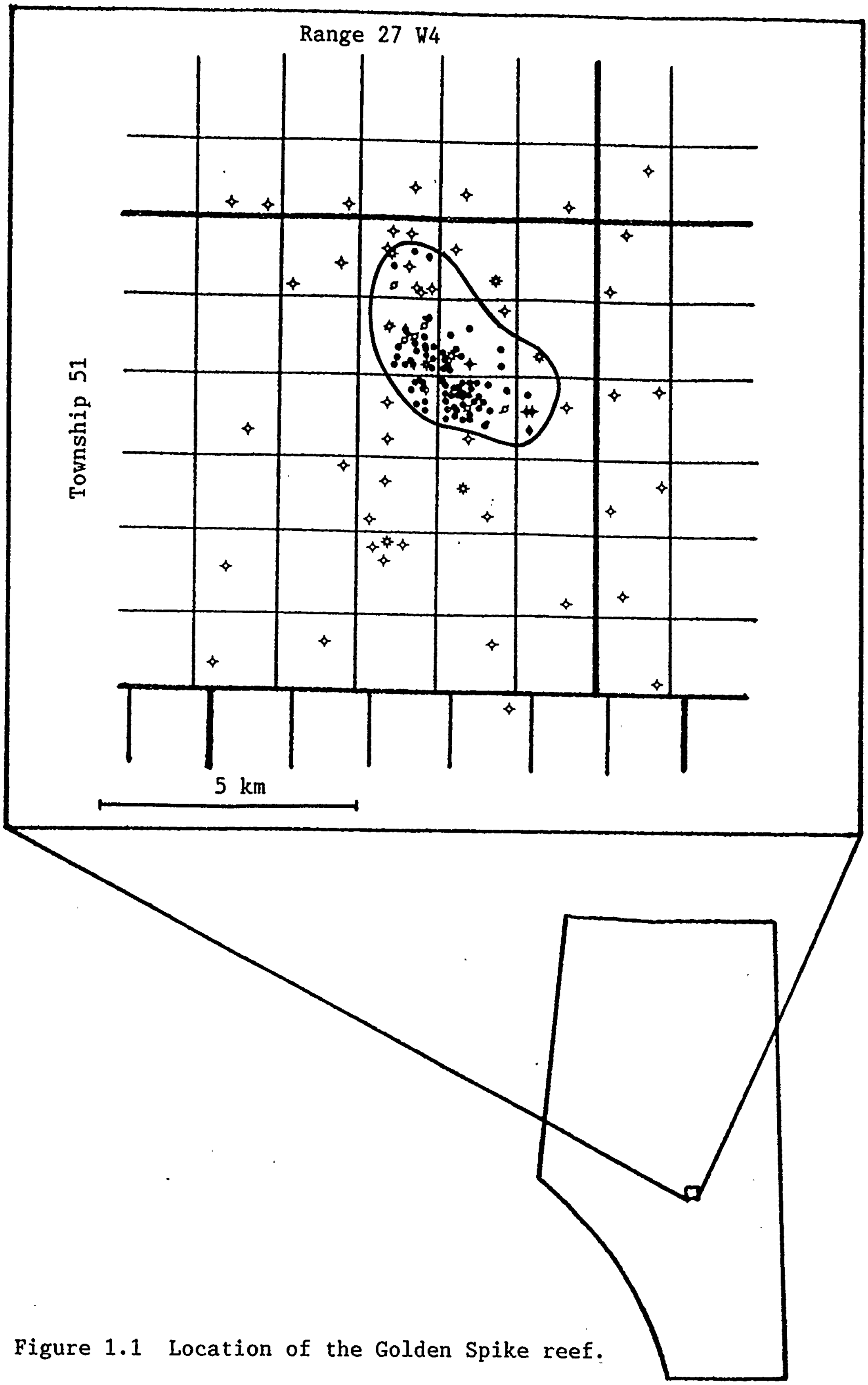

Figure 1.1 Location of the Golden Spike reef.

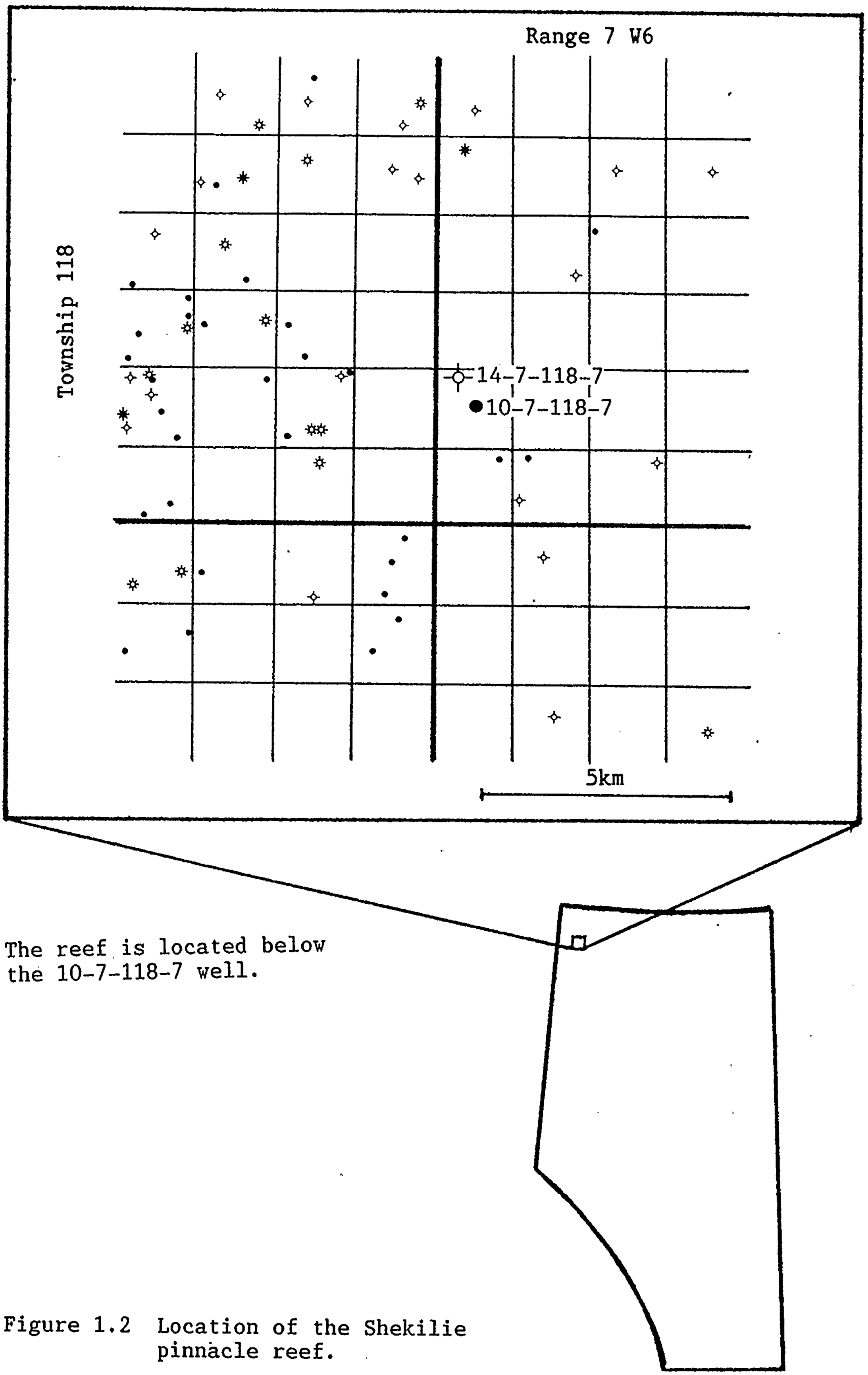

The reef is located below the 10-7-118-7 well.

Figure 1.2 Location of the Shekilie pinnacle reef.

geological settings. The Golden Spike reef is encased in shale which has a lower acoustic velocity than the reef mass. In comparison, the Shekilie pinnacle reef, which is much smaller than the Golden Spike reef both in height and areal extent, is surrounded by evaporites and dolomites with a higher acoustic velocity than the reefal material. These factors result in different seismic expressions for the two reefs. The seismic signatures of these types of reefs were summarized by Anderson and Brown (1987).

In this study, the Golden Spike reef served as a test model to gain familiarity with the operation of the physical modelling system and with the materials and methods used for construction of scaled replicas of the reefs. The Shekilie reef model was the basis for the majority of the analyses presented in this thesis.

Specific objectives of this study were to:

1. modify the modelling tank and develop software necessary for recording 3-D seismic surveys in the laboratory;
2. examine out-of-plane reflections present on two-dimensional seismic lines over and around the Golden Spike reef model;
3. review data acquisition parameters for 3-D seismic surveys;
4. investigate the impact of the "Fresnel zone effect" on the delineation of "small" pinnacle reefs;

5. study the effectiveness of the two-pass migration procedure for imaging these small targets;
6. compare the seismic responses obtained from numerical and physical modelling methods; and
7. assess the reliability of an interpretation based on three-dimensional seismic data over a known pinnacle reef.

Chapter Two: Seismic Modelling

2.1 Physical Modelling

2.1.1 Introduction

Physical seismic modelling involves the generation of full-wave seismic responses over scaled geological models in the laboratory. This method has been employed by many researchers to investigate acoustic propagation through a variety of earth models. McDonald et al. (1983) provide a detailed historical account of the physical modelling method and describe a selection of various seismic modelling projects which have been undertaken at the Seismic Acoustic Laboratory (SAL), University of Houston.

Many other seismic modelling projects of interest have been published. Hilterman (1970) investigated reflection and diffraction patterns associated with anticlinal, domal and fault structures. French (1974) studied the oblique seismic reflection profiles of two-dimensional and three-dimensional models. He concluded that the simultaneous three-dimensional migration procedure is instrumental in the elimination of ambiguities caused by sideswipe and blind structures on seismic reflection profiles. Newman (1980) investigated 3-D migration by Kirchhoff summation using a buried channel model. Kotcher et al. (1984) used the physical modelling method to study the effect of static errors in areal seismic data caused by glacial erosion over Silurian patch reefs from the northern Michigan reef belt. Hospers (1985) used physical modelling to study sideswipe reflections and other external and internal reflections from salt plugs in the Norwegian Basin. Cheadle (1988) and Lyatsky (1988) used the physical modelling system at the University of Calgary to study the acoustic responses from the permafrost-affected sediments in the Beaufort Sea, and shallow coal seams, respectively.

2.1.2 The Physical Modelling System

The physical modelling system at the University of Calgary was developed and described by Cheadle et al. (1985). The major components of the physical modelling system are a water-filled tank (3 m wide, 4 m long, and 2 m high), two perpendicular beams containing motorized carriages, two spherical ITC-1089C ultrasonic piezoelectric transducers, a pre-amplifier, a pulse generator, an IBM-XT personal computer and a digital storage oscilloscope.

A scaled earth model is constructed from synthetic compounds and is submerged in the tank for the experiment. The piezoelectric transducers act as source and receiver and are moved across the model on the motorized carriages. The acquisition geometry of the survey is programmed using the IBM-XT which controls the positions of the transducers. A zero-phase signal is obtained by the summation of three wave trains generated from the pulse generator. The received signal is digitized by a high-speed storage oscilloscope. A direct link between the oscilloscope and a Perkin-Elmer computer allows the transfer of a seismic trace, containing a maximum of 4096 samples plus the trace header, onto magnetic tape. At this stage, the data collected using the physical modelling system can be handled using standard seismic data processing procedures.

In order to accommodate 3-D seismic experiments, the physical modelling system was expanded in this study with additional components. To record an array of receivers distributed about a source position, and without having to move the model or the source transducer, a third transducer was added. Another preamplifier was also connected to scale the recorded signal from the new transducer. Modification of existing software to control the movement of all the transducers was implemented. With both receivers operating, the storage capacity on the digital oscilloscope was limited to 2048 samples for a given seismic trace.

2.1.3 Model Scale Factors and Materials

The principles of physical similitude (Buckingham, 1914) govern scaled modeling of physical equations between the real and the simulated environments in the laboratory. McDonald et al. (1983) and White (1965) discuss the concepts of scaling for physical models. The spatial or length scale factor, the time scale factor, and the velocity scale factor follow the basic physical law:

$$d = v \cdot t \tag{2.1}$$

where d is distance, v is velocity, and t is time.

In general, every dimension on the original field experiment is directly proportional to a corresponding dimension on the model. Equation (2.1) can be written as:

$$Xd = Yv \cdot Zt \tag{2.2}$$

where X, Y, and Z are dimensionless scaling factors which satisfy the condition of $X = Y \cdot Z$.

The time scale factor is selected such that the scaled frequency bandwidth of the model data is comparable to the field data. Also, it is advantageous to select the time scale factor to ensure that the scaled sampling interval is an integral number of milliseconds. Currently, the spherical piezoelectric transducers operate at a central frequency of 238 kHz. The sampling intervals available on the digital oscilloscope are 50, 100, 200, and 500 ns. Thus, if the time scale factor is 4000 with a sampling interval set at 500 ns, then the scaled central frequency of the source is 238 Khz/4000 (~60 Hz) and the scaled sample interval is 500 ns·4000 (2 ms). Typical time scale values range from 4000 to 10000. Selection of velocity scale values are constrained by the acoustic properties of the available modelling materials. For velocities commonly encountered in the Alberta basin, the velocity of the modelling material is scaled up between the factors of 1 and 3 to the field values. The distance scale factor can be obtained using equation (2.2). The distance scale factor is chosen to be as small as possible to minimize the effects of positioning errors but not so small as to make the scaled model too cumbersome to construct and handle. Ideally, the availability of a wide selection of transducers with a variety of central frequencies will enable a more flexible choice of spatial scale factors.

Epoxy resins, RTV rubber, and plexiglass are used as modelling materials to simulate the acoustic responses of the earth layers. Different acoustic properties can be achieved by mixing different proportions of epoxy resins and rubber compounds. Table 2.1 is a list of modelling compounds tested and their corresponding acoustic properties. The velocities of these samples are obtained from laboratory measurements at the University of Calgary, Composition and Weight Mixing Ratio() of Materials

code #	Material A	Material B	Material C	P-WAVE VELOCITY (m/s)	DENSITY kg/m^3
1	STYCAST 2741LV (1)	15LV (1)	ECCOGEL 1265A (1)	2450	1150
2	STYCAST 2741LV (3)	15LV (3)	ECCOGEL 1265A (2)	deformed badly under pressure	1260
3	STYCAST 2741LV (1)	15LV (1)		2483	1220
4	STYCAST 2741LV (1)	15LV (1)	Cat. S (1)	did not set	
5	STYCAST 2741LV (4)	15LV (2)	SYLGARD 184 (1)	too much air trapped inside	
6	STYCAST 2741LV (1)	15LV (1)	ECCOGEL 1265A (2)	2330	1140
7	STYCAST 2741LV (2)	15LV (1)	ECCOGEL 1265A (3)	2180	1170
8	STYCAST 2741LV (2)	15LV (1)	ECCOGEL 1265a (1)	2430	1270

Table 2.1 List of modeling compounds tested and their acoustic properties.

*() Mixing proportion by weight.

9	Silicone 3120 (15)	Cat. S (1)		too soft & rubbery	
10	ECCOGEL 1265A (1)	ECCOGEL 1265B (1)		did not set	
11	STYCAST 2741LV (4)	15LV (2)	ECCOGEL 1265A (3)	2439	1230
12	STYCAST 2741LV (2)	15LV (1)	ECCOGEL 1265A (6)	2383	1150
13	STYCAST 2741LV (2)	15LV (1)		2458	1300
14	STLGARD 184 (10)	Cat. S (1)	ECCOGEL 1265A (11)	did not set	
15	STYCAST 2741LV (3)	15LV (3)	STLGARD 184 (1)	1904	1170
16	STYCAST 2741LV (4)	15LV (4)	STLGARD 184 (1)	2013	1220
17	STYCAST 2741LV (5)	15LV (5)	STLGARD 184 (1)	2065	1220

Table 2.1 (Continued) List of modeling compounds tested and their acoustic properties.

*() Mixing proportion by weight.

18	STYCAST 2741LV (3)	15LV (1)	2578	1280
19	STYCAST 2741LV (3)	15LV (2)	2515	1280
20	STYCAST 2741LV (4)	15LV (1)	2635	1390
21	STYCAST 2741LV (1)	15LV (2)	did not set	
22	STYCAST 2741LV (2)	15LV (3)	did not set	
23	STYCAST 2741LV (3)	15LV (1)	did not set	
24	STYCAST 2741LV (7)	15LV (1)	2409	1430
25	STYCAST 2741LV (5.5)	15LV (1)	2442	1390
26	STYCAST 2741LV (6)	15LV (1)	2489	1400
27	PLEXIGLASS		2750	1200
28	PVC		2400	1450

Table 2.1 (Continued) List of modeling compounds tested and their acoustic properties.

*() Mixing proportion by weight.

while the densities, ρ, are derived from the formula:

$$\rho = \rho_w W_a \;/\; (W_a - W_w) \qquad (2.3)$$

Where W_a is the weight of the sample in air, W_w is the weight of the sample immersed in water, and ρ_w is the density of water.

It is important to prevent the formation of air bubbles during the course of pouring epoxy resin in the process of model construction, as a small air bubble becomes a large cavity after the scale factor is applied.

2.1.4 Limitations of Physical Modelling

The reproduction of field data in the laboratory is limited by the accuracy and precision of model building and by the accuracy of the recording system. Presently, only a limited number of earth layers with constant acoustic properties can be modelled. Capability of modelling porosity and permeability of rock formations needs to be further investigated. The central frequency of the transducers restricts the choice of time scale factors. The finite range of the velocity values of the available modelling materials and the acoustic velocity in water limits selection of the velocity scale factor. The distance scaling factor and the recording configurations of the model survey are also constrained by the physical properties of the modelling tank system.

The data acquisition parameters are restricted by the accuracy of the stepping motors and the physical size of the transducers. The stepping motors of the source and receiver carriages have a positional precision of ± 0.5 mm. The transducers are 1 cm in diameter, thus restricting the near offset of the model seismic survey to 1 cm. For a distance scale of 1 : 15000, the near offset of the modeled survey will have the value of 150 m in the field.

2.2 Numerical Modelling

2.2.1 Introduction

Numerical modelling is commonly employed to aid in the interpretation of seismic data. Methods of numerical modelling used by geophysicists are: vertical-incidence, normal-incidence raytracing, and methods based on solutions to the wave equation. Vertical-incidence modelling is commonly used to produce synthetic seismograms by convolving a source wavelet with a reflectivity sequence derived from borehole logs. Normal incidence raytracing is widely used in the industry to produce synthetic seismic sections and there are many commercially available software packages. Although algorithms based on solutions to the wave equation are available, these methods are, at present, seldom used since they are computationally intensive and thus are expensive to run. The method of normal-incidence raytracing is used for the numerical modelling part of this study.

After creating a desired model geometry, the next step in raytrace modelling is to specify the source and receiver locations. For each shot, downward travelling rays are generated at many takeoff angles from the source location. Each ray is propagated through the model according to Snell's Law and interactions at acoustic impedance boundaries are governed by the Zoeppritz equations. Rays which are reflected back to the surface within a specified distance from the receiver are captured. For each captured ray, an appropriately scaled spike is located on the output trace at a time determined by integrating along the captured raypath. The trace containing scaled spikes for every reflection is then convolved with a user-specified wavelet producing the synthetic model trace.

2.2.2 Raytracing Software

Sierra Modeling Software, a commercially available seismic modelling package, was used to generate synthetic data over the Golden Spike and Shekilie reef models. Information on the operation and the assumptions of the programs was obtained from the Sierra Geophysics Exploration Software User Notes (1983). The modelling procedure was divided into three stages: (1) building the model using the program MIMIC, (2) specifying the source and receiver locations and raytracing with one of the QUIK programs - QUIKRAY, QUIKSHOT, QUIKCDP, or QUIKVSP, and (3) convolving the raytraced data with a suitable wavelet and displaying the results on a graphics terminal using the program SLIPR.

The size and shape of the numerical models were specified using the MIMIC module. In the process of model construction, the first step was the specification of the grid size in the horizontal plane. The shape and depth of either two or three dimensional layers was input. The last step in model construction was completed by supplying the acoustic properties of each layer. If density values were not specified for the model layers, default values would be generated according to Gardner's equation (Gardner et al., 1974):

$$\rho = 0.31 \times (V_p)^{.25} \qquad (2.4)$$

where ρ is density in g/cm^3, and V_p is the P-wave velocity in m/s.

In this study, the QUIKRAY module was used to simulate zero-offset synthetic sections. This program utilizes the method of normal-incidence raytrace modelling and it assumes coincident source and receiver locations to produce synthetic zero offset seismic traces. Upon the specification of the receiver/shot stations of the zero offset lines, generation of the working ray set, ray capture and amplitude computation proceeded automatically using the default values of the QUIKRAY program. The program defaulted to P-wave propagation only. The capture radius was half of the receiver interval. The interaction at the boundaries was transmission without mode conversion. The ray time limit was 10 seconds. Contained within the normal-incidence raytraced data were the implicit assumptions that multiples and noise had been eliminated, and that mode conversion did not occur. The SLIPR time-domain processing module sorted the spike seismograms generated in the raytracing modules and arranged the data by shot point and group number. A wavelet with user-specified shape and central frequency was convolved with the spike series produced by the QUIKRAY program. An array of display options were available to display the synthetic traces.

2.2.3 Limitations of Normal-incidence Raytracing

The raytrace method of modelling has some potentially important deficiencies. Wavefront effects such as amplitude contributions from the Fresnel zone and non-spherical spreading of the wavefront are not accounted for by raytracing methods. For the SIERRA package, the QUIK programs assume all raypaths within a layer are straight. Diffractions which should be generated from any boundary discontinuity or discontinuity in the slope of an interface are excluded from the QUIK programs. Head waves which have been refracted at the critical angles are also not considered.

Chapter Three: Golden Spike Model Study

3.1 Background

Golden Spike is an isolated pinnacle reef located approximately 22 km west of Edmonton (Twp 51, R27W4, Figure 1.1). The reef is approximately 175 m in height and 2.4 km by 3.6 km across at the base. Average depth of burial is 1650 m below the surface (Trott, 1981). The pool was discovered in 1949 by Imperial Oil Limited. McGillivray and Mountjoy (1975) gave a detailed account of the facies and related reservoir characteristics of this reef mass. Trott (1981) performed a gravity survey over this reef and showed that the reef generated a small Bouguer anomaly of about 0.25 mGal.

Golden Spike was selected as a preliminary model for this study due to the excellent well control, the relatively simple geometric shape of the reef mass, and the significant velocity contrast between the reef mass (5500 m/s) and its surrounding sedimentary rocks (4600 m/s). Experience gained from this model aided in recognition of problems associated with detailed model construction and scale parameter selection and also provided familiarization with the physical modelling system.

3.2 Geology

Figure 3.1 shows a stratigraphic column for the lithologies in central and northern Alberta (after Energy Resources Conservation Board, 1987). Belyea et al. (1964) provide excellent regional overviews for the stratigraphy of the Upper Devonian in western Canada. Mountjoy (1980) provides a detailed account concerning the development of Upper Devonian carbonate buildups in this part of Alberta. Stokes (1980) studied the depositional episodes of reef growth and the eventual termination of growth of hydrocarbon-producing Leduc reef buildups. Anderson (1986) has summarized the geological history of the oil-bearing Leduc Formation reefs. A brief summary of their work is given below.

The Golden Spike reef is a Leduc Formation limestone build-up which developed on the Cooking Lake carbonate platform. Surrounding and overlying the reef are calcareous shales of the Duvernay and Ireton formations. Above the Ireton Formation are a series of predominantly carbonate sediments, including the Nisku, Calmar, Graminia, and Wabamun units. These formations are stratigraphically contained in the Upper Devonian System.

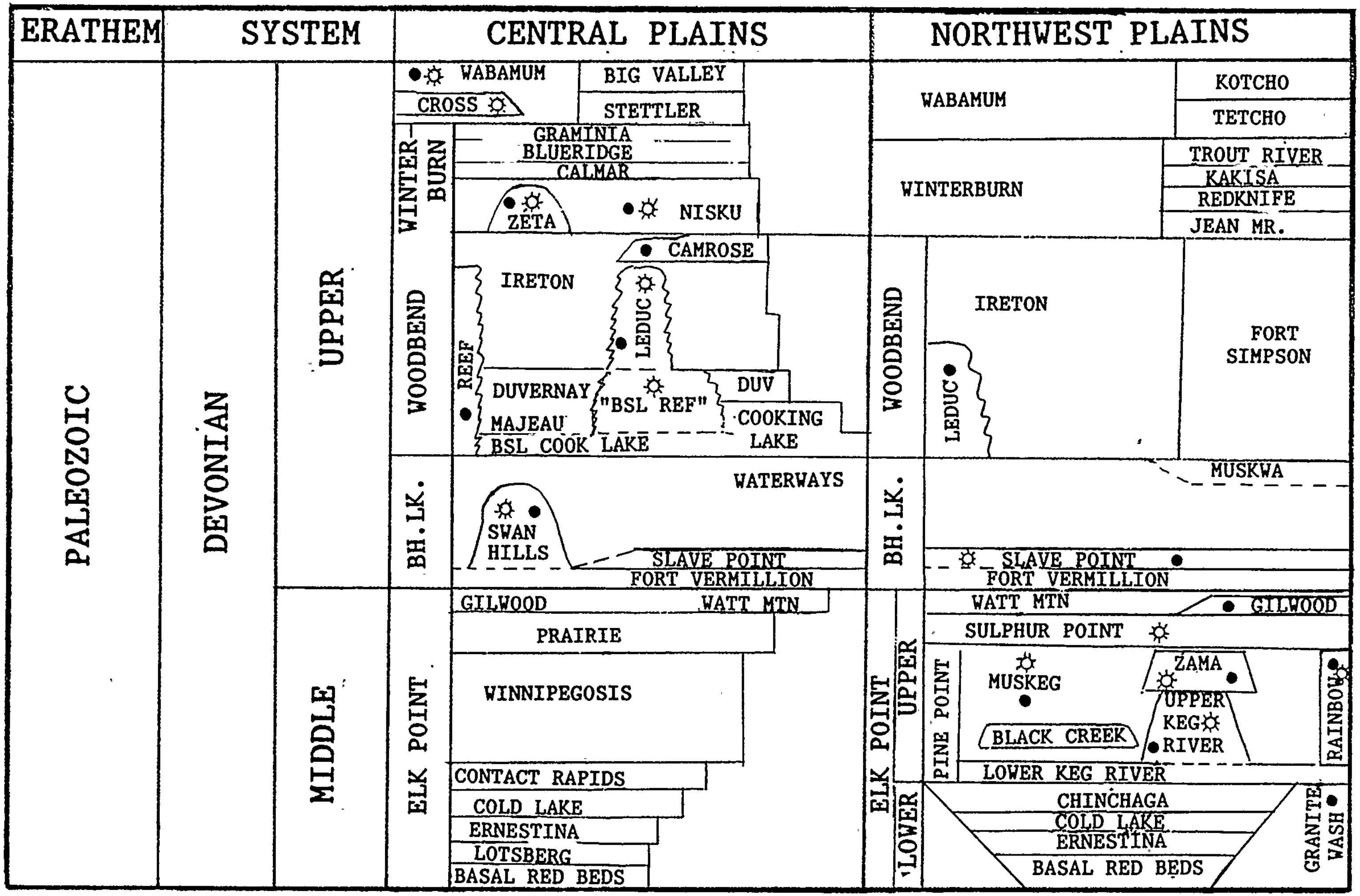

Figure 3.1 Stratigraphic column for central and northwestern Alberta (After ERCB, 1987).

3.3 Data Base

Approximately 118 wells drilled in the vicinity of the Golden Spike reef mass provide excellent subsurface geological control for building the reef model. Using a surface-fitting technique, computer-generated contour maps for the topography of various geological interfaces were produced. The shape of the model reef mass was based on the contour map (Figure 3.2) generated from these wells for the top of the Leduc Formation.

Five sonic logs from each of the reef crest, reef flank, and off-reef locations were digitized. Average interval velocities for the Cooking Lake, Leduc, Ireton, Nisku, Calmar and Wabamun units were also calculated. Interval densities were also obtained from available density logs. Table 3.1 contains acoustic impedance values calculated for each of the geological intervals. The uncertainty bounds for the velocities and densities are on the order of 1.0×10^2 m/s and 1.0×10^2 kg/m^3.

3.4 Modelling Details

3.4.1 Model Construction

Prior to construction of the model, appropriate scale parameters were selected (Table 3.2). The proposed

Range 27 W4

Township 51

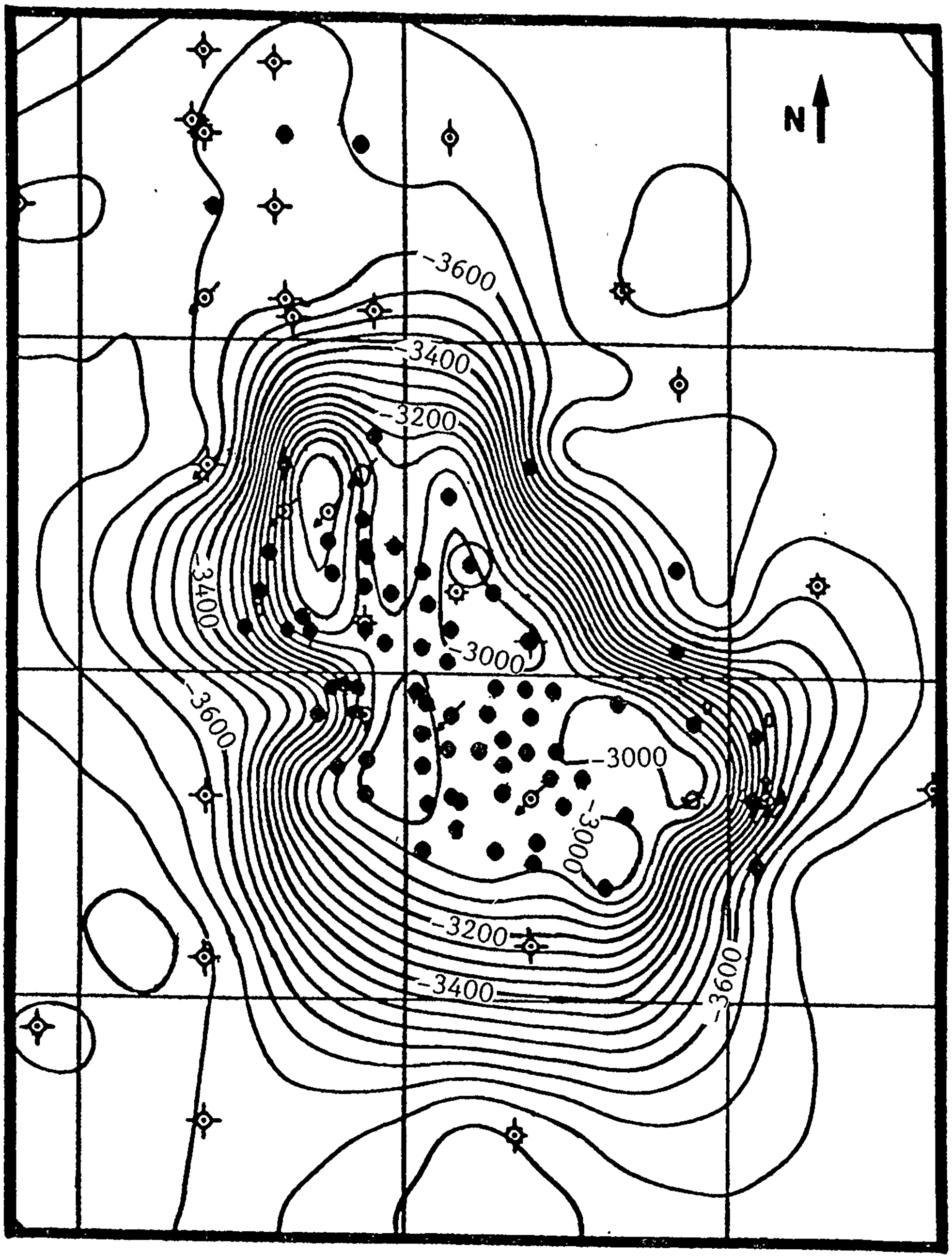

All values are in feet below sea level
Contour Interval: 50 feet

1 km

Figure 3.2 Contour map of the top of the Leduc Formation for Golden Spike (Courtesy of Chevron Canada Resources Ltd.).

GEOLOGICAL INTERVAL	VELOCITY $_{avg}$ m/s	DENSITY $_{avg}$ kg/m^3	ACOUSTIC IMPEDANCE kg/(s·m^2)
Top sonic log/ Wabamun Gp	3400	2600	8.8×10^6
Wabamun Gp/ Calmar FM	5800	2400	1.4×10^7
Calmar FM/ Nisku FM	4900	2300	1.1×10^7
Nisku FM/ Ireton FM	5900	2200	1.3×10^7
Ireton FM/ Leduc FM	4600	2300	1.1×10^7
Leduc FM/ Cooking Lake FM	5500	2400	1.3×10^7
Cooking Lake FM/ Beaverhill Lake FM	5900	2300	1.4×10^7

Table 3.1 Average acoustic impedances of the geological intervals for the Golden Spike reef.

PARAMETER	DIMENSION	SCALE FACTOR	MODEL	FIELD
distance	L	16000	1 cm	160 m
time	T	8000	200 ns	1.6 ms
velocity	L/T	2	1500 m/s	3000 m/s
frequency	1/T	1/8000	250 khz	31 hz

Table 3.2 Scale parameters for the Golden Spike reef model.

construction materials are indicated on a cross-section of the Golden Spike reef model (Figure 3.3). The Cooking Lake platform, composed of epoxy resin, was poured into a square mold and allowed to harden. The scaled model of the reef mass was milled from a block of plexiglass to match the even 100-foot contours on the Leduc structure map (Figure 3.2), as shown in Figure 3.4. The actual size of the modelled reef layer is approximately 23 cm wide, 33 cm long and 1.2 cm high. The contouring terraces were subsequently smoothed with a pneumatic hand-held chisel. The next layer to be included, the Duvernay/Ireton interval, was poured in two stages due to the large volume of epoxy resin required to complete this interval. The thickness of this layer posed two problems: (1) it was difficult to handle large volumes of epoxy resin and to mix them thoroughly; and (2) it was difficult to fully cure large volumes of the compound. After curing of the first half of this layer, the second portion was poured onto the model. The second pouring of epoxy resin for the Duvernay/Ireton interval never hardened, the surface remained sticky to the touch, indicating incomplete mixing of compounds. At this stage, construction of the Golden Spike reef model was ceased. Experience gained during construction of this model was invaluable to the successful completion of the Shekilie model.

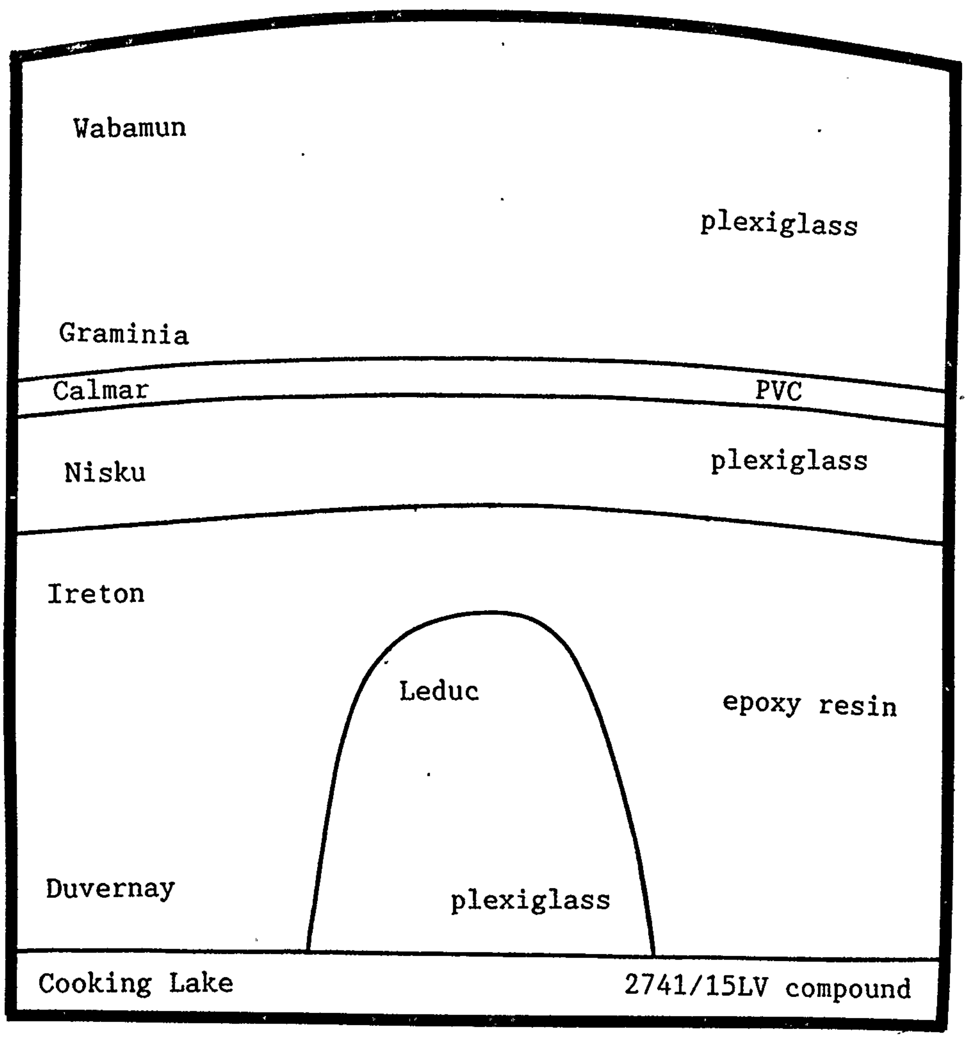

vertical exaggeration: 40X

horizontal scale: 10 cm

Figure 3.3 Cross-section of the Golden Spike reef model.

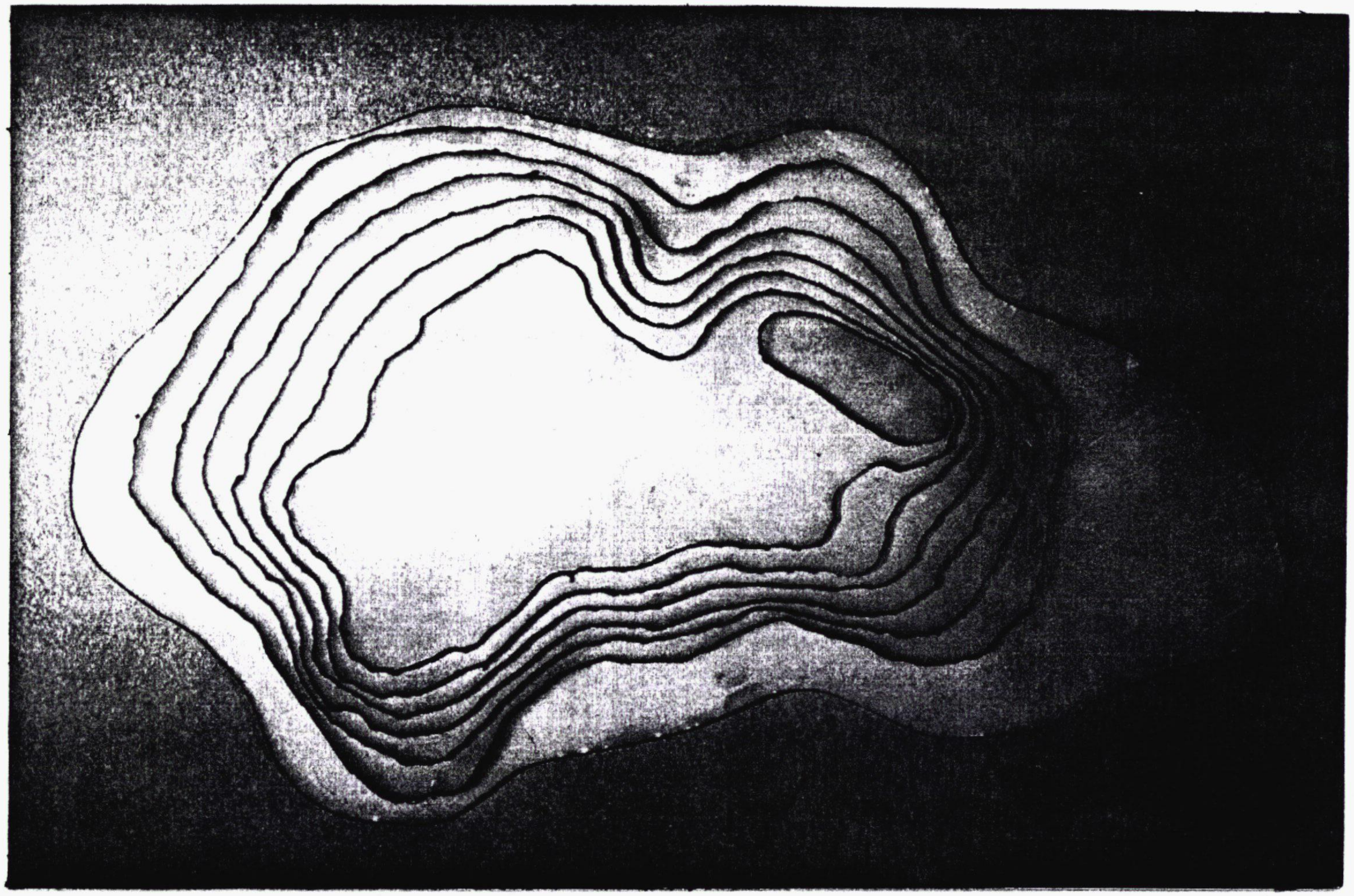

Figure 3.4 Picture of the modeled Leduc reef mass milled from a block of plexiglass.

3.4.2 Data Collection

To gain a better understanding of the origin and significance of seismic reflections generated from the model, it was decided that zero-offset surveys would be collected after each addition of a model layer. Zero-offset lines were collected over the model by a pair of transducers positioned as close together as possible, but without being in physical contact. The zero-offset sections should be equivalent to unmigrated stacked sections.

Seismic data were collected with the Golden Spike model resting on a plexiglass table on the bottom of the water-filled tank. The scaled central frequency of the source pulse was approximately 30 Hz. The sampling interval was 200 ns which corresponds to 1.6 ms after scaling. This decimal sampling rate led to difficulties later during data processing, as most processing software does not currently accept non-integer sampling rates.

Forty zero-offset lines were collected over the reefal layer and the Cooking Lake platform layer resting on a plexiglass table submerged in the water tank. Figure 3.5 shows the location of these lines over the reef mass. The line and shot spacings used were 1 cm and 0.2 cm respectively which are equivalent to 160 m and 32 m in the field after scaling. There were 240 shots per line. Data were not collected over the model after the Duvernay/

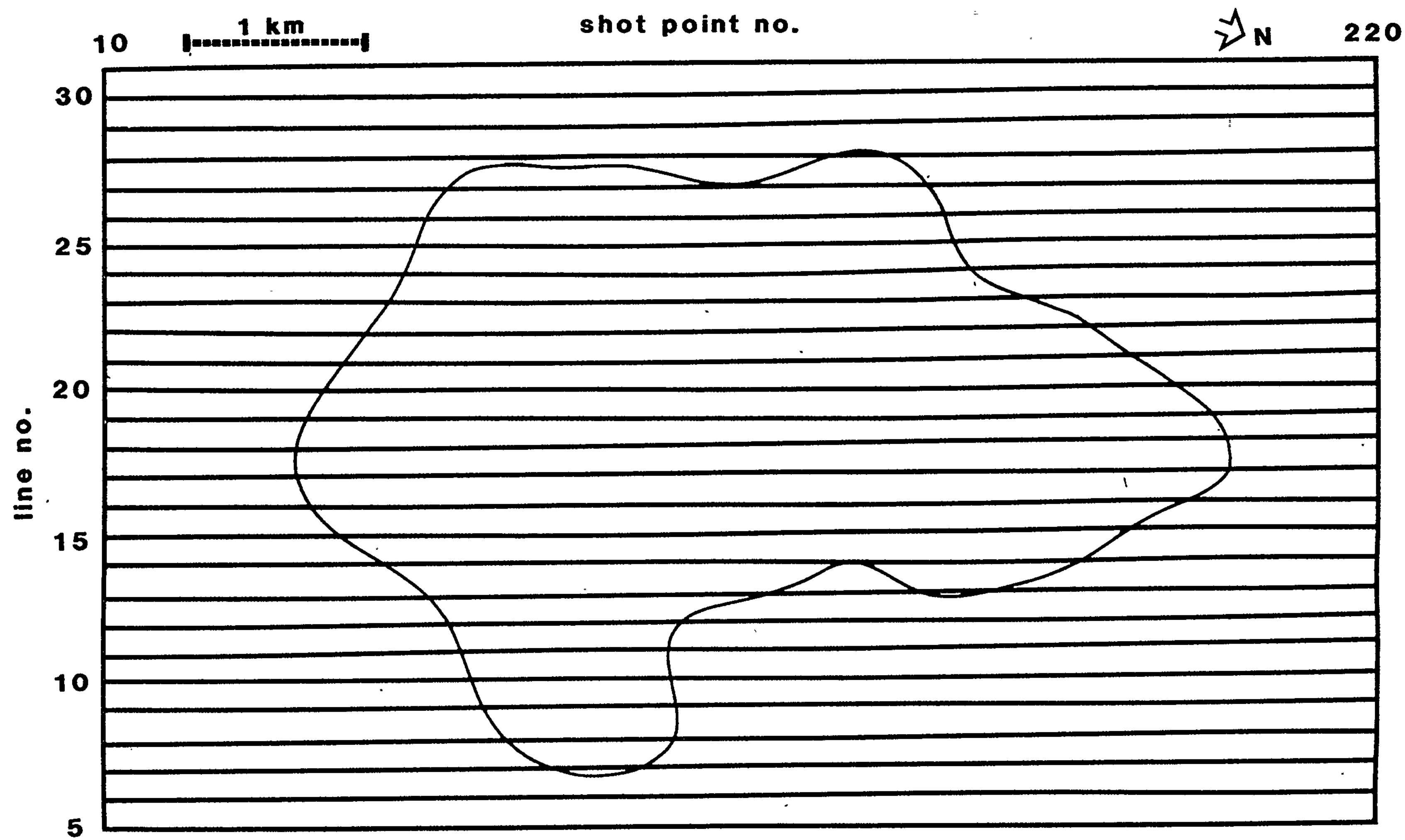

Figure 3.5 Location of the zero-offset lines over the Golden Spike model (Cooking Lake + Leduc Formation).

Ireton interval was constructed, because of incorrect acoustic properties which resulted from the improperly cured modelling compounds.

3.5 Discussion

All zero-offset lines collected over the reefal layer and the Cooking Lake platform (Figure 3.5) were displayed and examined. A variety of complex reflection events were demonstrated. Two representative lines, one crossing the centre of the reef mass and the other passing along the northeast flank of the reefal build-up are discussed in detail along with relevant synthetic sections from numerical modelling.

Line 21, positioned across the crest of the reef model, is shown with various reflection events identified (Figure 3.6). Event (a) is generated by the water/plexiglass acoustic contrast at the location of the Leduc reef and illustrates the normal-incidence time structure of the top of the reef along this profile. Event (b) is generated by the water/epoxy resin acoustic contrast representing the water/Cooking Lake platform contact. Event (c) is produced from the flat bottom of the plexiglass table upon which the model rests in the physical modelling tank. A velocity "pull-up" of this event under the reef mass can clearly be observed. This

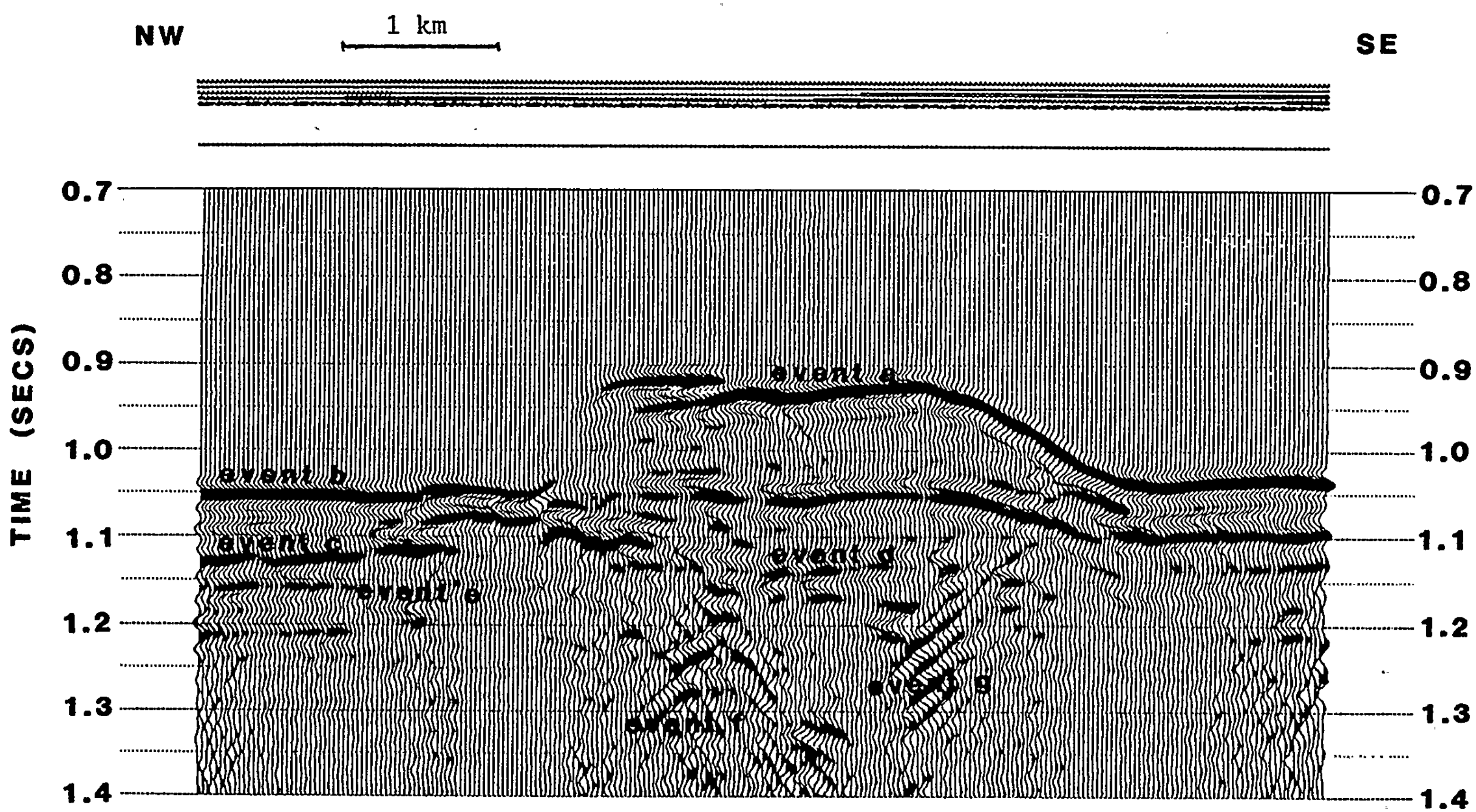

Figure 3.6 Line 21: zero-offset data across the centre of the Golden Spike model.

velocity anomaly is present since the traveltime through the plexiglass reef is less than the traveltime through an equivalent thickness of water which has lower acoustic velocity. The velocity anomaly observed under this model is more exaggerated than the anomaly which would have been observed if the Ireton shale had been added to the model, since the acoustic velocity of the modelled shale is faster than the velocity of water. Event (d) is a multiple reflection generated between the top of the reef and the bottom of the modelling table. Events (e) are strong diffractions originating from very sharp curves or discontinuities in the model. Events (f) are identified as multiply reflected diffractions. Events (g) are identified as probable reflected refractions based on their strong amplitudes and abrupt linear appearance.

Using the SIERRA modelling package (section 2.2), 2-D models along several of the profiles across the model are computed. Zero-offset lines were raytraced using the QUIKRAY module. The spike series produced from the raytracing module were subsequently convolved with a zero-phase Ricker wavelet having a central frequency of approximately 30 Hz, using the program SLIPR.

Figure 3.7 displays the 2-D numerically modelled seismic section in the same location as line 21 on the physical model (Figure 3.6). The loss in amplitude from the steep slope on the northwest side of the reef is much more dramatic from the physical modelling data than that

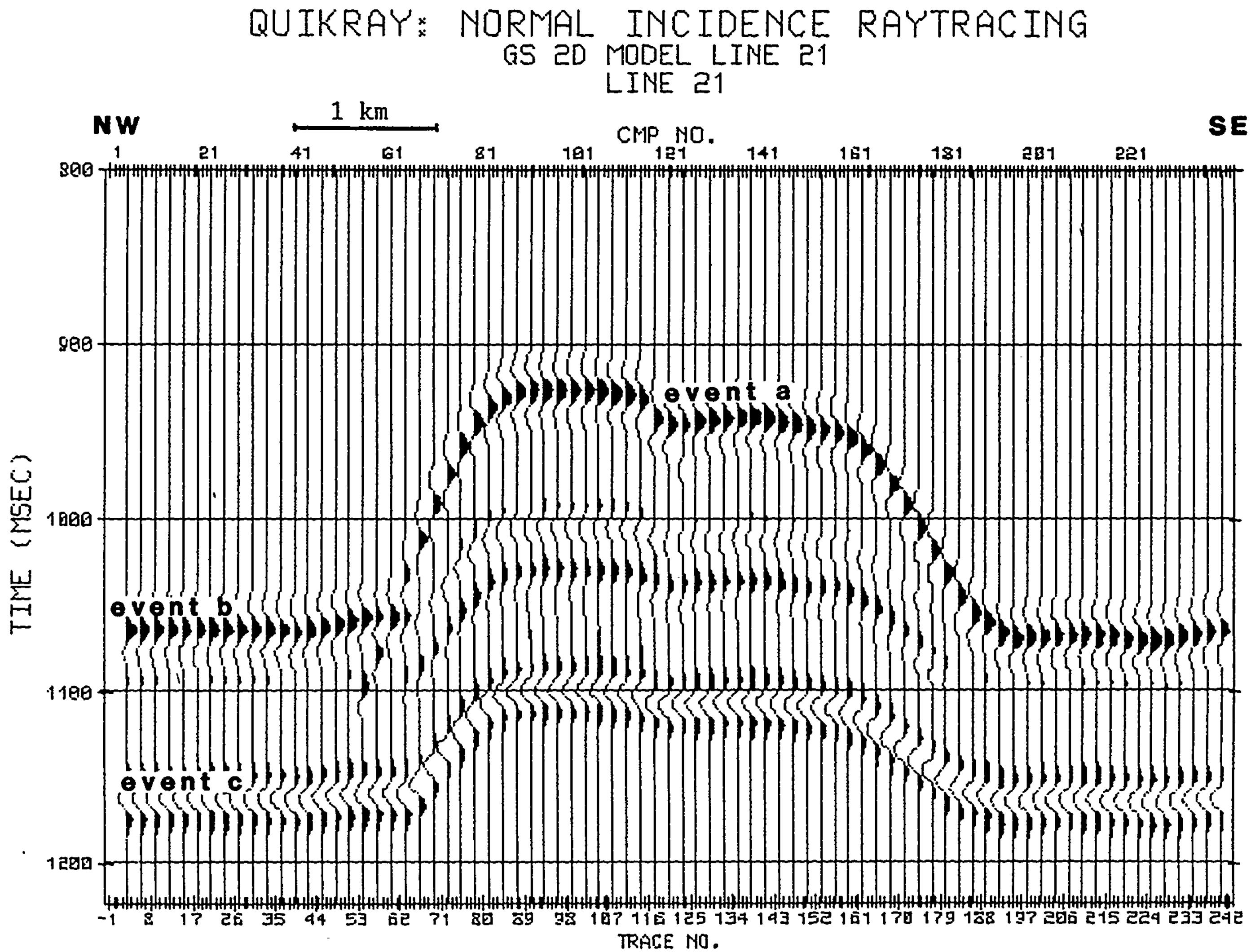

Figure 3.7 2-D numerical model along the profile of line 21 of the physicallly modelled survey.

which is predicted from two-dimensional modelling based on the curvature in the plane of the seismic line of the reef flank. The additional loss in amplitude in the physical modelling case is caused by the 3-D curvature of the reef flank and is a result of wavefront propagation where energy is reflected from an area rather than a curve as is assumed in numerical raytrace modelling. Moreover, many of the complex diffraction patterns seen in the physical modelling section (Figure 3.6) are not present in the numerical modelling section as this numerical modelling program does not account for diffractions and multiples. This example serves to illustrate that perfectly positioned 2-D lines over the crest of a feature may not be sufficient to correctly image that feature. Fresnel zone effects therefore limit the utility of 2-D seismic data. For instance, a 2-D migration of the physical modelling data over the crest of this feature, based on known parameters of the reef model, will not restore the correct amplitudes of the reef flank. Thus, 3-D migration becomes more desirable as the amount of curvature, in the plane perpendicular to the vertical plane containing the seismic line, increases. The concepts of Fresnel zones and areas of reflection are discussed further in section 4.5.

Line 10 from the physical modelling dataset is shown in Figure 3.8 with various reflection events identified. This line is positioned over the northeast toe of the reef

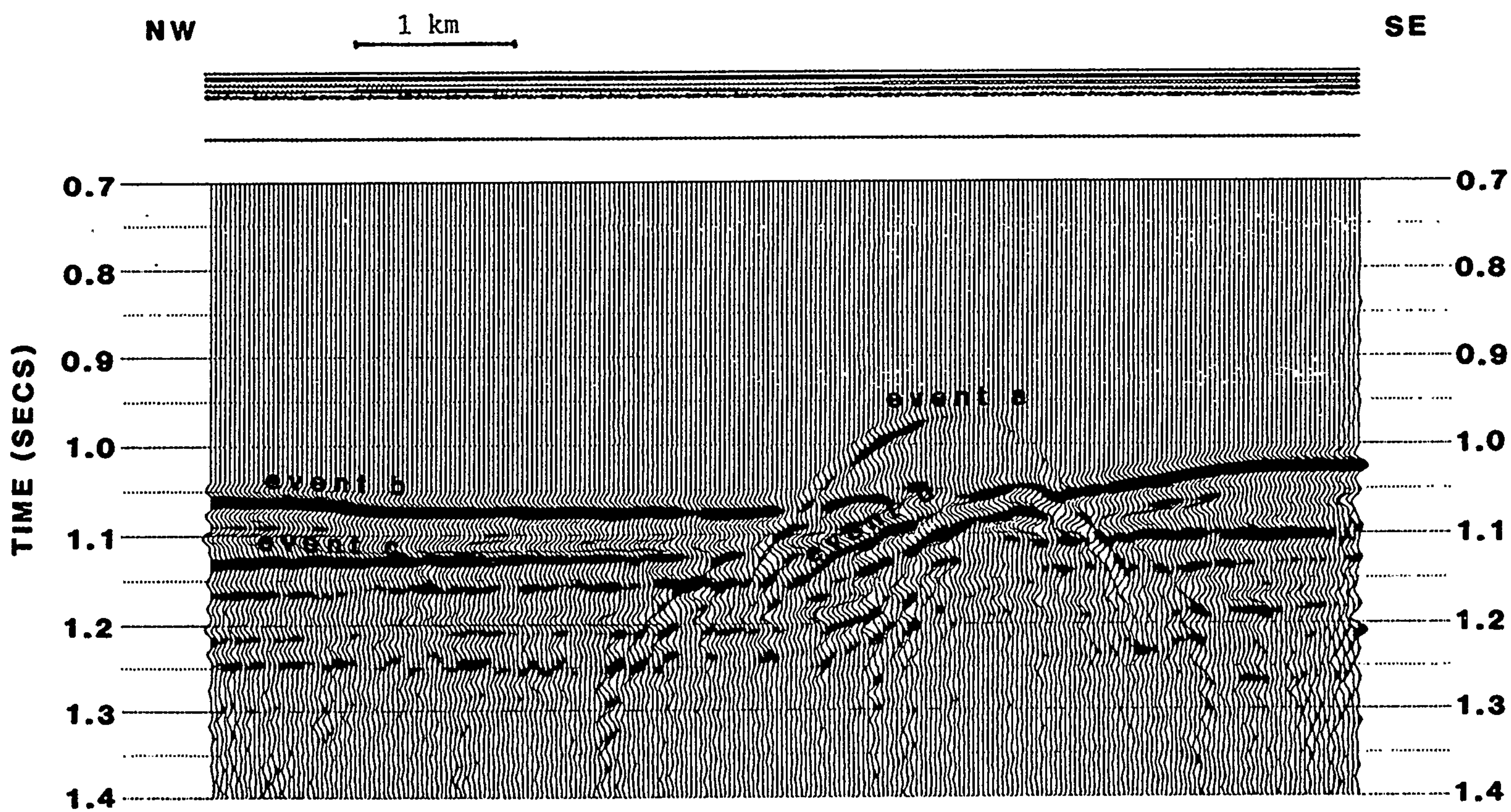

Figure 3.8 Line 10: zero-offset data over the northeast flank of the Golden Spike model.

(Figure 3.5). Event (a) is again generated by the water/plexiglass acoustic contrast at the location of Leduc reef. Event (b) is generated by the water/epoxy resin acoustic contrast representing the water/Cooking Lake platform contact. Event (c) is produced from the bottom of the plexiglass modelling table. Event (d) is an out of plane reflection from the bottom of the plexiglass modelling table. Energy from this event arrives before energy from event (c) because of its travel path through the high-velocity reef mass.

A numerical 2-D model in the same relative location as line 10 is shown on Figure 3.9. Comparison of Figures 3.8 and 3.9 reveals significant sideswipe energy present on the physical modelling line. Evidence for out-of-plane energy identification is given by the early arrival of energy from event (a) on the physical modelling data, and by the absence of a reflection event (d) on the numerical model. These strong out-of-plane reflection events again illustrate the need for a 3-D analysis of seismic data over structural features.

Time slices were created and examined for the entire unmigrated survey using an Apollo workstation. Horizontal seismic sections (time slices) from the top of the reef at 1024 ms, from the middle of the reef at 1056 ms, and from below the reef at 1184 ms are shown on Figure 3.10 and a contour of the physical reef model at the level corresponding to the time slice is superposed on each

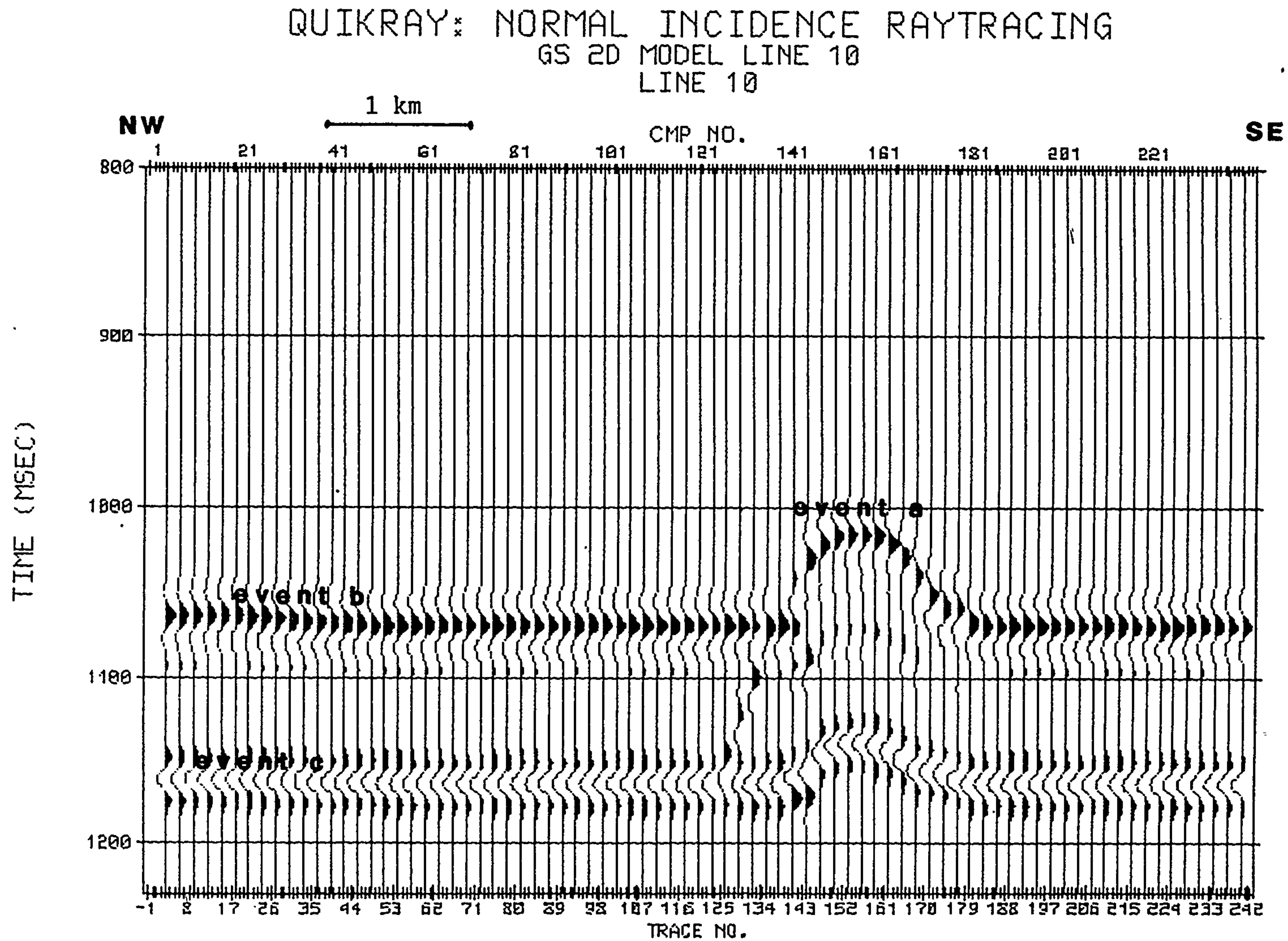

Figure 3.9 2-D numerical model along the profile of line 10 of the physically modelled survey.

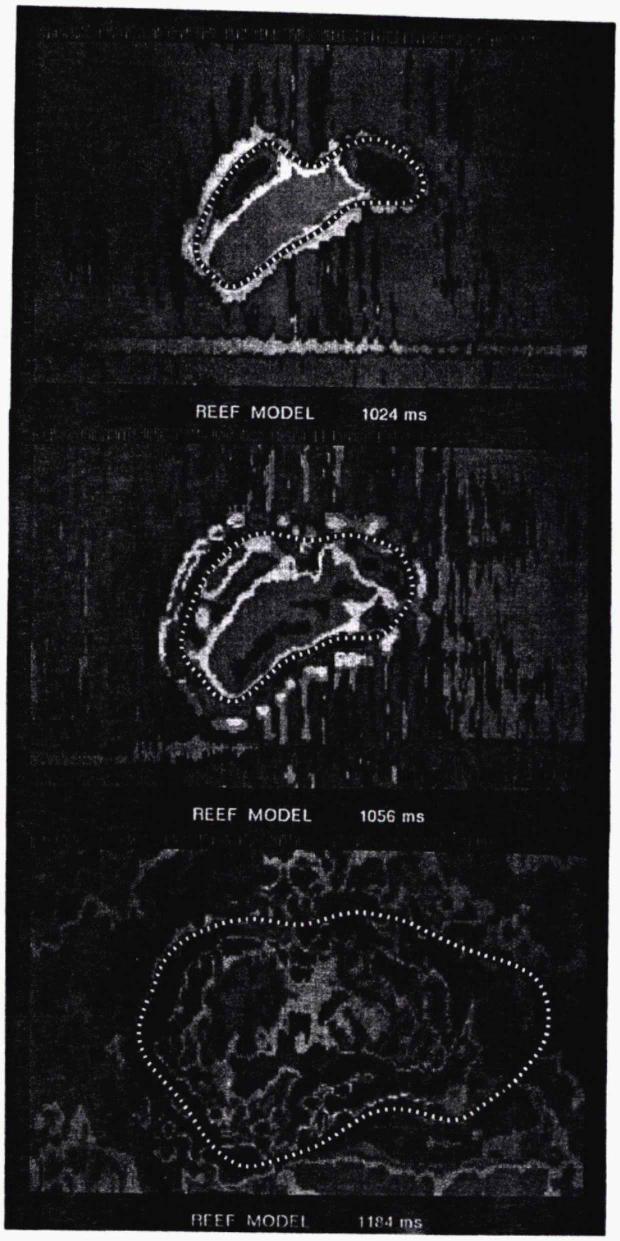

Dashed line indicates the actual reef contour at the corresponding time. Note, since the time of 1184 ms is below the reef mass, the contour of the base of the physical reef model is shown.

2 km

Figure 3.10 Time slices through the Golden Spike dataset.

display. Note, since the time slice at 1184 ms is from below the reef, the contour of the base of the physical reef model is shown. The largest positive amplitudes are represented on the time slices in red, the largest negative amplitudes in blue and zero amplitude in green. The time slices give a graphical demonstration of the dispersal of energy from the edges of the reef. The time slices are also valuable interpretational aids for assigning geological significance to reflection energies based on lateral morphologies and for helping in the identification of the various events indicated on the vertical seismic sections. Further work such as 3-D migration will be performed on the Shekilie example.

Chapter 4: Shekilie Pinnacle Reef Model Study

4.1 Background

The Shekilie Basin is located in the northwestern corner of the province of Alberta. The study area is situated within the Shekilie Basin in the vicinity of Townships 117 to 118 and Ranges 7 to 8, west of the sixth meridian (Figure 1.2). The Shekilie Basin is the most northerly of the Keg River evaporite basins. Exploration for hydrocarbons in the Shekilie Basin is of economic interest due to the presence of oil-bearing pinnacle reefs encountered in the Upper Keg River Member. The reefs found in this basin are approximately 120 m in height, and 200 to 700 m across at the base (ERCB, 1988). The depth of burial is approximately 1700 m. The Shekilie pinnacle reef study was chosen because of the difficulties associated with imaging such small and subtle features. The availability of detailed three-dimensional seismic coverage provided control for the study.

4.2 Geology

The geological setting of the Shekilie Basin is not well documented. However, the diagenetic history is very similar to the neighbouring Zama and Rainbow Basins which have been studied extensively (Langton and Chin, 1968; Hriskevich, 1970; McCamis and Griffith, 1967; Barss et al., 1970; Anderson, 1986). The Middle Devonian stratigraphy of this area is shown in Figure 3.1. A brief description of the geological setting of Upper Keg River reefs is given below.

The Cold Lake Formation, lying directly upon the Precambrian surface, consists of halite, suggesting very restricted marine conditions. Following deposition of the Cold Lake Formation, cyclic deposition of anhydrites and dolomites indicates fluctuating sea levels, with anhydrites deposited during the more restricted marine environment. This sequence of sediments is termed the Chinchaga Formation and is overlain by the Lower Keg River limestone platform which developed during an abrupt change to more open marine conditions. The Lower Keg River platform provides the base for the Upper Keg River reef growth. Numerous isolated pinnacles of the Upper Keg River Member have an average height of approximately 120 m with an areal extent of 4 to 35 hectares (ERCB, 1988). Upper Keg River Member reef growth was terminated by more restricted marine conditions. Black Creek Member salt may have been deposited at this time, as in the Rainbow and Zama basins. Interbedded anhydrites and dolomites of the Muskeg Formation were deposited until carbonate was again deposited from Sulphur Point to Slave Point time, interrupted only by the thin green shale of the Watt Mountain Formation. The Muskeg, Sulphur Point, Watt Mountain and Slave Point formations drape over the pinnacle reefs. This drape is probably due to dewatering of gypsum to anhydrite and/or the dissolution of Black Creek salt.

4.3 Data Base

Well logs in the Shekilie Basin were examined and categorized into reef crest, reef flank and inter-reef wells, based on the thickness of the Upper Keg River Member. Four sonic logs and one density log from each of these categories were digitized. Average interval velocities, densities and the corresponding acoustic impedances were calculated for various units and these data are presented in Table 4.1. The error limits for the velocity and density values are on the order of 1.0×10^2 m/s and 1.0×10^2 kg/m^3 respectively. These well logs provided control for the thickness and velocity values chosen for the modelled layers.

A 3-D seismic survey, over a reef crest well, 10-7-118-7W6, and an inter-reef well, 14-7-118-7W6, (Figure 1.2), was provided by Canterra Energy Limited. This dataset was collected in February 1986, by Western Geophysical Company of Canada. The energy source,

GEOLOGICAL INTERVAL	VELOCITY $_{avg}$ m/s	DENSITY $_{avg}$ kg/m^3	ACOUSTIC IMPEDANCE kg/(s·m^2)
Top sonic log/ Slave Point FM	3500	2500	8.8×10^6
Slave Point FM/ Watt Mountain FM	5900	2700	1.6×10^7
Watt Mountain FM/ Sulphur Point FM	5600	2400	1.3×10^7
Sulphur Point FM/ Muskeg FM	6100	2700	1.7×10^7
Muskeg FM/ Upper Keg River Mem	6300	2900	1.8×10^7
Upper Keg River Mem/ Lower Keg River Mem	5600	2600	1.5×10^7
Lower Keg River Mem/ Chinchaga FM	6200	2700	1.7×10^7
Chinchaga FM/ Cold Lake FM	6100	2900	1.8×10^7
Cold Lake FM/ Basement	4500	2000	9.0×10^6

Table 4.1 Average acoustic impedances of the geological intervals for Shekilie pinnacle reefs.

receiver configurations and instruments used in this survey are listed in Table 4.2. The processing history of this dataset is shown in Table 4.3. Interpretation of the seismic data was carried out on the Crystal® workstation at Western Geophysical Company of Canada. As part of this thesis, several reflectors were interpreted over the dataset. The reflectors that were picked are shown on an east-west seismic line from the 3-D dataset over the selected reef (Figure 4.1). Reflections generated from the reef and the drape above the reef in the overlying units are apparent on this section. Two-way time contour maps produced for the Upper Keg River and Muskeg reflectors are shown on Figures 4.2 and 4.3 respectively. The shape of the reef and the drape of the overlying units used for the physical model are based on these contour maps.

4.4 Modelling Details

4.4.1 Model Construction

Appropriate scale parameters and modelling materials were selected prior to construction of the Shekilie model (Table 4.4). Care was taken to select parameters such that the scaled sample interval (1 millisecond) was an integral number of milliseconds and that the physical

ACQUISITION:	
Acquired for:	Canterra Energy Ltd.
Acquired by:	Western Geophysical Co. of Canada
Party:	341
Recording date:	February 1986
SOURCE:	
Energy source	Dynamite
Number of charges	one hole inline
Charge size	2 kilogram
Shot depth	18 meters
Shot interval	100 meters
INSTRUMENTS:	
Model	Sercel SN348B
Amplifier	1FP
Filter	out / 125 Hz
Sampling interval	2 ms
Record length	3.0 s
Tape format	SEG-B
Tape density	6250 BPI
RECEIVERS:	
Type of geophone	14 Hz LRS - 1011
Number of geophones per group	9 over 25 meters
Number of groups recorded	240
Group interval	70 meters
Average percent coverage	1200 %

Table 4.2 Field survey parameters for the Shekilie pinnacle reef.

PROCESSING		
	date:	May 1986
1.	Demultiplex	
	processing sample rate	2 ms
	processing record length	2.0 s
2.	Pre-processor	
	trace header update for cell sort	
3.	Cell sort	
	cell size	35 x 50 meters
4.	Geophone/instrument phase compensation	
	filter operator length	600 ms
5.	Amplitude compensation	
	time function exponential value of 2.5	
6.	Prefilter	
	frequency	10 - 90 Hz
	slope	18 - 36 DB/OCT
7.	Deconvolution	
	type	minimum phase inverse filter
	autocorrelation window	300 ms - 1300 ms
	minimum predictive distance	spiking 2 ms
	operator length	100 ms
	percent white noise	0.1 %
8.	Trace equalization	
	2000 RMS	
	window	-400 ms start time delay 3000 ms stop time
9.	Weathering and drift statics	
	method	refraction intercept
	datum elevation	600 meters ASL
	replacement velocity	2750 meters/s
	weathering velocity	610 meters/s
10.	Automatic statics (first iteration)	
	NMO with one regional velocity function	
	type (MISER®)	automatic surface consistent
	gate 1	400 - 1200 ms
	maximum shift	+ or - 24 ms

Table 4.3 Processing history of the Shekilie field survey.

11.	3-D velocity analysis	
	type (VELAN®)	Semblance
	3-D velocity interpolation	
12.	Automatic statics (sond iteration)	
	NMO with 3-D velocity interpolation	
	type (MISER®)	automatic surface consistent
	gate 1	450 - 1200 ms
	maximum shift	+ or - 24 ms
	residual shot/receiver statics corrections	
13.	Normal Moveout application	
	mute applied after N.M.O.	
	distance (meters)	time(ms)
	300	0
	350	300
	500	500
	1300	1200
14.	Trim statics	
	correlation window	400 - 1200 ms
	model	5 traces
	maximum shift	+ or - 10 ms
15.	Stack	
	flexicell® - strength factor	1 : 2
	equal weights with 1200 % average fold	
16.	Finite difference migration	
	2 pass migration (pass one E-W, pass two N-S)	
	percent velocity used	95 %
17.	Bandpass filter	
	frequency	12 - 75 Hz
	slopes	18 / 36 DB/OCT
18.	Gain	
	type	RMS
	window	200 - 700 ms

Table 4.3 (Continued) Processing history of the Shekilie field survey.

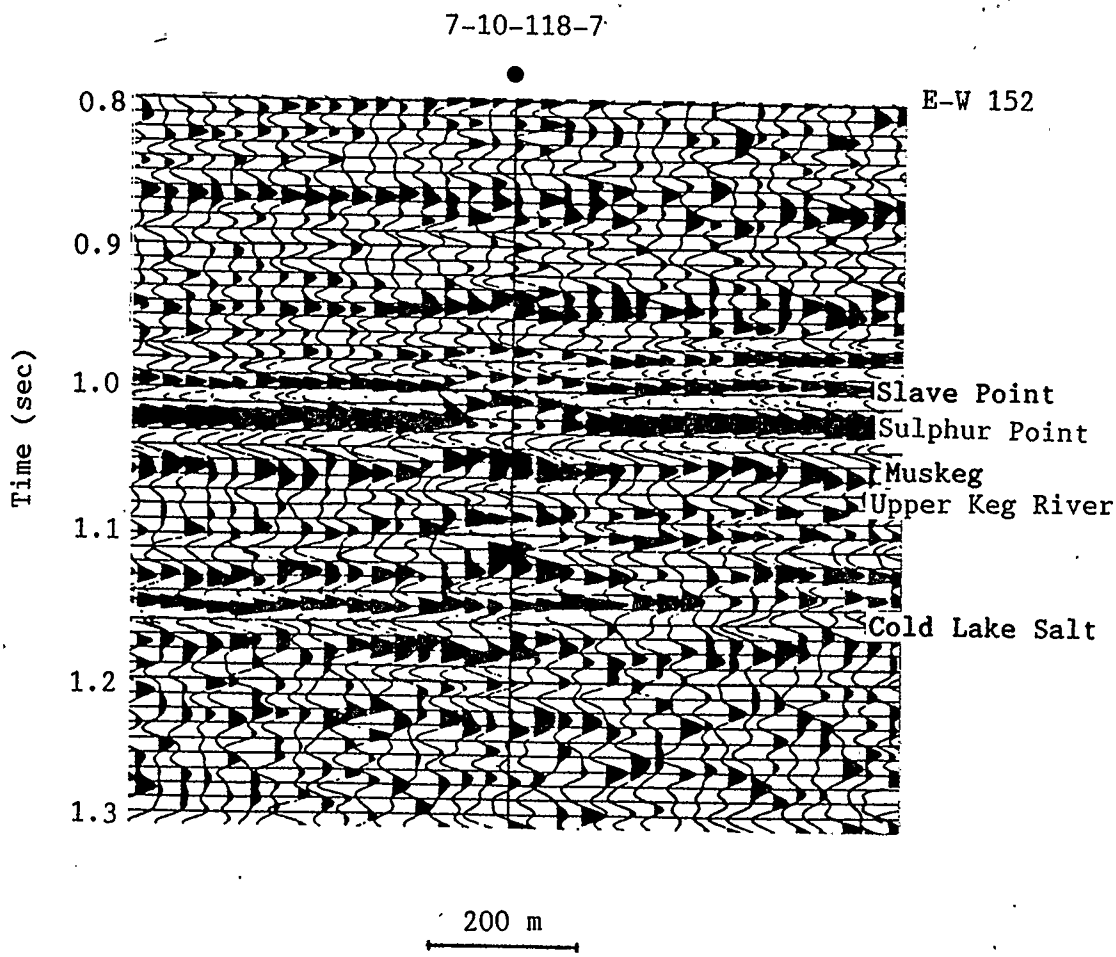

Figure 4.1 Field seismic line over the Shekilie pinnacle reef.

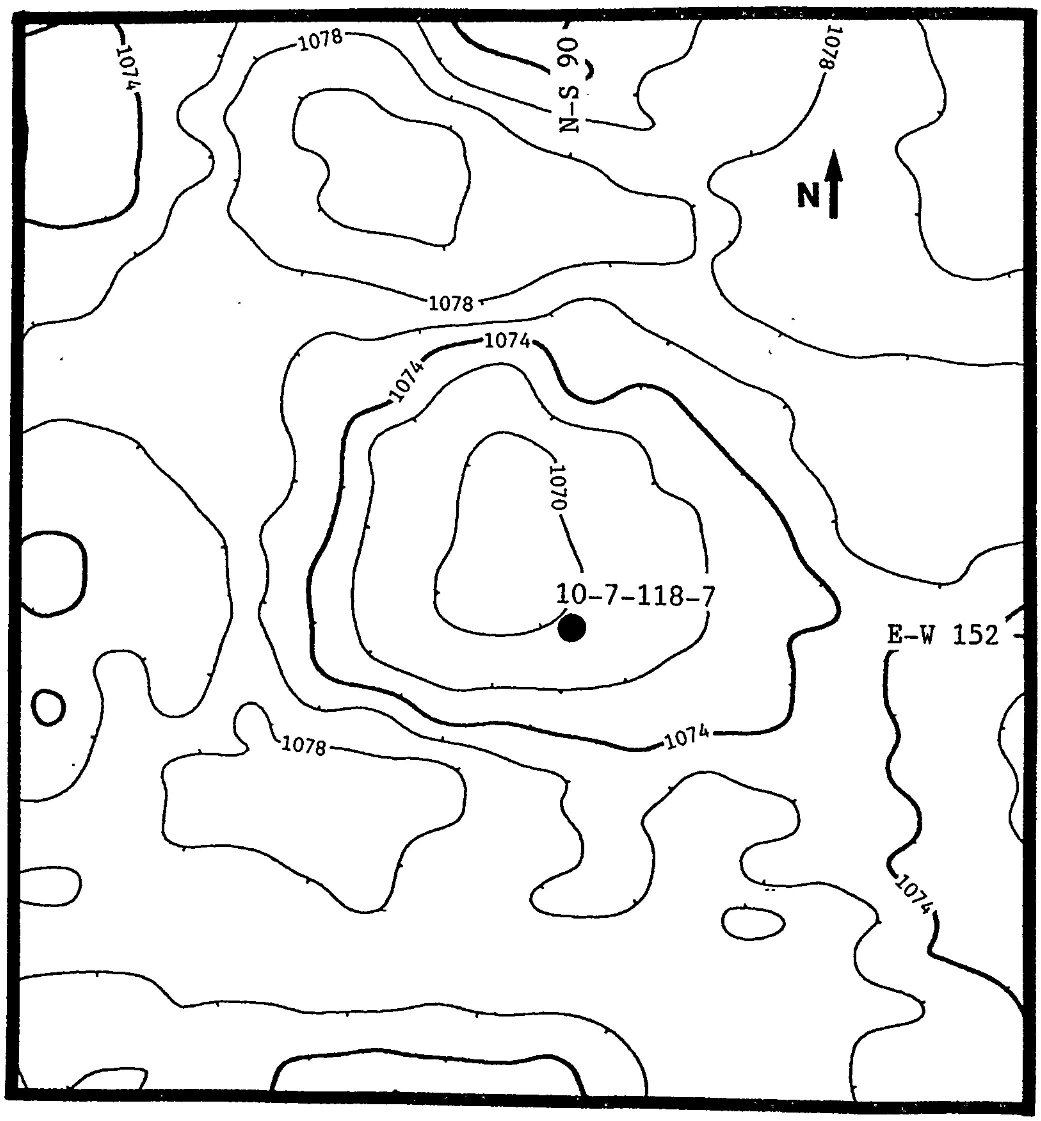

All values are two-way traveltime in ms
Contour interval: 2ms

200 m

Figure 4.2 Time contour map of the top of the Upper Keg River Member.

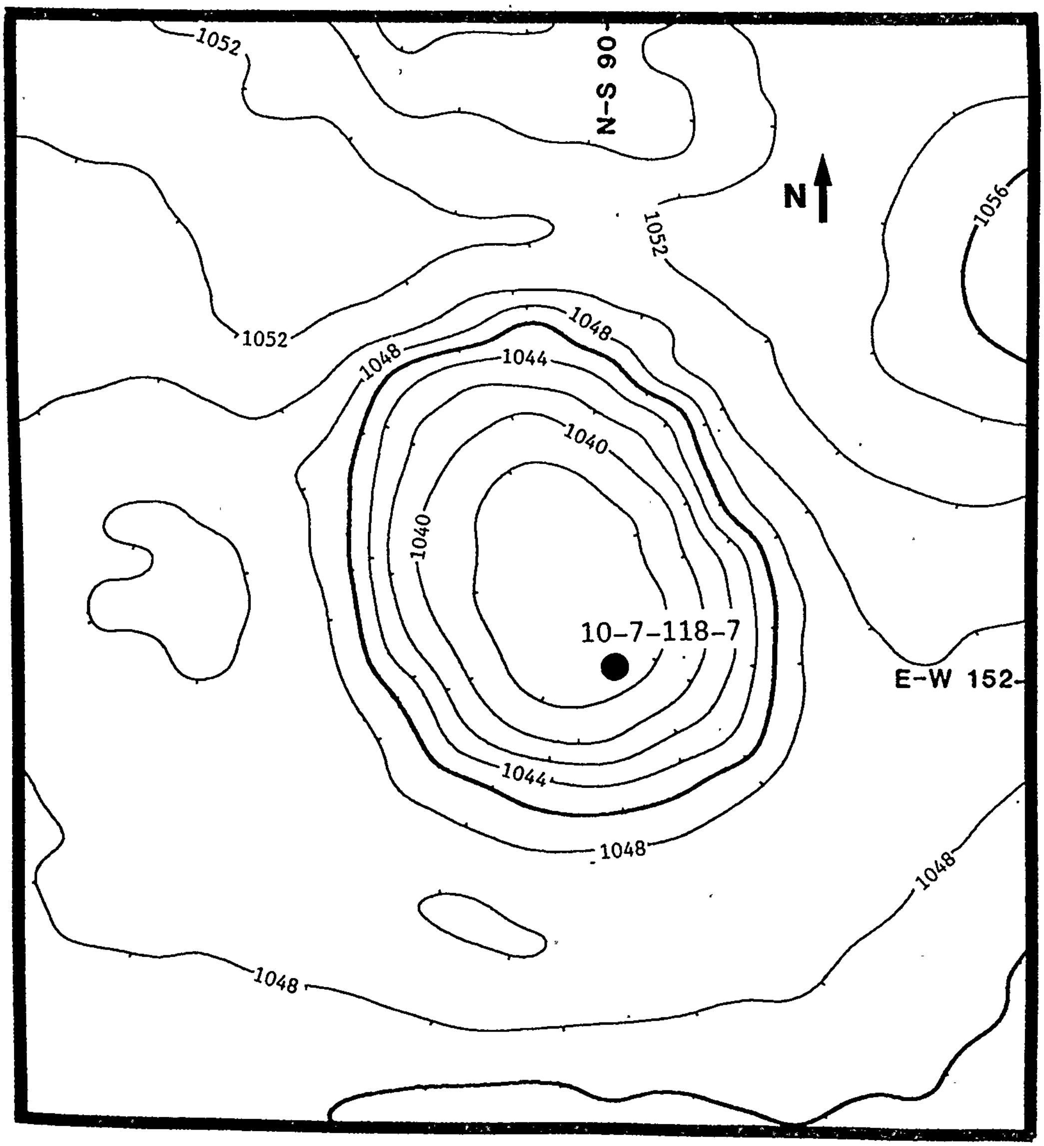

All values are two-way traveltime in ms
Contour interval: 2ms

200 m

Figure 4.3 Time contour map of the top of the Muskeg Formation.

PARAMETER	DIMENSION	SCALE FACTOR	MODEL	FIELD
distance	L	11500	1 cm	115 m
time	T	5000	200 ns	1 ms
velocity	L/T	2.3	1500 m/s	3450 m/s
frequency	1/T	1/5000	250 khz	50 hz

Table 4.4 Scale parameters for the Shekilie pinnacle reef model.

dimensions of the model (31 cm x 35 cm x 4.5 cm) allowed for relative ease of construction and handling. A cross-section of this reef model is shown on Figure 4.4 with the velocities and thicknesses used for model construction as indicated.

The Shekilie model was constructed, as with the Golden Spike model, one layer at a time. The thicknesses and the velocities of the modelled layers were based on the well log information. The Cold Lake, Chinchaga, and Lower Keg River units were poured consecutively, allowing time for each layer to dry fully. The Muskeg Formation layer was milled from a single piece of plexiglass based on contours interpreted from the 3-D seismic data (Figure 4.3). The shape of the Upper Keg River reef was cut as a cavity, in the plexiglass representing the Muskeg Formation, according to the interpreted Keg River Member contour map (Figure 4.2). The Upper Keg River Member hollow was then filled with epoxy resin and allowed to dry. The cavity was not completely filled, in order to allow for slight topography on the Lower Keg River Member platform as shown in the cross-section (Figure 4.4). A very thin paste of epoxy compound, used to model the Lower Keg River, was applied to the bottom of the Muskeg and the Upper Keg River units,-filling this cavity, pressed against the lower part of the model, clamped, and allowed to dry. The Sulphur Point Formation was added next on top of the Muskeg Formation, and gentle drape was accomplished by

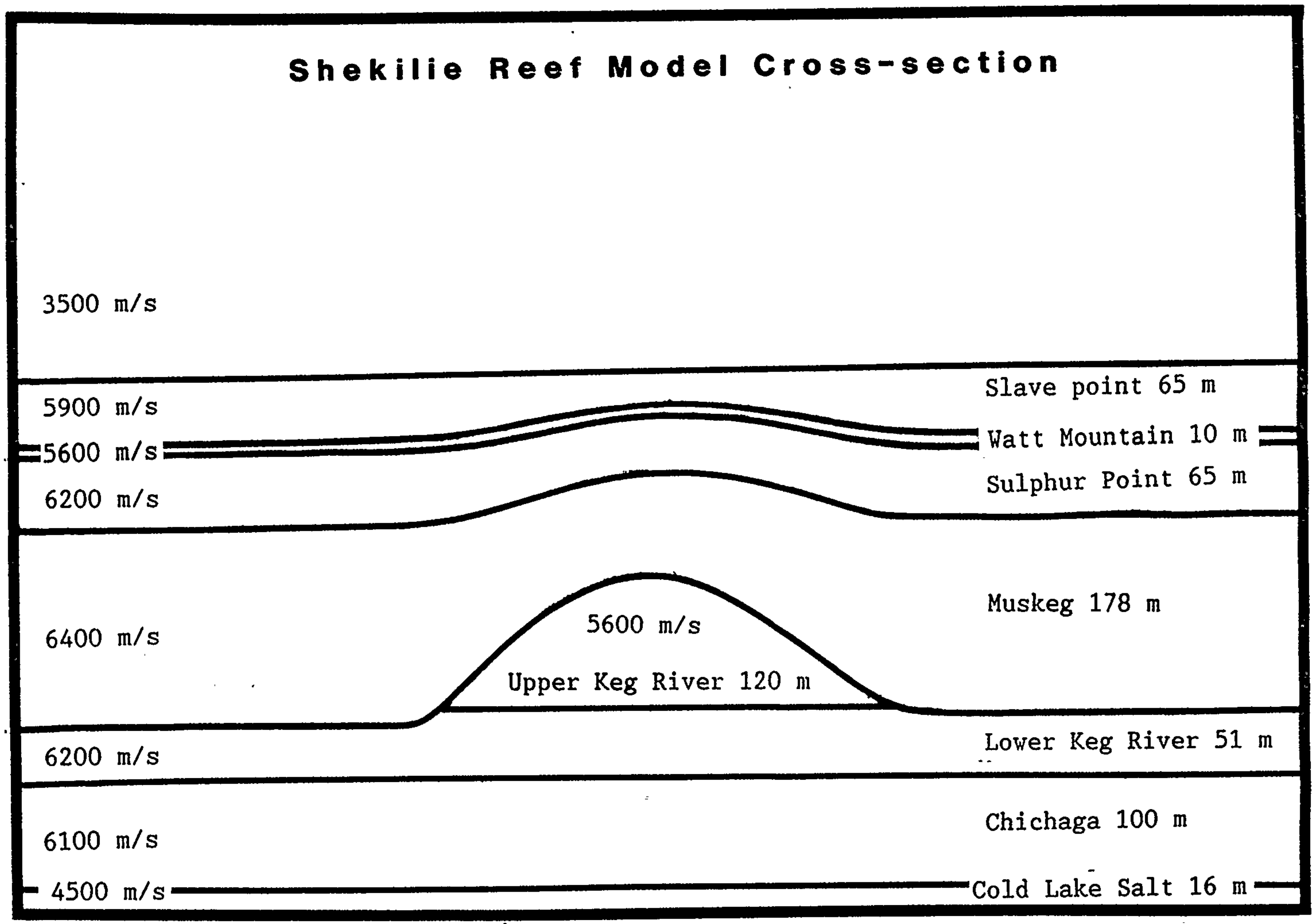

Figure 4.4 Cross-section of the Shekilie reef model.

100 m

adding more epoxy resin above the location of the reef after the initial pouring had dried. A thin layer of Watt Mountain Formation was applied and the model was completed by the addition of the Slave Point Formation. Drape on the Slave Point Formation was omitted from the model for two reasons: (1) since this layer is in contact with the water background and has a stronger reflection coefficient than would be observed in the field, that is, the scaled velocity in water is less than the velocity in shale, it is advantageous to have a uniform reflector for reference; and (2) to simplify analysis of the effects of structure at Muskeg and Keg River levels since it was believed that energy from this artificially strong reflection would interfere with the weaker events below.

4.4.2 3-D Survey Acquisition Design

As part of this thesis, 3-D seismic survey acquisition parameters were reviewed. A thorough understanding of these parameters was necessary prior to data collection so that an adequate survey could be designed to properly image the structure of interest. Knowledge of these factors is also required for interpretation of the final data.

3-D seismic surveys provide subsurface coverage over an area, rather than along a line as in the case of conventional 2-D seismic acquisition. Ideally, the data should be distributed over a uniform grid with equal trace multiplicity at each grid point or common midpoint (CMP). Each CMP should contain traces with an evenly distributed range of source-receiver offset distances and the traces within each CMP should have evenly distributed source-receiver azimuths. On land, the most frequently used acquisition technique to achieve these desired properties is the crossed-lines method whereby a number of source lines and receiver lines are positioned perpendicular to each other, forming a regular grid of crossing lines.

Data are recorded by receivers along a number of receiver lines for each shot. The areal distribution of receivers is termed the patch and the choice of patch configuration determines maximum offset. The natural CMP spacing with this method is one half the shot spacing in the direction of the shot lines and one half the receiver group spacing in the direction of the receiver lines. The bin is introduced as a small cell for which all traces whose shot-receiver midpoints fall within the cell are stacked together. The concept of binning is necessary for an areal dataset because, in practice, midpoints are usually scattered, as the shots and receivers are not positioned in an exactly regular grid. The lateral dimensions of the bin are usually chosen to equal the along-line CMP spacing, again to achieve the desired properties of evenly distributed multiplicity, offset distances and azimuths.

Receiver array design, patch size, bin size and recording aperture for dipping events are factors which govern the design of 3-D surveys. The design of the physical modelling 3-D survey was based on compatibility with the Canterra 3-D field survey so that the two datasets could reasonably be compared.

Since 3-D data are recorded with a distribution of offset azimuths, areal arrays should be employed to discriminate against coherent noise (Burg, 1964). However, areal arrays are difficult and expensive to employ in practice and usually linear arrays in the direction of the receiver lines are utilized. Horizontally travelling coherent noise arrives at the n-element array, with element spacing Δx, from many different azimuths, α, (Figure 4.5). It is noted that the array response, F, to plane waves of wavelength λ (Sheriff and Geldart, 1982) is:

$$F = |\sin\{n\pi(\Delta x/\lambda)\sin\alpha\}/[n\sin\{\pi(\Delta x/\lambda)\sin\alpha\}]| \qquad (4.1)$$

The response, F, varies from no attenuation for a broadside source, $\alpha = 0^{\circ}$, to the usual attenuation for an inline array, $\alpha = 90^{\circ}$. For an n-element array, the improvement in signal to random noise ratio is $n^{1/2}$, provided that the signal is vertically incident and that the element spacing is larger than the correlation

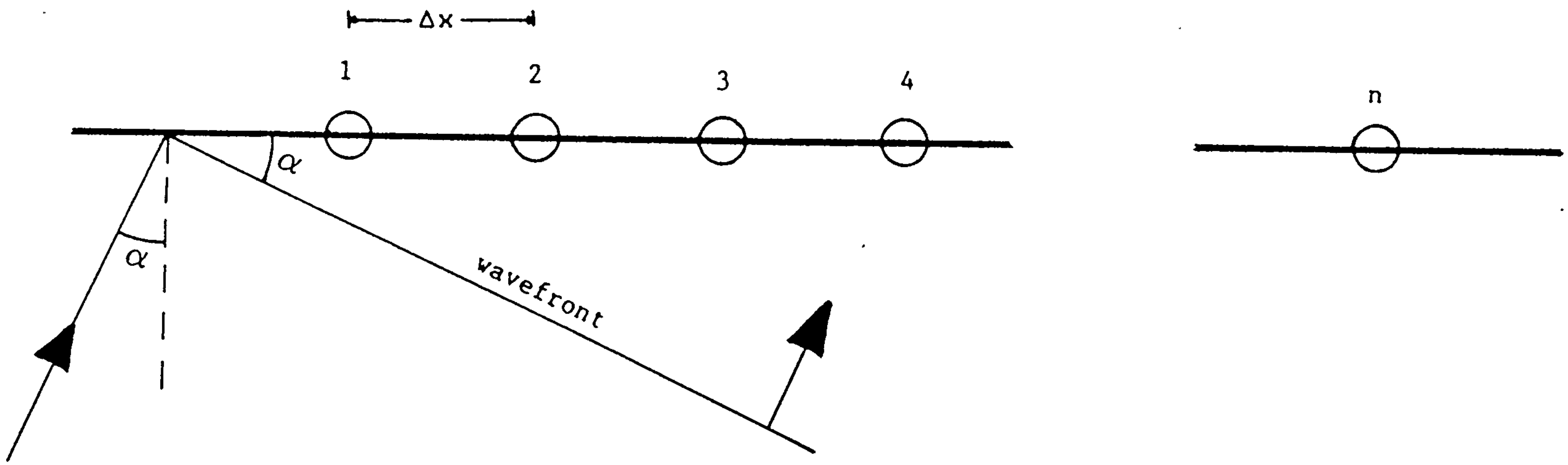

Figure 4.5 Plan view of wavefront approaching linear array at broadside angle, α (After Sheriff and Geldart, 1982).

distance of the random noise. Since linear arrays do not attenuate multi-azimuth, horizontally travelling coherent noise in a consistent fashion, and since the arrays will attenuate non-vertically incident signal, array lengths are generally kept as short as possible while keeping element spacing larger than the correlation distance of the random noise.

The spatial sampling interval represents the natural bin size of the recorded data. The requirement of adequately sampled data is of major importance since aliased energy tends not to be moved by the migration process (Claerbout, 1985).

For zero-offset data, differences in reflection traveltime between two surface points are produced only where reflecting interfaces are not parallel. Referring to Figure 4.6, the difference between two-way traveltime for the two reflection raypaths for a horizontal surface with two dipping planar reflection interfaces is:

$$\Delta t = 2(t_1 + t_2)$$

$$t_1 = \Delta x \sin\theta_{upper}/(V_{upper}\cos\theta_r)$$

$$t_2 = \Delta x \cos(\theta_{upper}+\theta_r)\sin\theta_r/(V_{upper}\cos\theta_r)$$

$$\Delta t = 2\Delta x[\cos(\theta_{upper}+\theta_r)\sin\theta_r+\sin\theta_{upper}]/(V_{upper}\cos\theta_r) \quad (4.2)$$

where t_1 is the extra traveltime in the upper dipping layer, t_2 is the extra traveltime in the lower dipping layer, Δx is the receiver interval, θ_{upper} is the angle

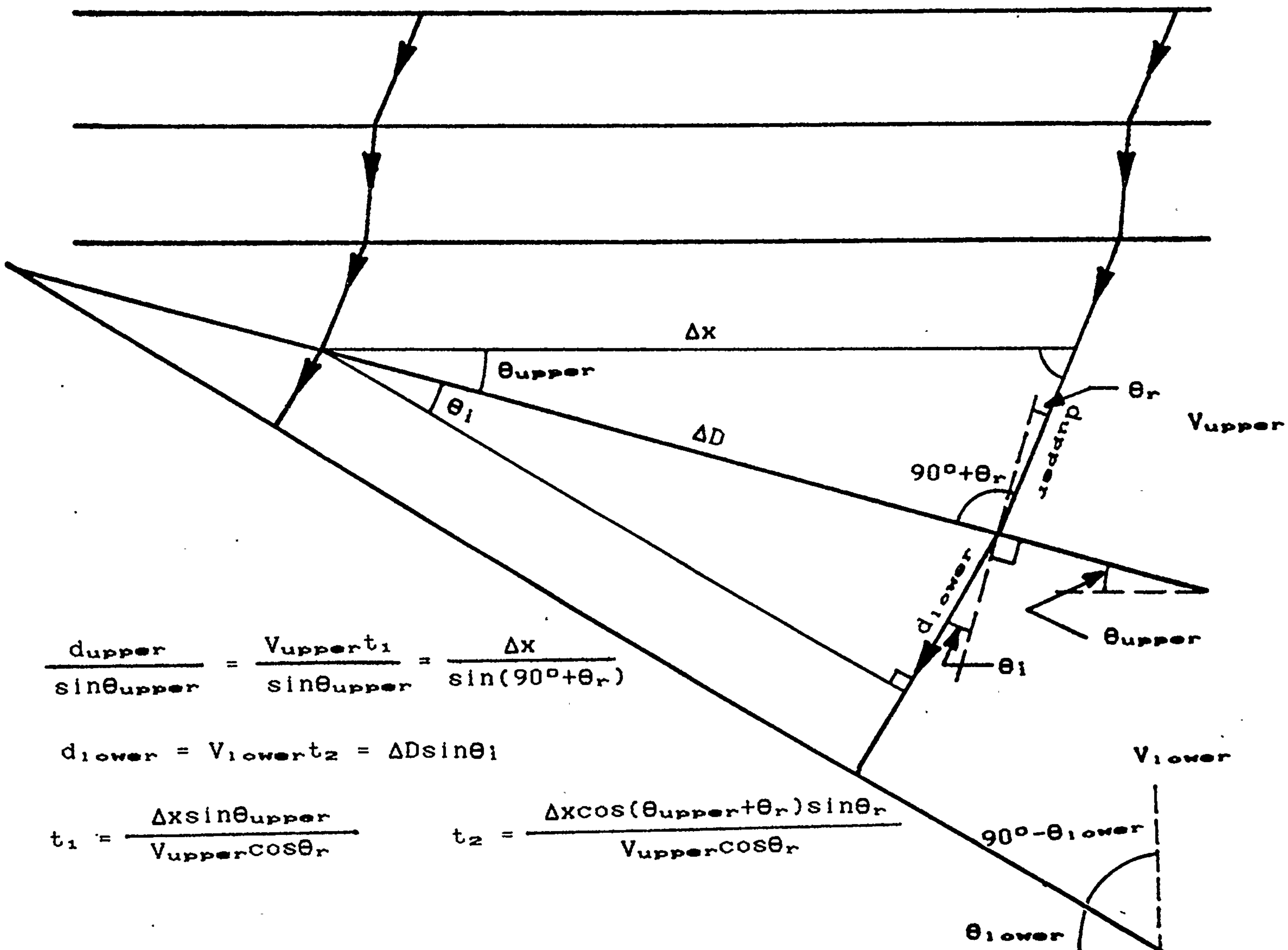

Figure 4.6 Raypath diagram for two dipping interfaces.

between the upper dipping layer and a horizontal layer, θ_r is the angle of refraction, V_{upper} is the velocity in the upper dipping layer.

For the model case, we assume that all interfaces are parallel except formations which have drape and that drape geometry is such that $V_{lower} \geq V_{upper}$ and $\theta_{lower} \geq \theta_{upper}$ for concentric drape caused by salt dissolution or for non-concentric drape due to differential compaction caused by gypsum-to-anhydrite dewatering. The function, Δt, is monotonically increasing with increasing θ_{upper} for all values of θ_{lower}. The bounds on the traveltime differences are:

$$t_{min} = 2\Delta x \sin\theta_{lower}/V_{lower} \qquad \text{for } \theta_{upper} = 0^{\circ} \qquad (4.3)$$

and

$$t_{max} = 2\Delta x \sin\theta_{lower}/V_{upper} \qquad \text{for } \theta_{upper} = \theta_{lower} \qquad (4.4)$$

By induction, these bounds are valid for any number of draped units with V_{upper} replaced by the velocity above the uppermost draped layer.

To prevent spatial aliasing on the stacked section, there must be two spatial samples per wavelength of the highest frequency in the signal, f_n (Copper and Cook, 1984). Therefore, bounds for the maximum unaliased dip present, θ_{max}, can be obtained by substutiting $1/2f_n$ into equations (4.3) and (4.4):

$$V_{upper} / 4f_h\Delta x \le \sin\theta_{max} \le V_{lower} / 4f_h\Delta x \quad (4.5)$$

The recording aperture is the horizontal distance over which data must be recorded to capture energy which is normally incident on dipping reflections. Data must be acquired with a sufficient recording aperture to ensure that all unaliased energy from dipping interfaces is captured. This distance can be calculated by normal incidence raytracing upon a reflector with dip equal to θ_{max} overlain by horizontal interfaces.

4.4.3 Data Collection

4.4.3.1 Physical Modelling Data

Seismic data were collected with the Shekilie model resting on a plexiglass table on the bottom of the water-filled tank. The scaled central frequency of the source pulse was approximately 50 Hz, with highest frequency, $f_h \sim 80$ Hz. The temporal sampling interval used for data collection was 200 ns which corresponds to 1 ms after scaling. The method of data collection in the physical modelling system differed from data collection in the field since recording in the laboratory was restricted to one receiver channel at a time. Receiver arrays and the patch geometries in the laboratory were simulated by moving the receiver and repeating the source.

To acquire a better understanding of the origin and significance of seismic reflections generated from the model, zero-offset surveys were collected over the model during various stages of the model construction. The ability to see the seismic wavefield in stages, as model complexity increased, proved valuable for gaining insight into the origin and significance of various recorded reflections.

The first zero-offset survey, consisting of 25 lines with 48 shots per line, was gathered over the model at the completion of the Lower Keg River unit. The line and shot intervals were 1 cm and 0.5 cm which are equivalent to scaled distances of 115 m and 57.5 m respectively. Figure 4.7 shows a zero-offset line from this survey with the Lower Keg River, Chinchaga, and Cold Lake salt events identified. A reflection from the bottom of the modelling table is also indicated. The events on this section are laterally consistent as expected from uniform , flat layers. Figure 4.8 displays a zero-offset line, with the major events as indicated, but now collected directly over the reef crest upon the completion of Upper Keg River and Muskeg layers. The events identified on the previous figure are more difficult to identify on this section because at the crest the response is dominated by energy scattered from the Muskeg Formation drape structure.

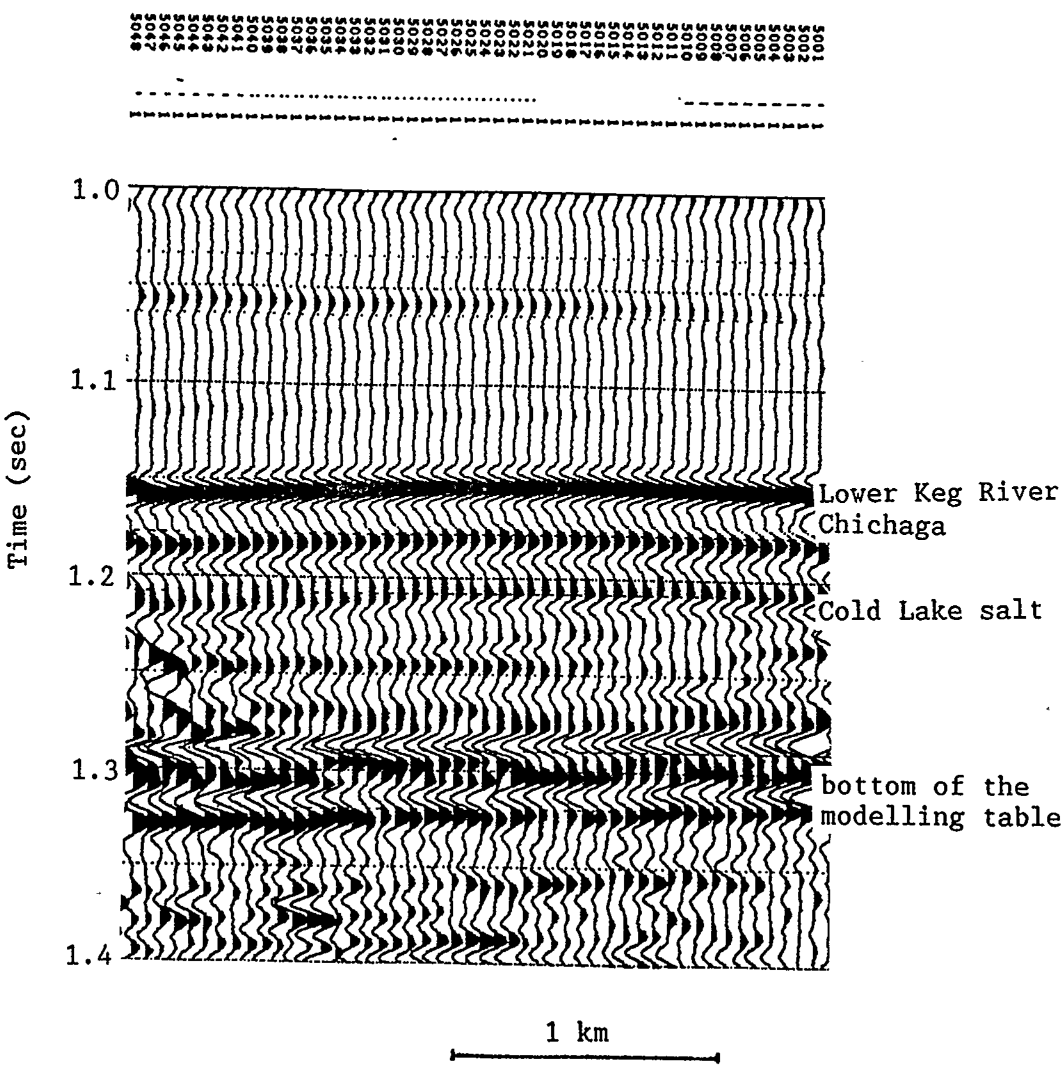

Figure 4.7 Lower Keg River zero-offset line.

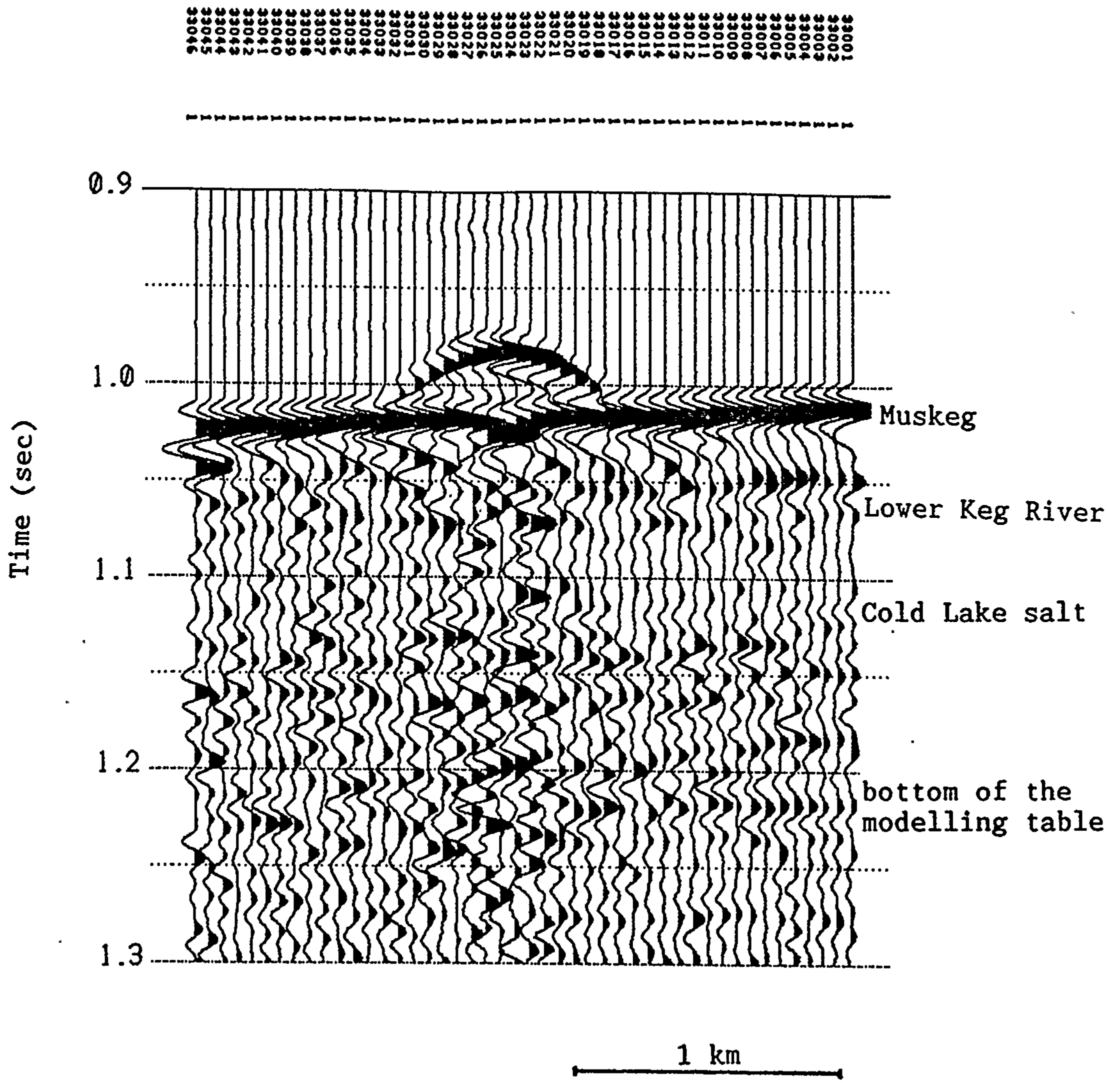

Figure 4.8 Muskeg zero-offset line.

Analysis of this section lead to the decision to exclude the drape on the Slave Point Formation. However, this section shows several interesting phenomena related to drape. Fresnel zone smearing of the flat portions of the Muskeg event almost cause the flat reflection event to continue through below the Muskeg structure. A section after inclusion of the Sulphur Point Formation is shown on Figure 4.9 with the major events identified. The reflection events on this section again show a fairly high degree of lateral consistency. This line does not cross the reef structure and no effects attributable to the reef are discernible on it. The model was completed by the addition of the Slave Point layer, with water used for the remainder of the model to the surface. A zero-offset section across the reef location using the completed model is displayed on Figure 4.10. The main events are again identified. Although this section is over the same Muskeg drape feature as in Figure 4.8, the seismic response in this case is not dominated by scattered energy. The reflection coefficient from the boundary at the top of the Muskeg Foramtion is much smaller with the addition of the high-velocity Sulphur Point Formation so that any reflections from the drape feature are weaker and do not tend to dominate. The "ringy" appearance of this section is caused by source-generated direct arrival energy. Specific details of the zero-offset data from the completed model are analyzed in section 4.5.2.

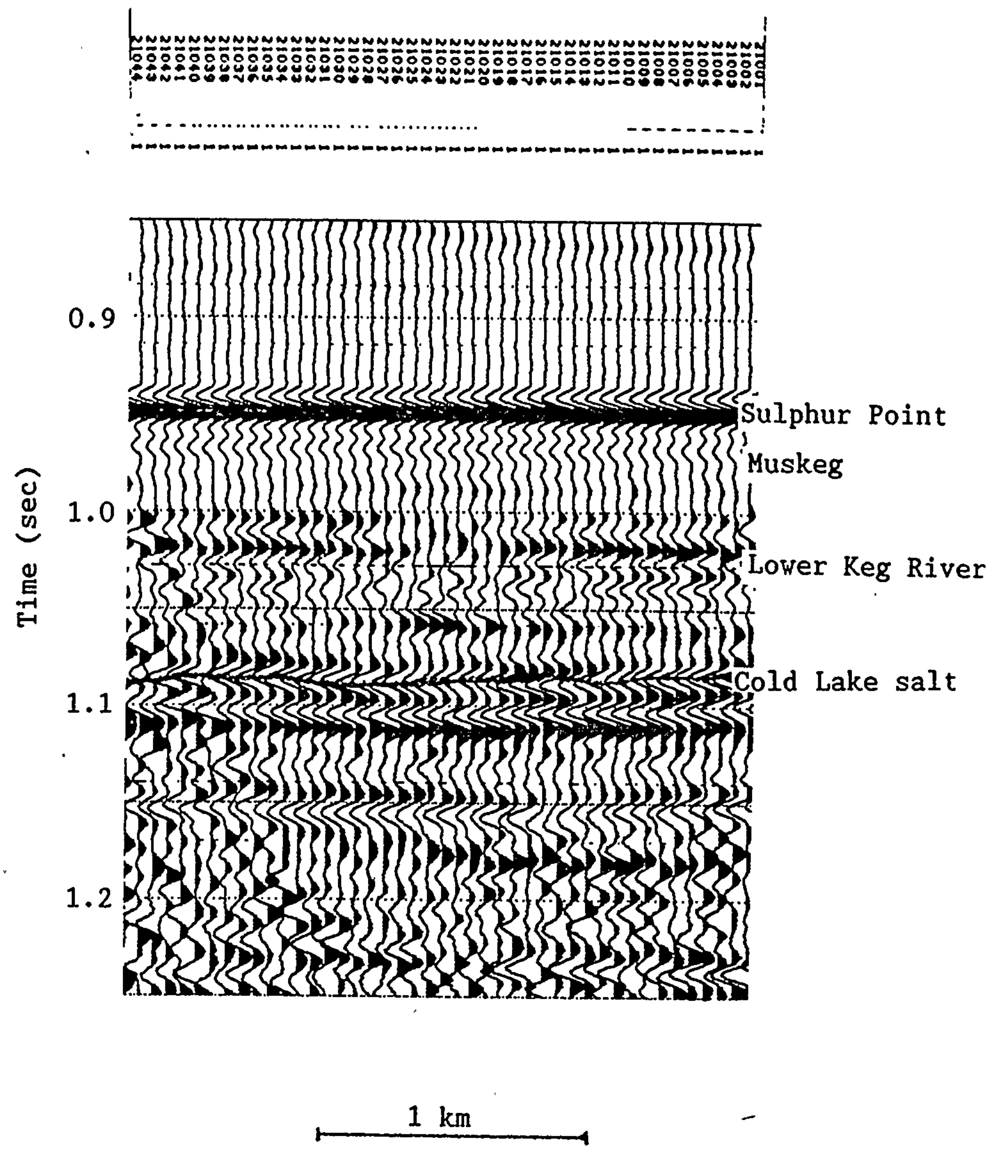

Figure 4.9 Sulphur Point zero-offset line.

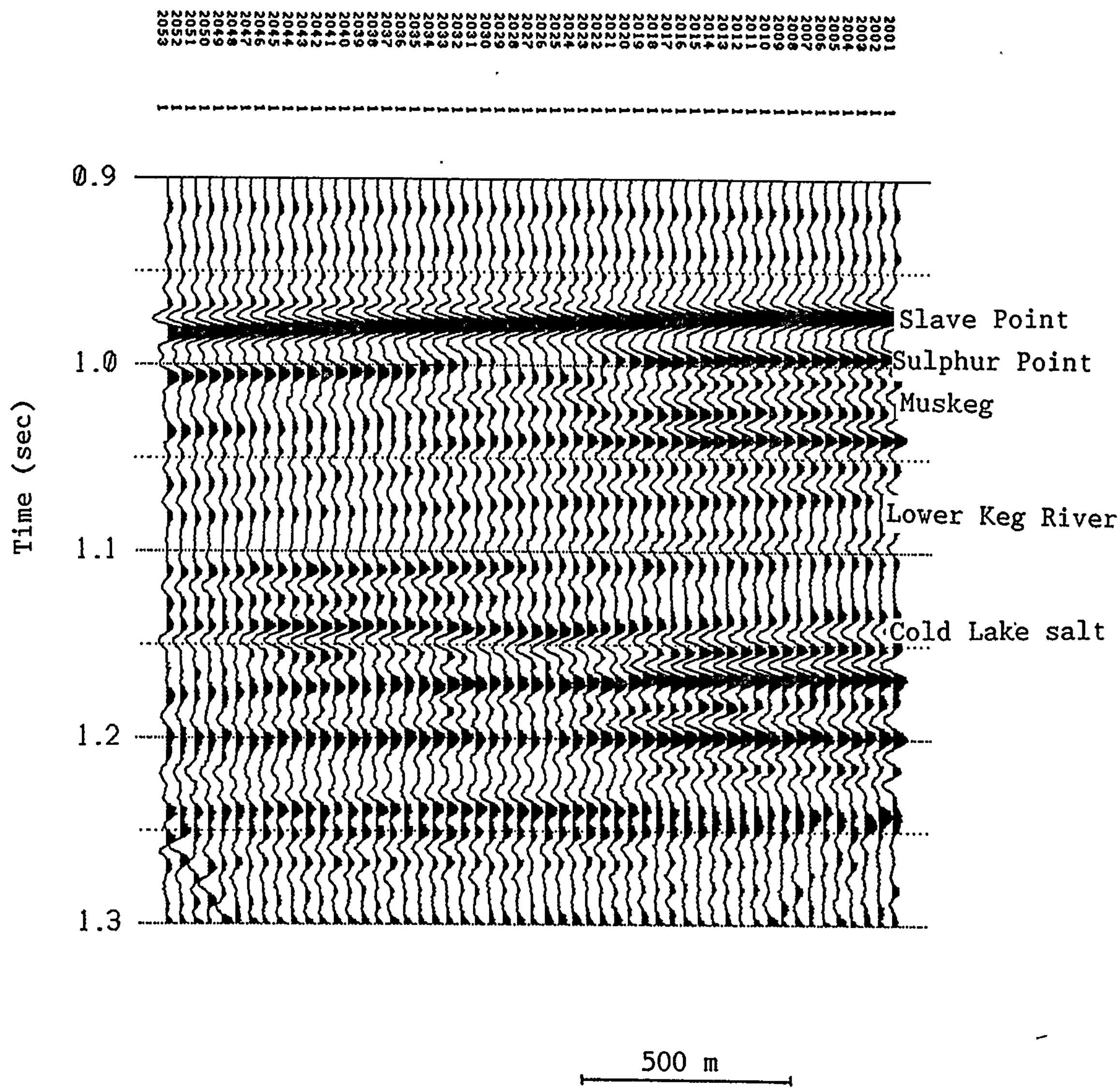

Figure 4.10 Physically modelled Slave Point zero-offset line over reef crest.

A full three-dimensional survey, with acquisition parameters similar to the Canterra field data, was collected over the completed Shekilie model. The crossed lines method of 3-D data acquisition, with shot and receiver lines perpendicular to each other, was used for this survey. The final acquisition pattern for the 3-D survey, shown on Figure 4.11, consisted of 133 shots with 240 receiver stations recorded per shot. The shot station spacing was 0.9 cm, corresponding to a scaled distance of 104 m. The 240 receivers were arranged in patches of 10 receiver lines with 24 receiver stations on each line. The receiver line and receiver station spacings were 1.8 cm and 0.6 cm respectively, corresponding to scaled distances of 207 m and 69 m respectively. Therefore, the scaled dimensions of the patch were 2070 m by 1656 m. For each receiver station, an inline array of six receivers, 1 mm apart, with an array length of 1 station was used. The average of the six traces was recorded in standard SEGY format for each station. The natural bin size or CMP spacing, equal to one half the source and receiver intervals, was 34.5 m by 52 m in this example.

Referring to equation (4.5), the maximum unaliased dip from the Upper Keg River reef, in the inline direction, for Δx = 34.5 m, is bounded by $32.3° \leq \theta_{max} \leq 35.4°$. In the crossline direction, for Δx = 52 m, the maximum unaliased dip from the Keg River reef is bounded by $20.7° \leq \theta_{max} \leq 22.6°$. Since there are reflecting interfaces in

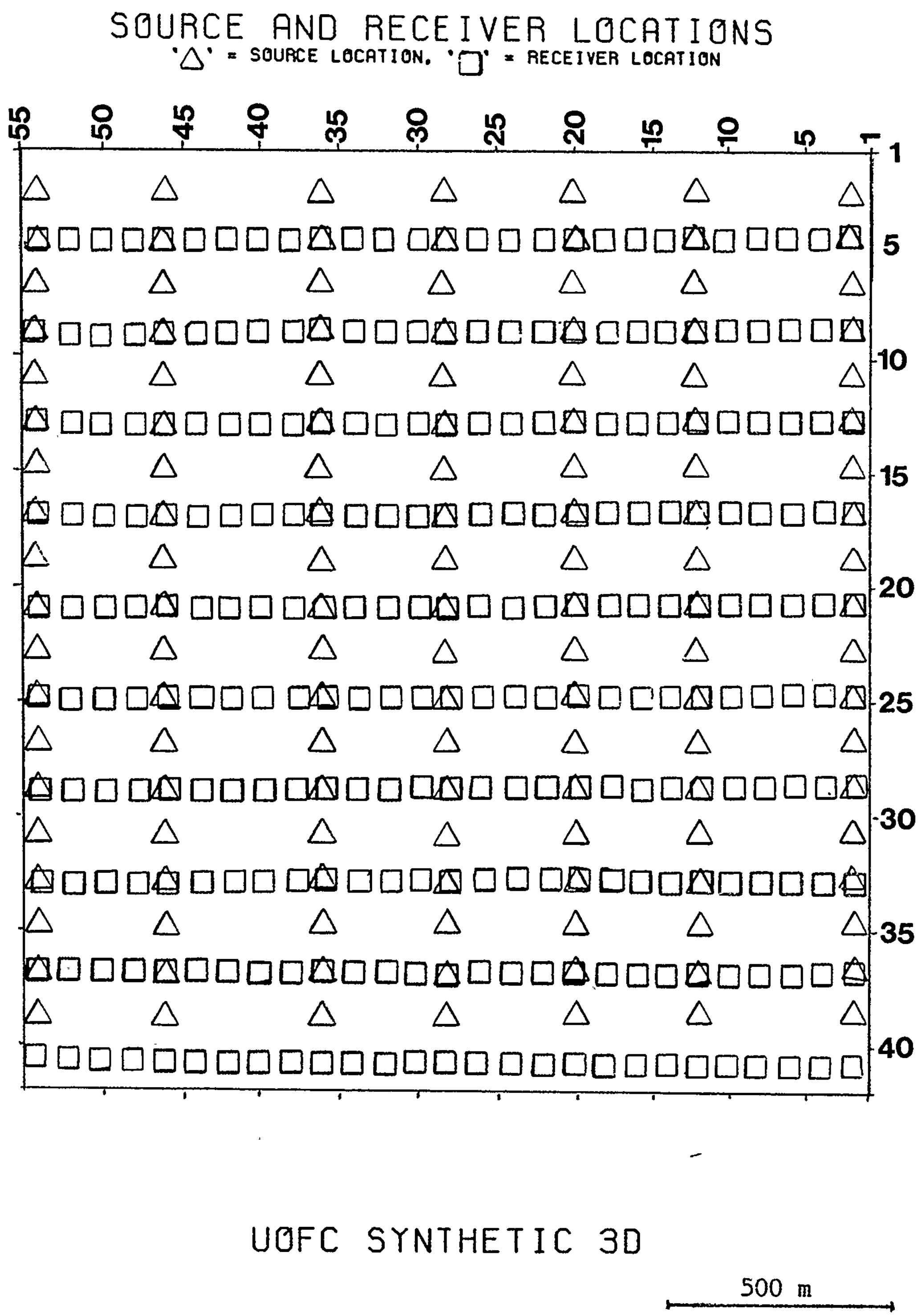

Figure 4.11 Shooting pattern of the modeled 3D survey.

the model with dip greater than θ_{max}, spatially aliased energy will be recorded. The amplitudes of reflections from steeply dipping interfaces will be diminished due to mis-stacking of the non-hyperbolic CMP events. The aliased energy will be migrated incorrectly and will be a source of error in the final result.

The scaled temporal sampling rate of the physical modelling data is 1 sample/millisecond. Data will alias above the frequency where there are less than two samples per wavelength. Therefore, frequencies up to 500 Hz are unaliased. Since the source wavelet is generated with frequencies less than 500 Hz, the temporal data are unaliased.

To satisfy recording aperture requirements, data were recorded about 750 m from the edges of the reef in the inline and crossline directions so that all unaliased energy from the flanks of the reef was captured. The requirements as determined by raytracing using θ_{max} from above, were 680 m in the inline direction and 460 m in the crossline direction.

After data collection for the three-dimensional survey was completed, a zero-offset survey with the same CMP coverage as the 3-D survey was recorded. Three other zero-offset surveys with similar acquisition parameters were also acquired, with the model raised from the modelling table at distances of 1.5 cm, 3.3 cm, and 5.0 cm respectively. These surveys were acquired to examine

Fresnel zone concepts discussed in section 4.5.1 and to investigate the effectiveness of migration in reducing these Fresnel zones. The interpretation and analysis of all physical modelling datasets is contained in section 4.5.

4.4.3.2 Numerical Modelling Data

Using the SIERRA modelling package (see section 2.2), numerically modelled data were generated over the Shekilie reef model. Construction of the numerical model was accomplished within the MIMIC program. The grid size for the model was 2500 x 2500 metres in the x-y plane with 400 divisions on each of the x and y axes. A cross-section of the model in the north-south direction is shown on Figure 4.12. Table 4.5 displays the depths of the formation tops and the P-wave velocities specified for each of the ten layers in this model. Figure 4.13 is a plan view of the top of the Muskeg layer. Muskeg drape (48 m) was simulated by tracing out the time contours from the field data shown in Figure 4.4. The Upper Keg River structure contours from the numerical modelling program are shown on Figure 4.14. Ten metres of relief on the Lower Keg River platform directly under the Keg River reef was included in the numerical model.

A series of zero-offset lines were specified over the

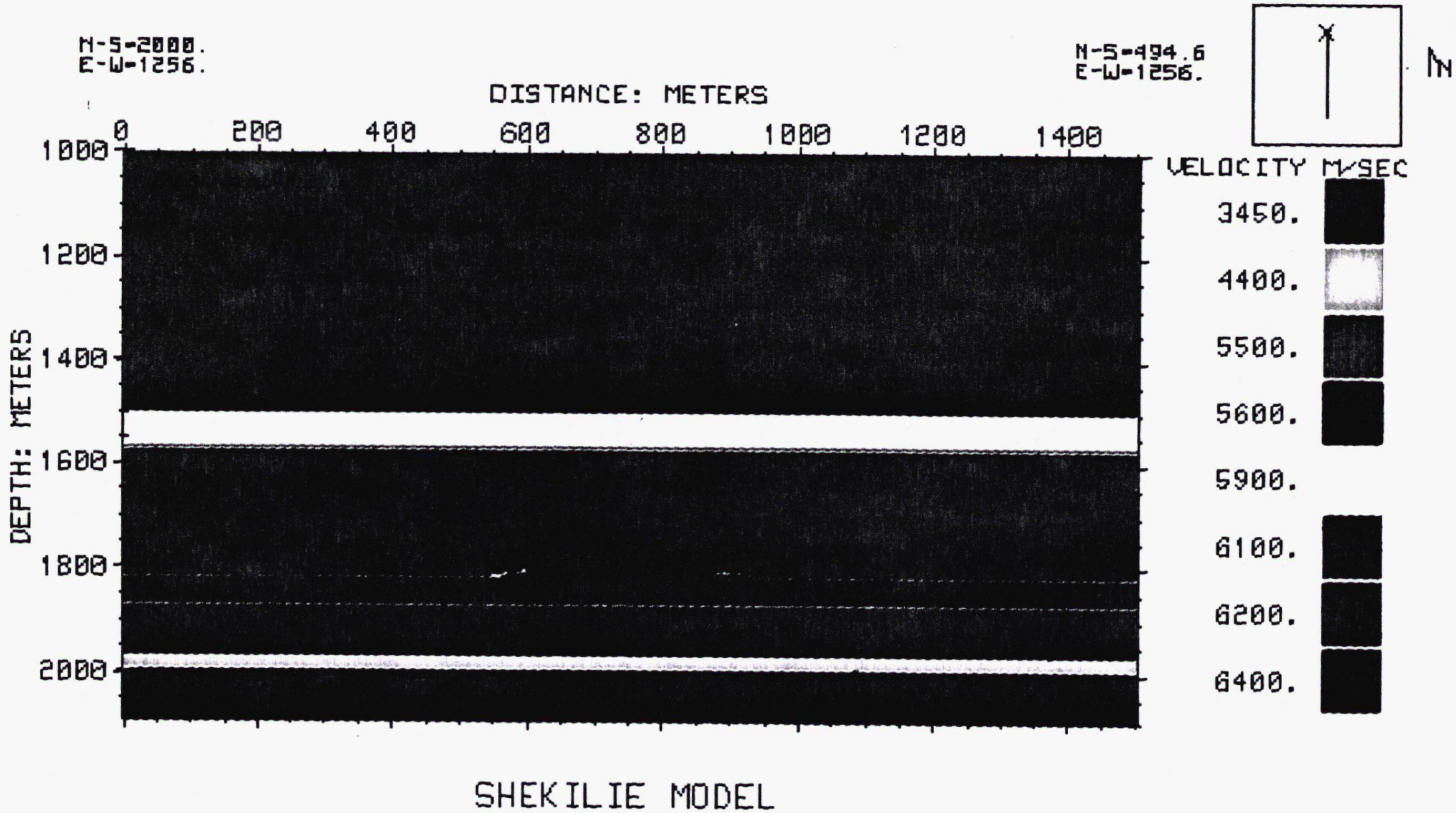

Figure 4.12 North-south cross-section of the Shekilie numerical model.

Formation tops	Depth(m)	P-wave velocity (m/s)
		3450
Slave Point	1500	5900
Watt Mount	1565	5500
Sulphur Point	1575	6200
Muskeg	1640 [1592]*	6400
Upper Keg River	[1688]*	5600
Lower Keg River	1818 [1808]*	6200
Chinchaga	1869	6100
Cold Lake Salt	1969	4400
	1994	6400

*[] indicates the depth values on the crest of the reef.

Note: The density values used in the numerical model were calculated using Gardner's equation (Gardner et al., 1974):

$$\rho = 0.31 \times (V_p)^{.25}$$

where ρ is density in g/cm^3, V_p is velocity in m/s.

Table 4.5 Depth of formation tops and P-wave velocities for the numerical model.

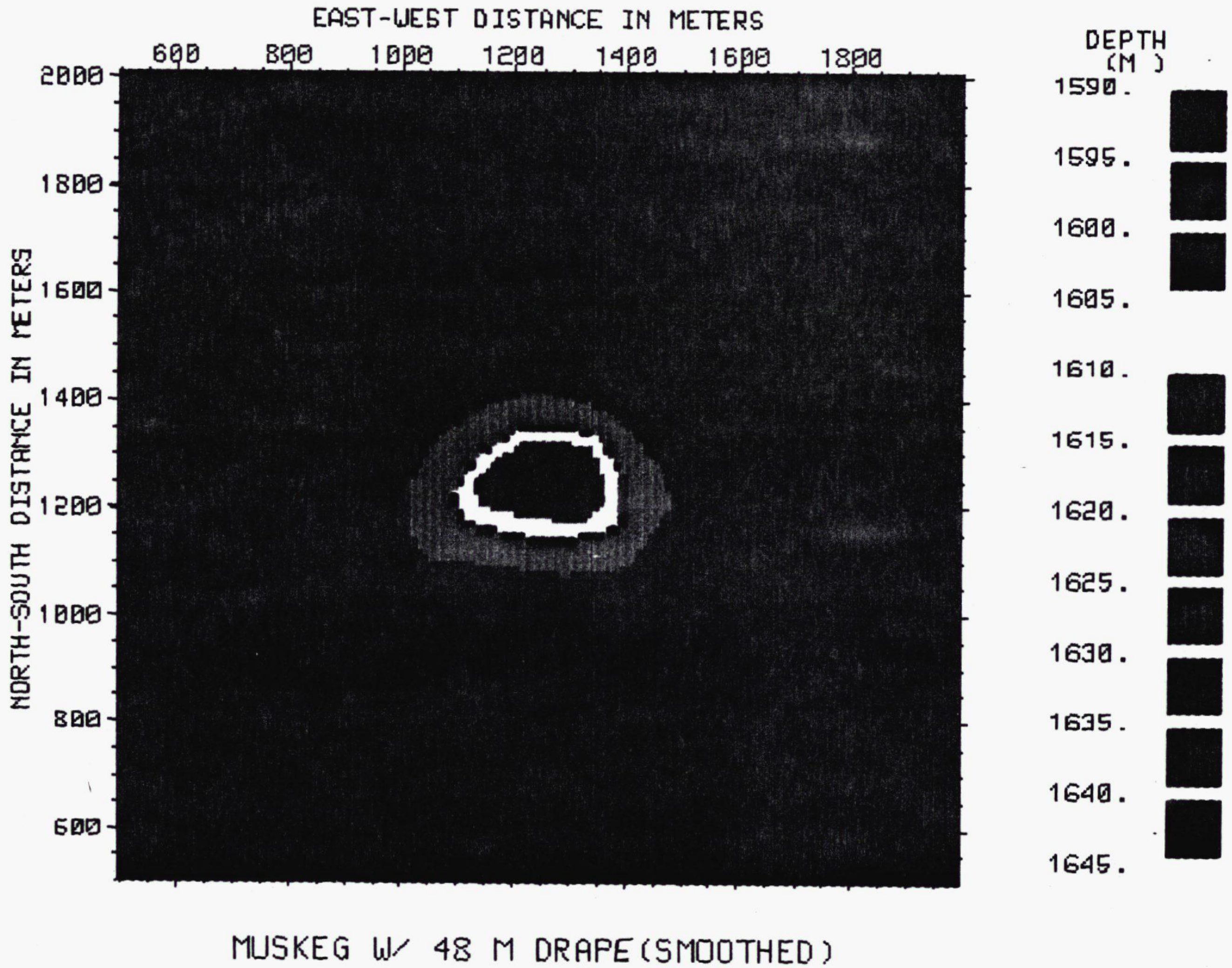

Figure 4.13 Plan view of the Muskeg layer for the numerical model.

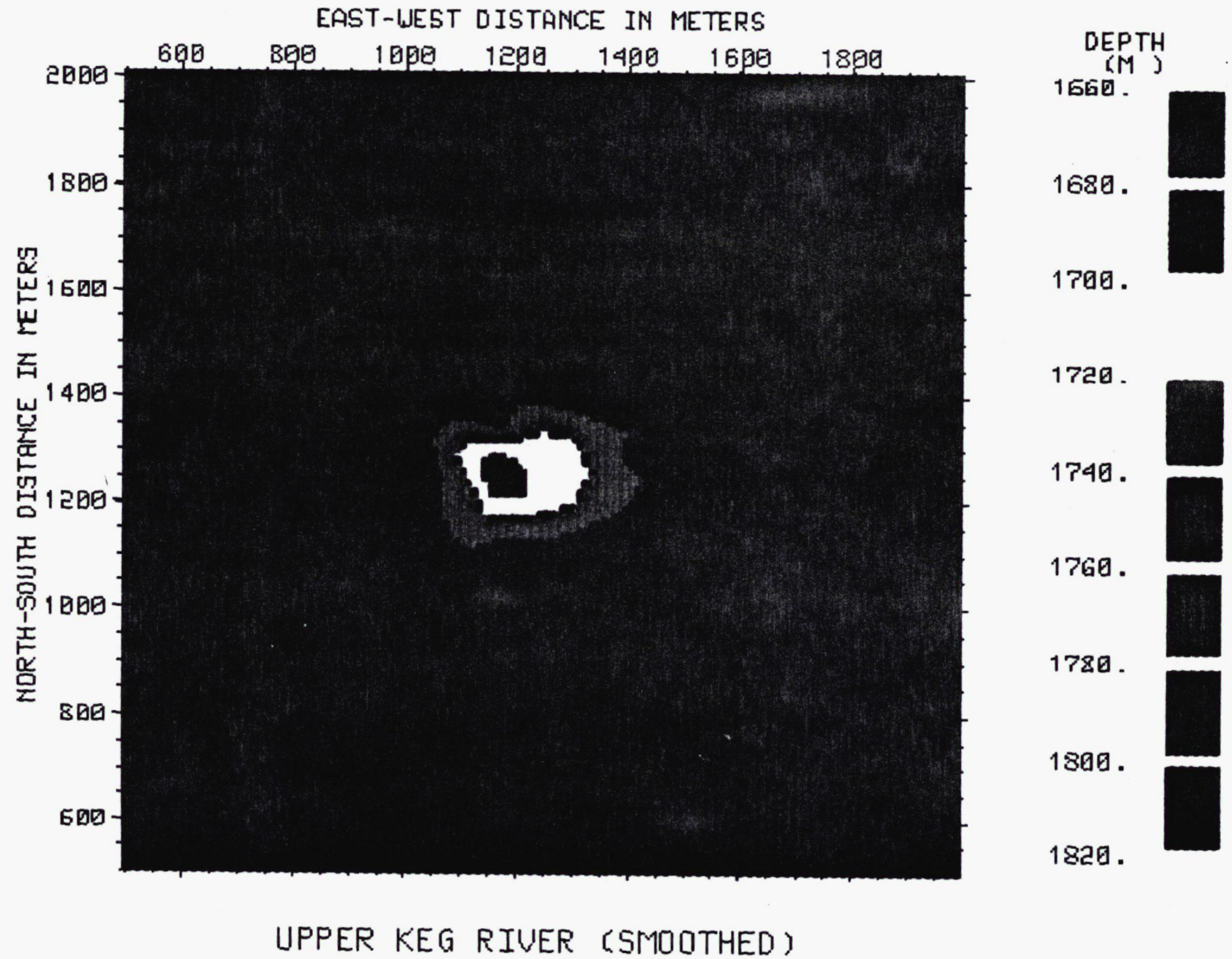

Figure 4.14 Plan view of the Upper Keg River for the numerical model.

model and raytraced using the QUIKRAY module. Nineteen lines with 27 shots on each line were generated (Figure 4.15). The line and shot spacings were 103 m and 69 m respectively. For comparison purposes, line 10a, at the same location as line 10 which lies directly over the reef structure, was raytraced again with 53 shots and a shot spacing of 34.5 m, the same number of shots and shot spacing as in the physical modelling case.

The SLIPR time-domain processing module sorted the spike seismograms generated in the raytracing modules and arranged the data by shot point and group number. A zero-phase Ricker wavelet with the same center frequency (approximately 50 Hz) as in the physical modelling experiment was designed (Figure 4.16). This wavelet was convolved with the spike series produced by the QUIKRAY program. The sample interval used was 1 millisecond. All the data were displayed without noise added.

Figure 4.17 displays the seismic traces from line 10a. The major events such as Slave Point, Sulphur Point, Muskeg, Upper Keg River, Lower Keg River, and Cold Lake salt are indicated. The Slave Point, Sulphur Point/Watt Mountain events are fairly uniform in reflection character and are continuous across the entire section. The Muskeg event is interrupted abruptly at the middle of the section due to interference with the drape feature on the top of the reef. A reflection associated with the Upper Keg River reef is clearly seen. The Lower Keg River and the

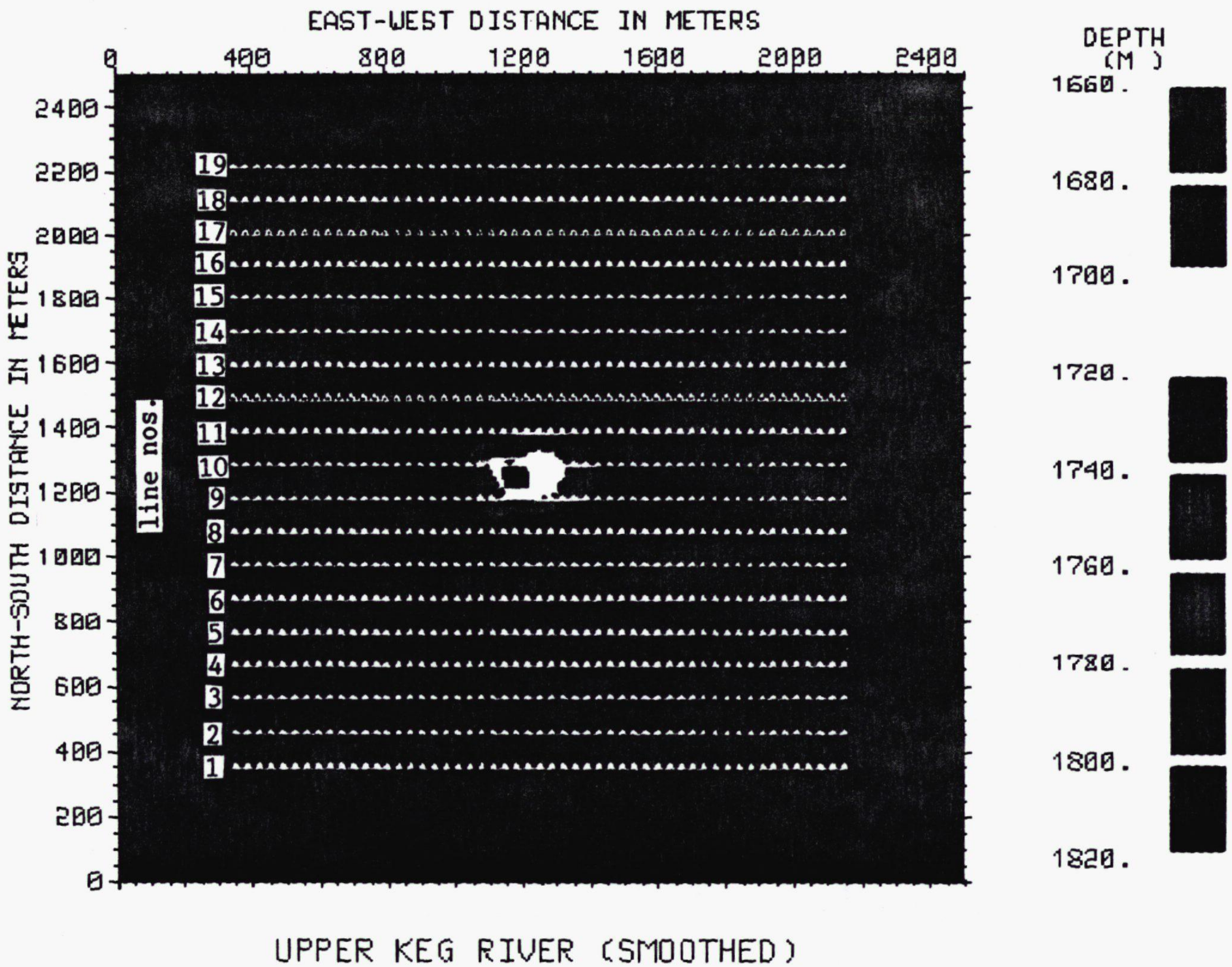

Figure 4.15 Zero-offset lines for the numerical model.

WAVELET DEFINITION

WAVELET TYPE:	ZP RICKER	
CENTER FREQ:	47.60	
WAVELET LENGTH:	64.0	(MSEC)
PHASE SHIFT:	0.0	(DEGREES)
TIME SHIFT:	0.0	(MSEC)
OVERSAMPLING:	1.	(TIMES)

NO ATTENUATION

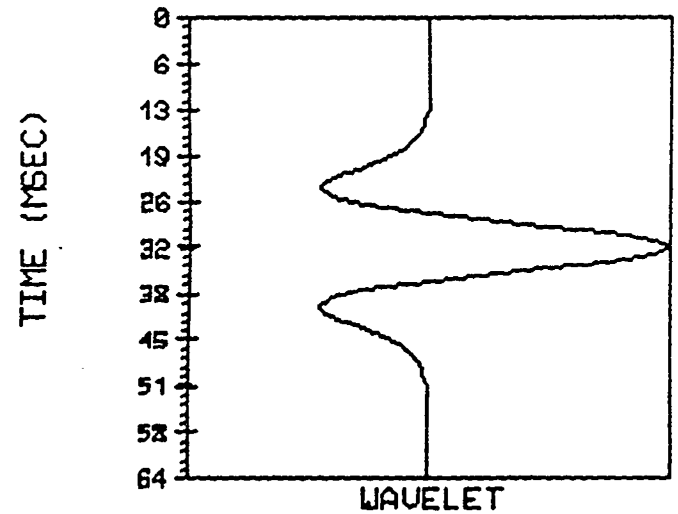

Figure 4.16 Ricker wavelet used to convolve the spike series.

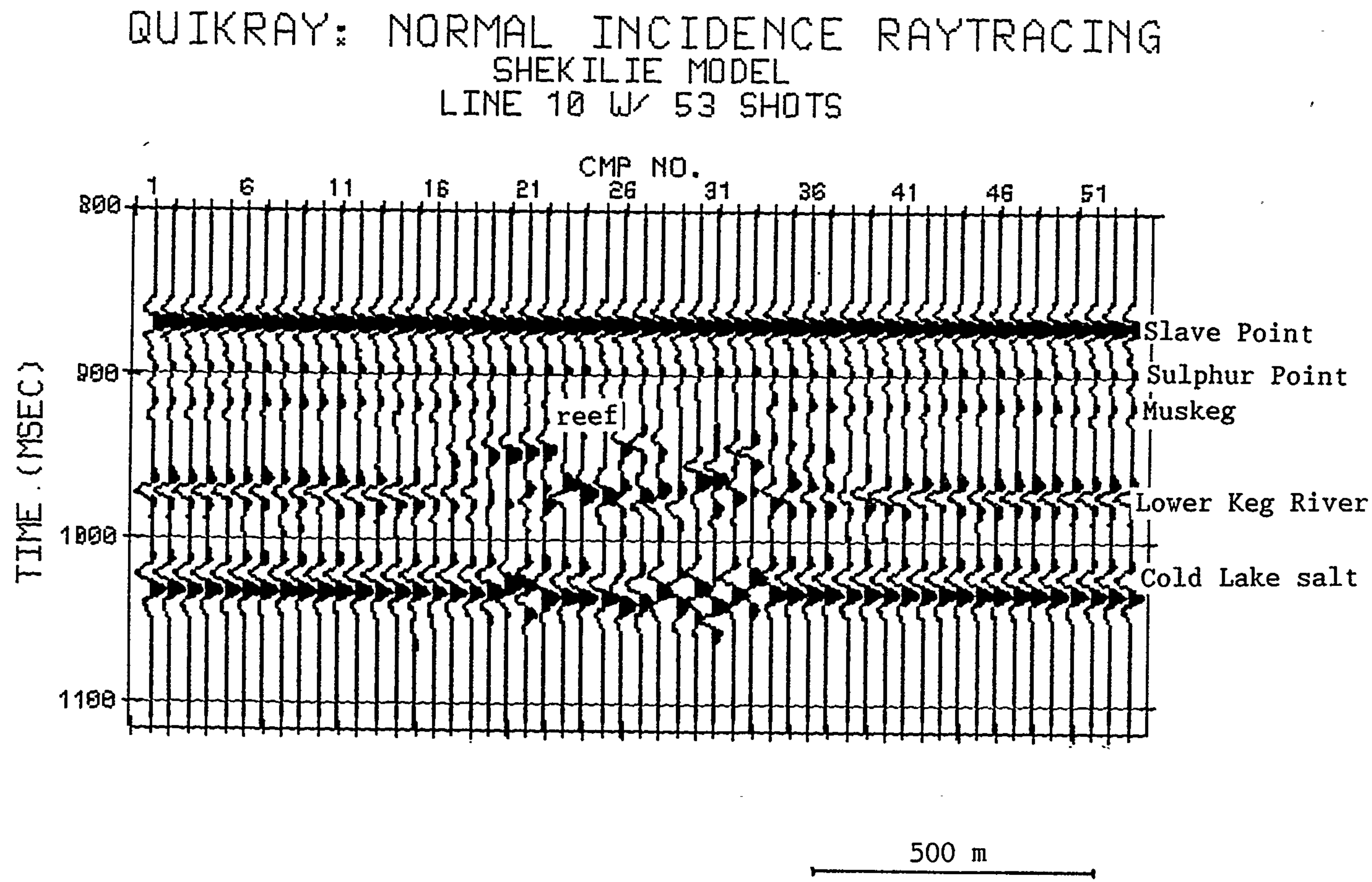

Figure 4.17 Numerically modelled seismic traces for zero-offset line 10a.

Cold Lake salt events are also affected by the presence of the reef. A velocity "push-down" is also seen on the Cold Lake salt event beneath the low-velocity reef.

The numerically modelled line 3, a typical off-reef profile, is shown on Figure 4.18. The major events are again identified. All the events on this section are uniform and continuous across the entire section. Some out-of-plane reflections from the reef mass can be observed just before 1100 ms on traces at both ends of the section.

4.4.4 Data Processing

Processing of the 3-D dataset collected over the Shekilie model was performed by Western Geophysical Company of Canada. Processing of the model data followed the procedures as outlined on Table 4.6.

Preliminary steps were format conversion, trace editing and insertion of geometry information into the trace headers. Data were converted into Western Geophysical format, bad traces were elimimated, traces were renumbered according to shot numbers and coordinates of the shot and receiver locations were put into the trace headers. Demultiplexing was not necessary since the physical modelling data was recorded trace sequentially as opposed to field data which is recorded time sequentially

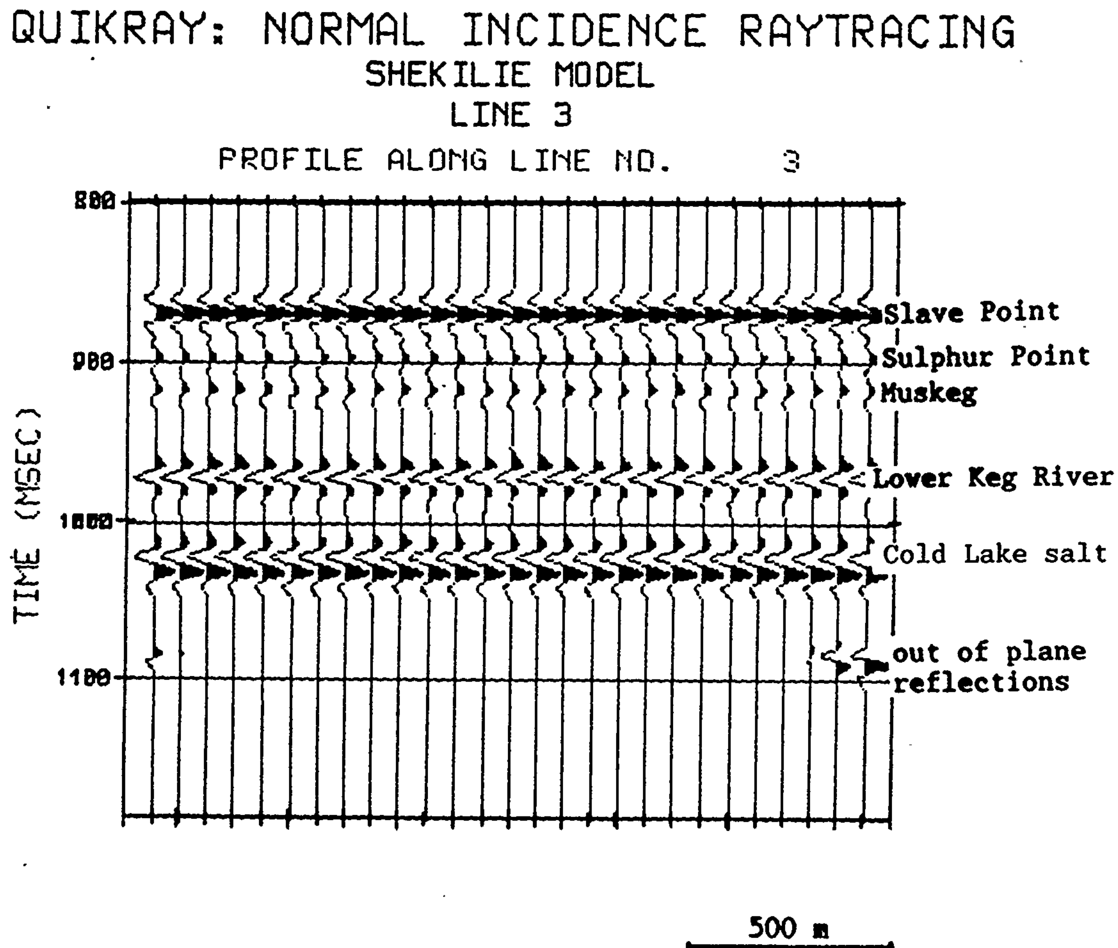

Figure 4.18 Numerically modelled seismic traces for zero-offset line 3.

Processing date:		July, 1988
1.	Format conversion	
	SEG-Y to Western code 4	
2.	Trace editing	
	removal of dummy traces	
	renumber traces with shot number	
3.	Geometry	
	insert shot and receiver location co-ordinates into trace headers	
4.	Cell sort	
	cell size	34.5 x 52 meters
	primary direction east to west	
5.	Automatic statics (first iteration)	
	NMO corrected data	
	type (MISER®)	automatic surface consistent
	gate	900 - 1200 ms
	maximum shift	+ or - 24 ms
6.	3-D velocity analysis	
	type (VELAN®)	semblance
	3-D velocity interpolation	
7.	Normal moveout application	
	mute applied after N.M.O.	
	distance(meters)	time(ms)
	100	0
	800	300
	1100	950
	1150	1040
	1600	1200
8.	Trim statics	
	correlation window	950 - 1200 ms
	model	30 traces
	maximum shift	+ or - 30 ms
9.	Flatten data	
	flattening window follows Slave Point reflector	
	zero crossing aligned at 990 ms	
10.	Bandpass filter	
	frequency	10 - 70 Hz
	slope	24 - 48 DB/oct

Table 4.6 Processing history of the physically modelled Shekilie 3-D survey.

11.	Gain	
	type	reflection strength
	window	300 ms
	stand out factor	2
12.	Finite difference migration	
	2 pass migration (pass one E-W, pass two N-S)	
	percent velocity used	100%

Table 4.6 (Continued) Processing history of the physically modelled Shekilie 3-D survey.

over a patch of receivers.

The traces were then sorted into CMP order. A surface consistant automatic statics program, MISER®, was used to correct small time shifts between the traces introduced by physical contact between the source and receiver transducers for traces with very small offset distances. Velocity analysis with a semblance statistics program, NMO correction, and selected muting were performed on the dataset. A trim statics procedure was applied to the records to further correlate the traces and to remove any time shifts that were not picked up by the MISER® program. The data were then flattened with respect to the Slave Point reflector to remove artificial dip introduced by the recording geometry problem and the slight tilt of the model. A bandpass filter and reflection strength gain were applied prior to the migration procedure. Two-pass finite difference migration was used with the first pass in the east-west direction and the second pass in the north-south direction.

Zero-offset surveys for the completed model placed at various depths were flattened on the Slave Point reflection. These flattened datasets were subsequently migrated using the same two-pass finite difference migration algorithm as in the 3-D model survey.

4.5 Analysis of Physical Modelling Data

4.5.1 Fresnel Zone Effects

Fresnel zone effects were anticipated to be significant in this dataset and the basic Fresnel zone concepts will be reviewed in this section. Many of the anomalous results analyzed on the physical modelling dataset can be interpreted and explained as Fresnel zone phenomena.

In general, raytracing methods are inadequate for describing reflection phenomena when the seismic wavelength is on the same order of magnitude as the size of the target to be resolved. When considering seismic reflection data from a three-dimensional object, the concept of the Fresnel zone is introduced to aid in the understanding of spatial resolution limitations and amplitudes of reflections that are returned to the surface. The Fresnel zone arises because wavefront propagation with a band-limited wavelet requires reflection from an area rather than from a point. In seismology, the first Fresnel zone is used as the measuring device for lateral or horizontal resolution of seismic data.

The concept of the Fresnel zone originates from classical optics. The Huygens-Fresnel principle states that "every unobstructed point of a wavefront, at a given instant in time, serves as a source of spherical secondary wavelets. The amplitude of the optical field at any point beyond is the superposition of all of these wavelets." (Hecht and Zajac, 1979). For the seismic reflection case, each point on the reflector is considered, where it has been energized by the passing wavefront, to be a source of spherical secondary wavelets. Figure 4.19 shows a spherical wavefront with a band-limited wavelet of dominant wavelength, λ, propagating from a point source S, arriving at a plane reflector at a depth, z. Energy from points on the reflector that are energized before the wavefront has propagated a distance $\lambda/4$ will arrive back at the surface within $\lambda/2$ and the majority of this energy will interfere constructively. The amplitude of a reflection recorded at the surface results from the superposition of secondary wavelets from this area, which is called the first Fresnel zone (Sheriff, 1977). For coincident source and receiver, the radius of the first Fresnel zone, r_1, (Figure 4.20), is obtained from:

$$z^2 + r_1^2 = (z + \lambda/4)^2 \qquad (4.6)$$

$$r_1 = (\lambda z/2 + \lambda^2/16)^{1/2} \qquad (4.7)$$

Generally, $z >> \lambda$; hence

$$r_1 = (\lambda z/2)^{1/2} \qquad (4.8)$$

$$= (vz/2f)^{1/2}$$

where $\lambda = v/f$, z is the depth, v the average velocity, and f the frequency.

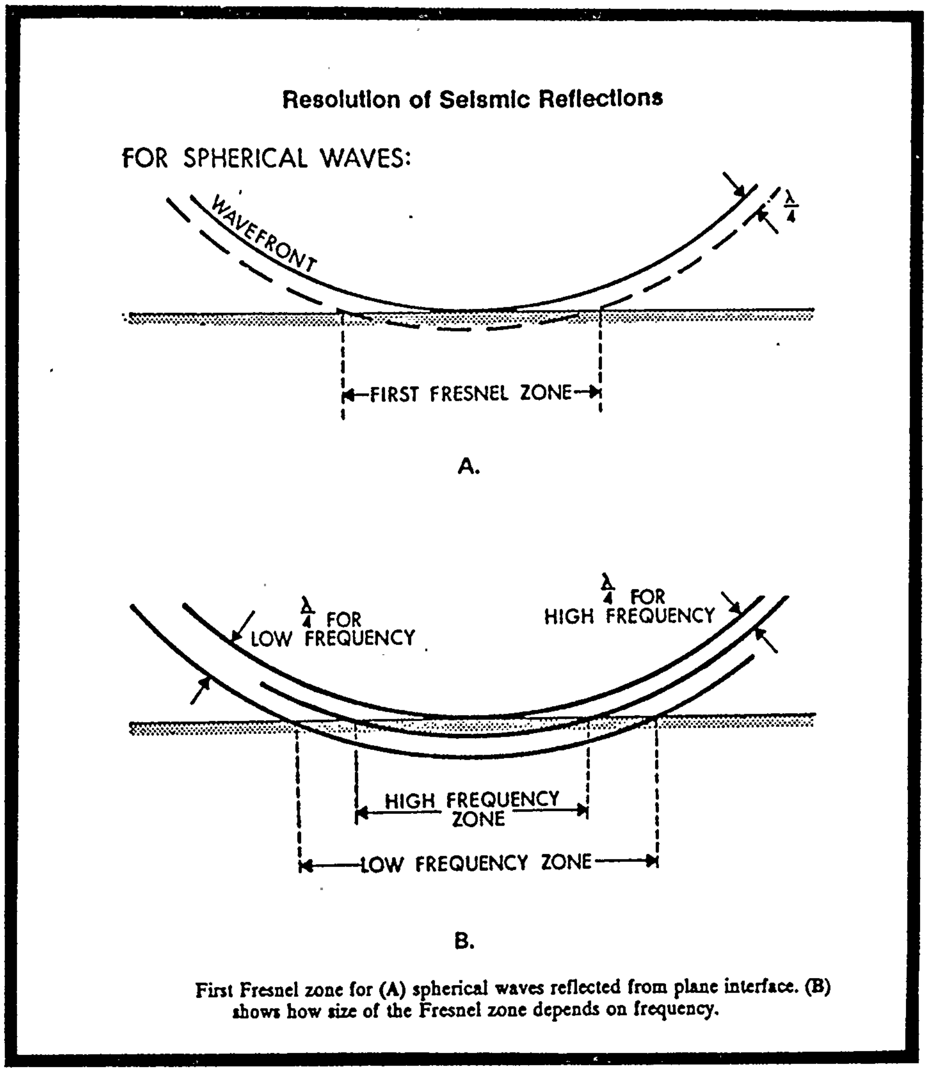

Figure 4.19 First Fresnel zone for a spherical wave reflected from a plane interface (After Sheriff, 1977).

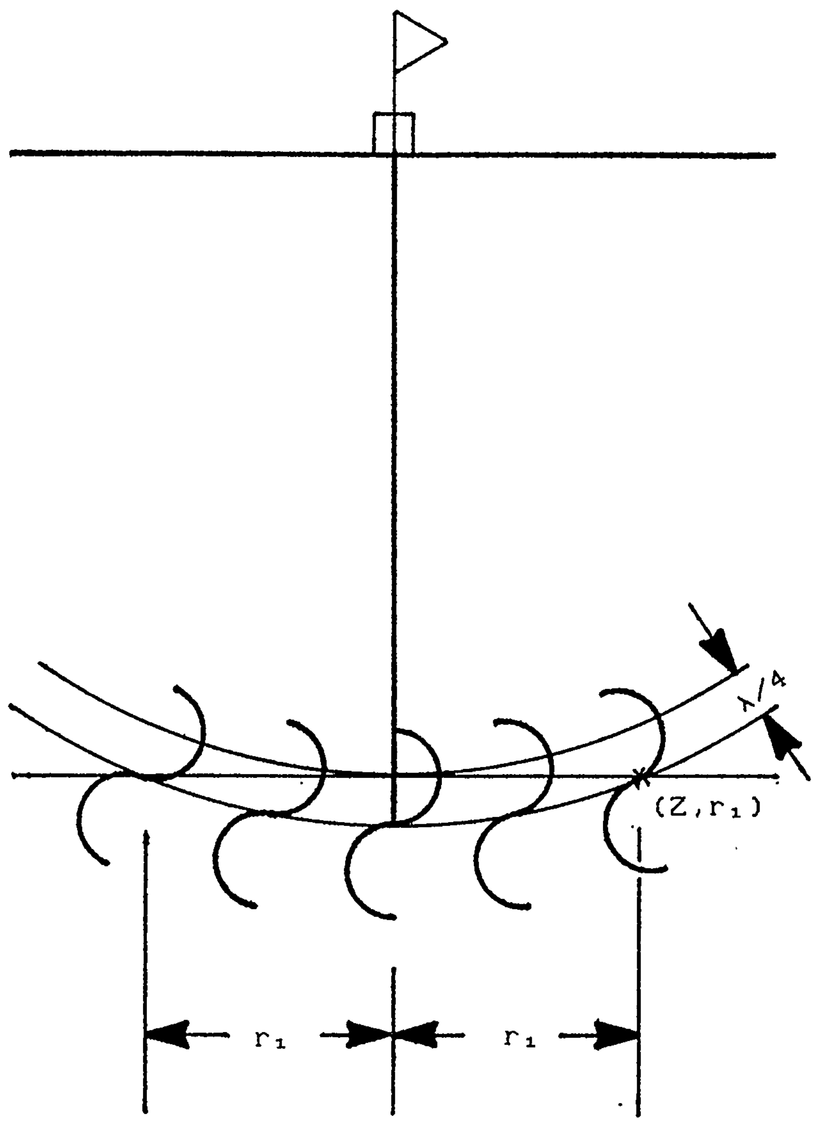

For an interface at depth, Z

$$z^2 + r_1^2 = (z + \lambda/4)^2$$

$$r_1 = (\lambda z/2 + \lambda^2/16)^{1/2}$$

Figure 4.20 Radius of the first Fresnel zone.

The Fresnel zone analysis can be extended into higher order for successive zones of constructive and destructive interference. However, the major contribution to the reflected signal comes from the first Fresnel zone (Sheriff and Geldart, 1982). For a nonzero-offset source and receiver configuration, the Fresnel zone is described by an ellipse (Berkhout, 1984). Hilterman (1982) has studied the seismic responses resulting from various sizes and shapes of targets approaching the limits of the Fresnel zone.

The radius of the Fresnel zone is dependent on the depth to the reflector, the velocity to the reflector, and the frequency content of seismic energy. The radius of the Fresnel zone can be decreased, hence lateral resolution can be increased, by increasing the dominant frequency of the seismic energy or by reducing the depth to the reflector. Reduction of reflector depth can be effectively accomplished through the downward continuation process involved in seismic migration (Sheriff, 1977; Berkhout, 1984). However, the improvement in lateral resolution due to migration is difficult to quantify since the accuracy of migration is affected by the presence of aliased energy, by the presence of noise, and by inexactness of chosen migration velocities.

4.5.2 Zero-offset 3-D Data

Zero-offset surveys were collected with the model placed at various depths to examine Fresnel zone phenomena and to study the effectiveness of migration for increasing horizontal resolution. These data demonstrate a variety of interesting reflection events which are discussed in the following sections.

A zero-offset structure section which does not cross the reef crest is displayed (Figure 4.21). Constant time, coherent events are present before the Slave Point reflection. These events are not related to the reflected signal and are therefore associated with direct arrival trailing energy or energy associated with the triggering of the source pulse. This energy will contaminate the recorded, reflected signal and is a source of error in these data.

Zero-offset, flattened sections over the reef crest are displayed, with events as indicated, for Slave Point depths of 1090 m (Figure 4.22), 1260 m (Figure 4.23), 1500 m (Figure 4.24), and 1680 m (Figure 4.25). The peak from the top of Muskeg drape occurs at the centers of the sections about 30 ms below the Slave Point event. The regional Muskeg reflection is as shown. Although the Muskeg reflections are not spatially aliased, $\theta_{max} \sim 17°$ (see Section 4.4.2) the flanks of the drape feature cannot be correlated even after migration (Figure 4.26). Also,

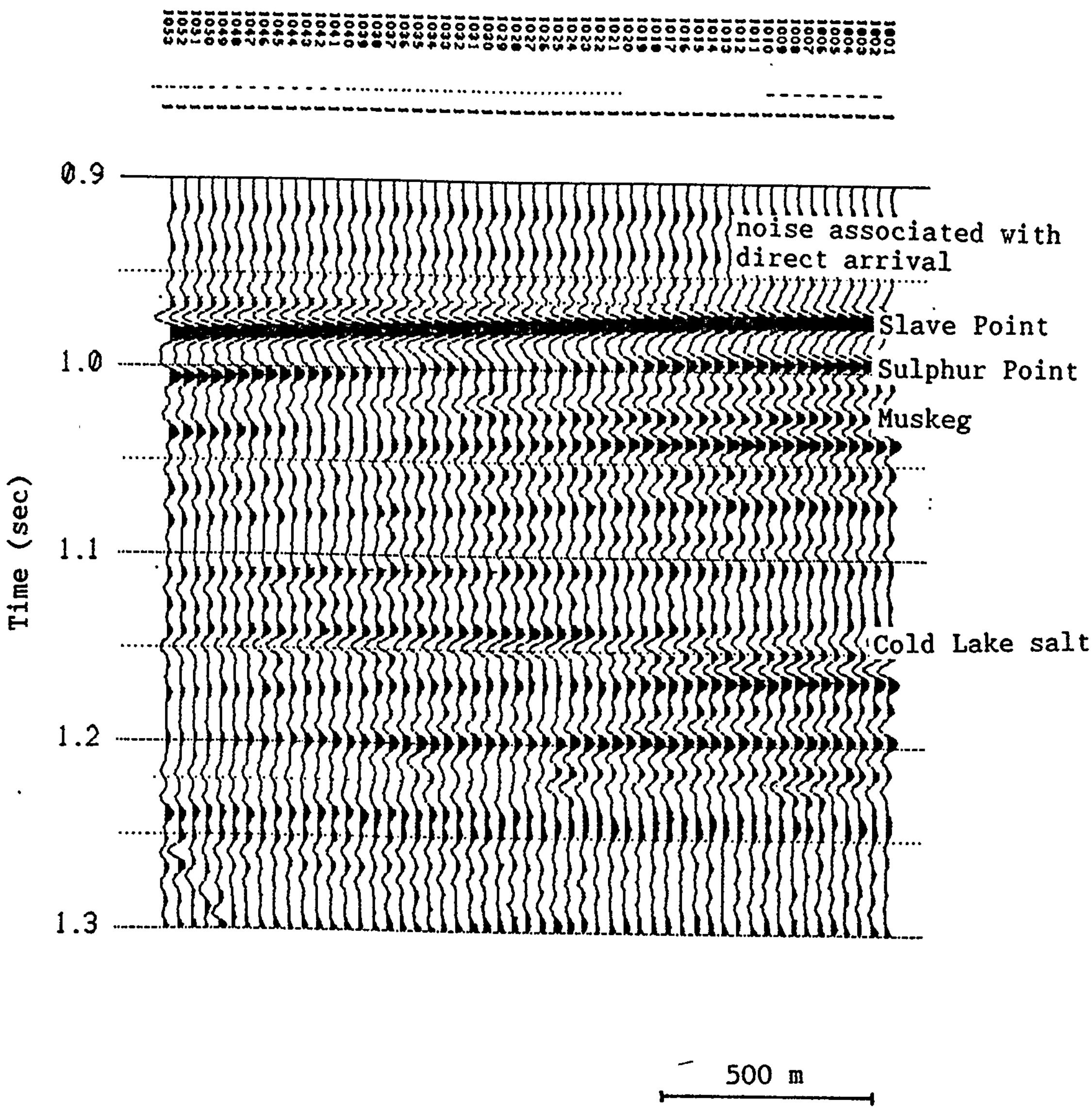

Figure 4.21 Off-reef zero-offset structure section.

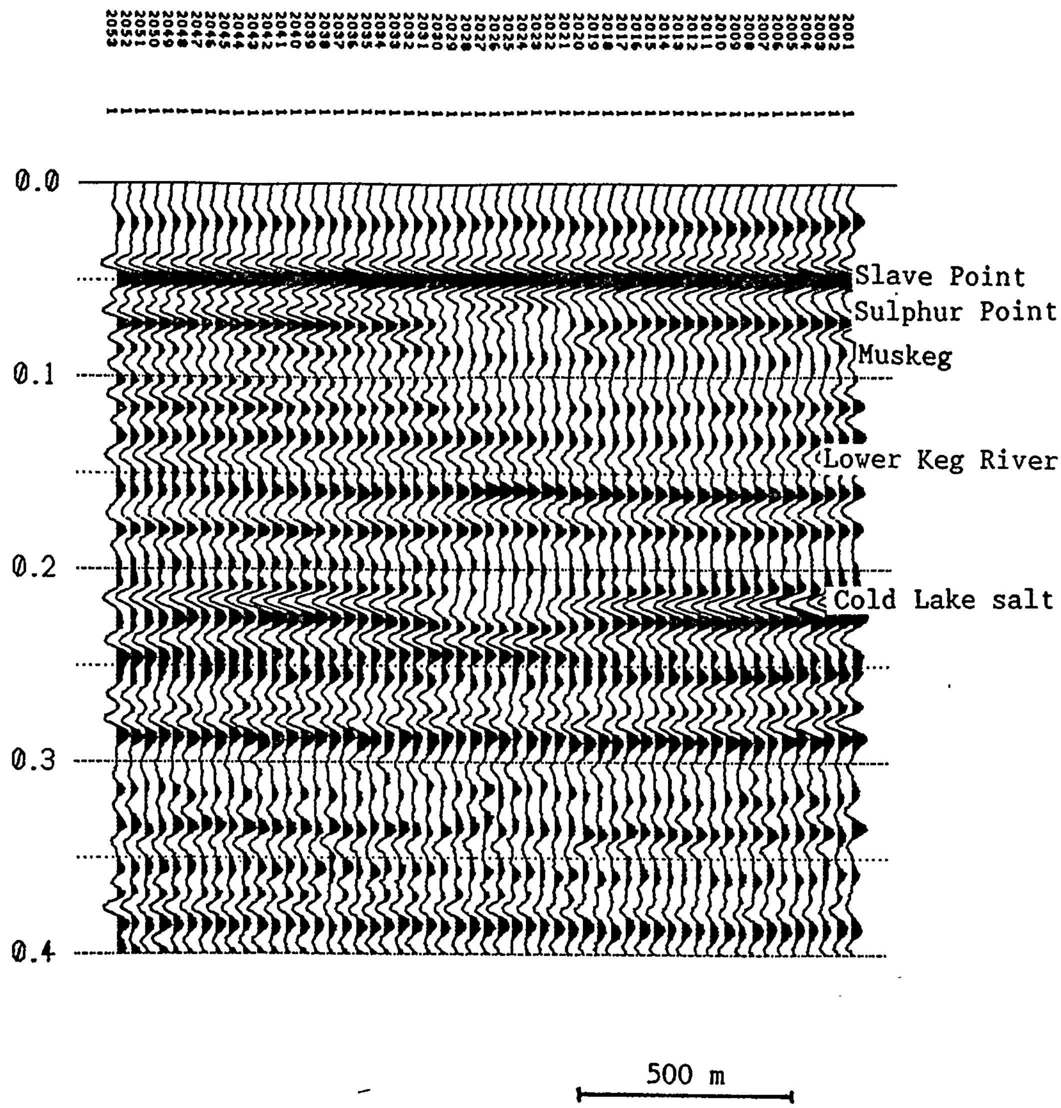

Figure 4.22 Zero-offset line over reef crest for Slave Point depth at 1090 m.

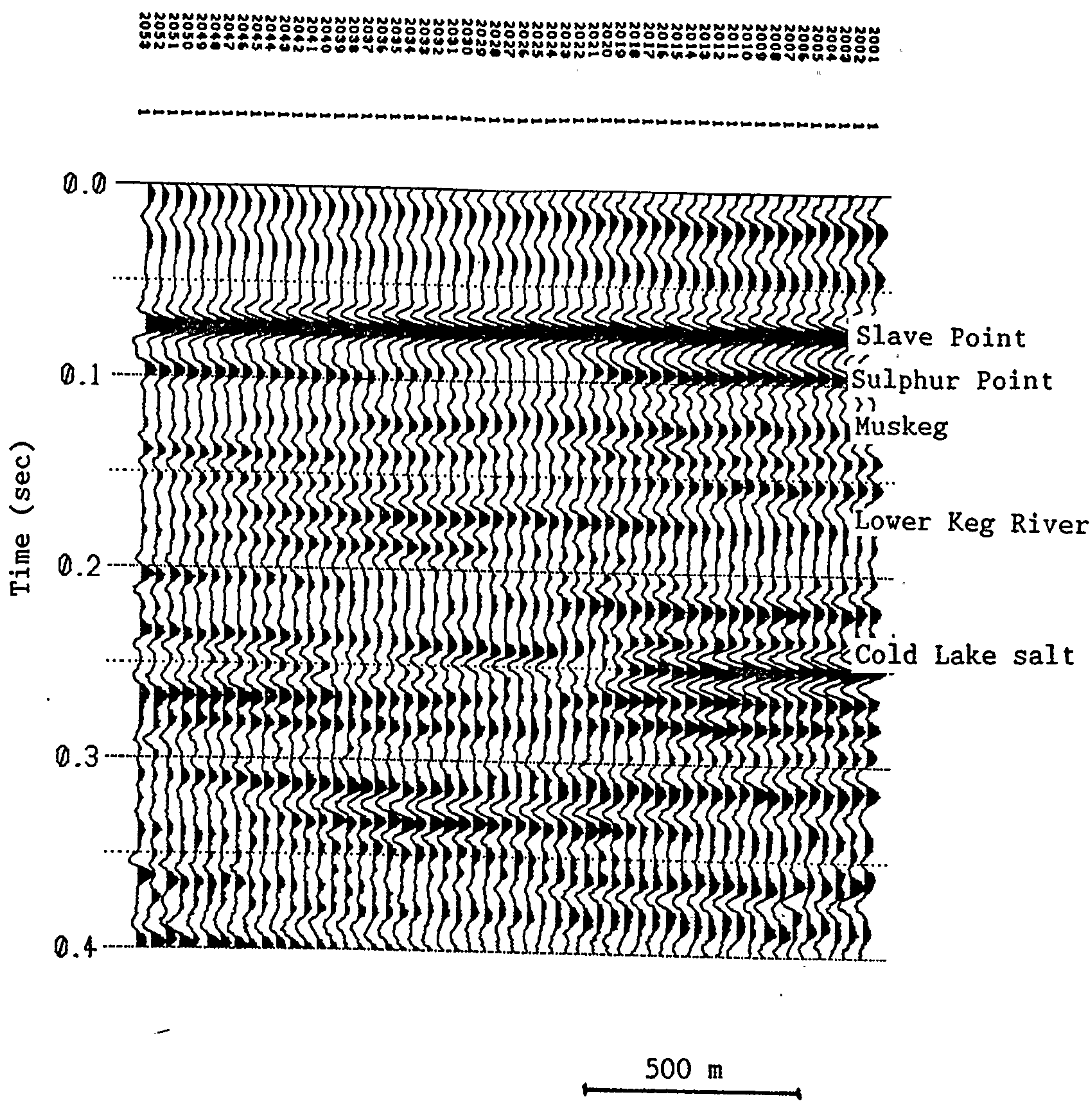

Figure 4.23 Zero-offset line over reef crest for Slave Point depth at 1260 m.

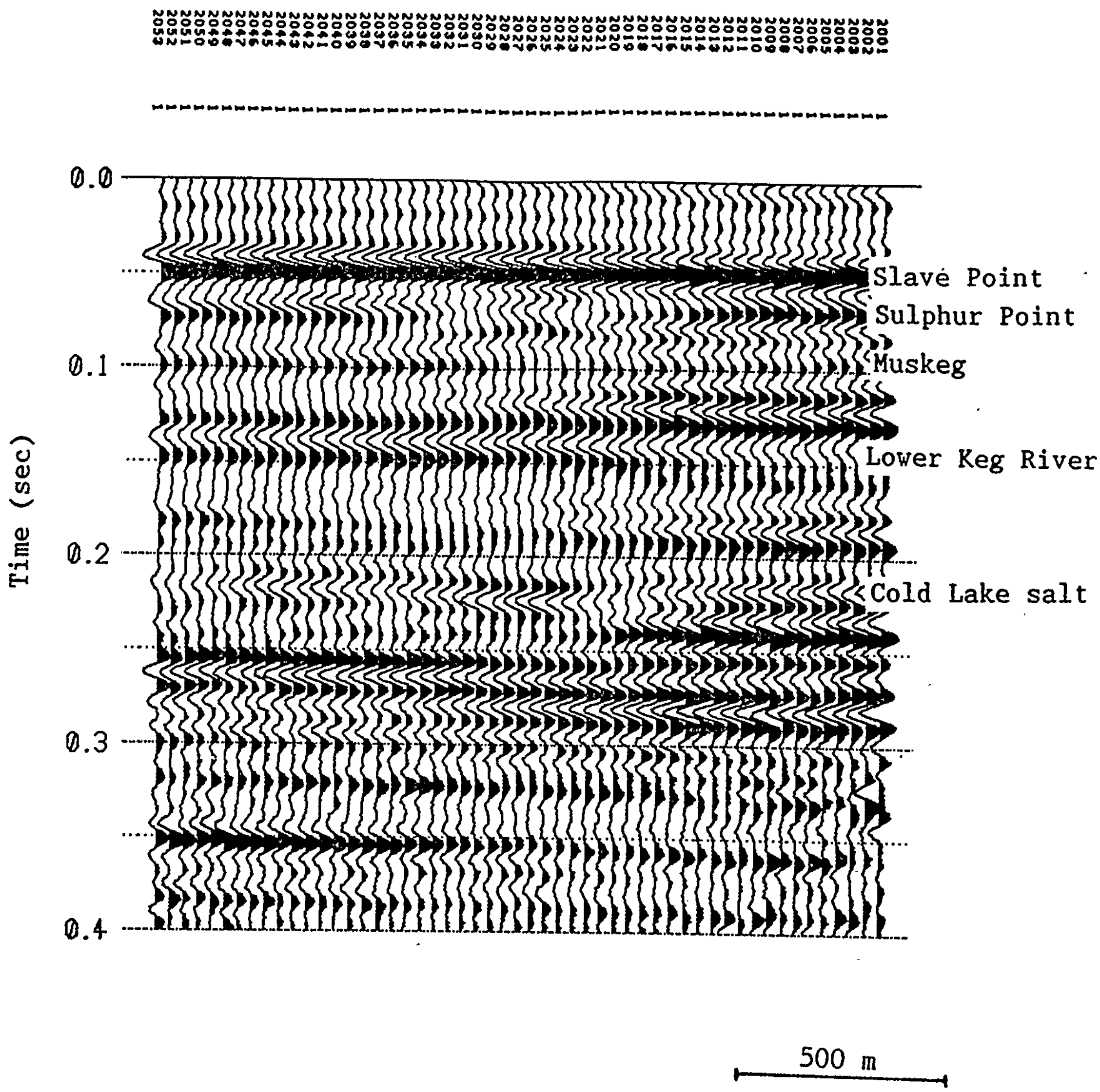

Figure 4.24 Zero-offset line over reef crest for Slave Point depth at 1500 m.

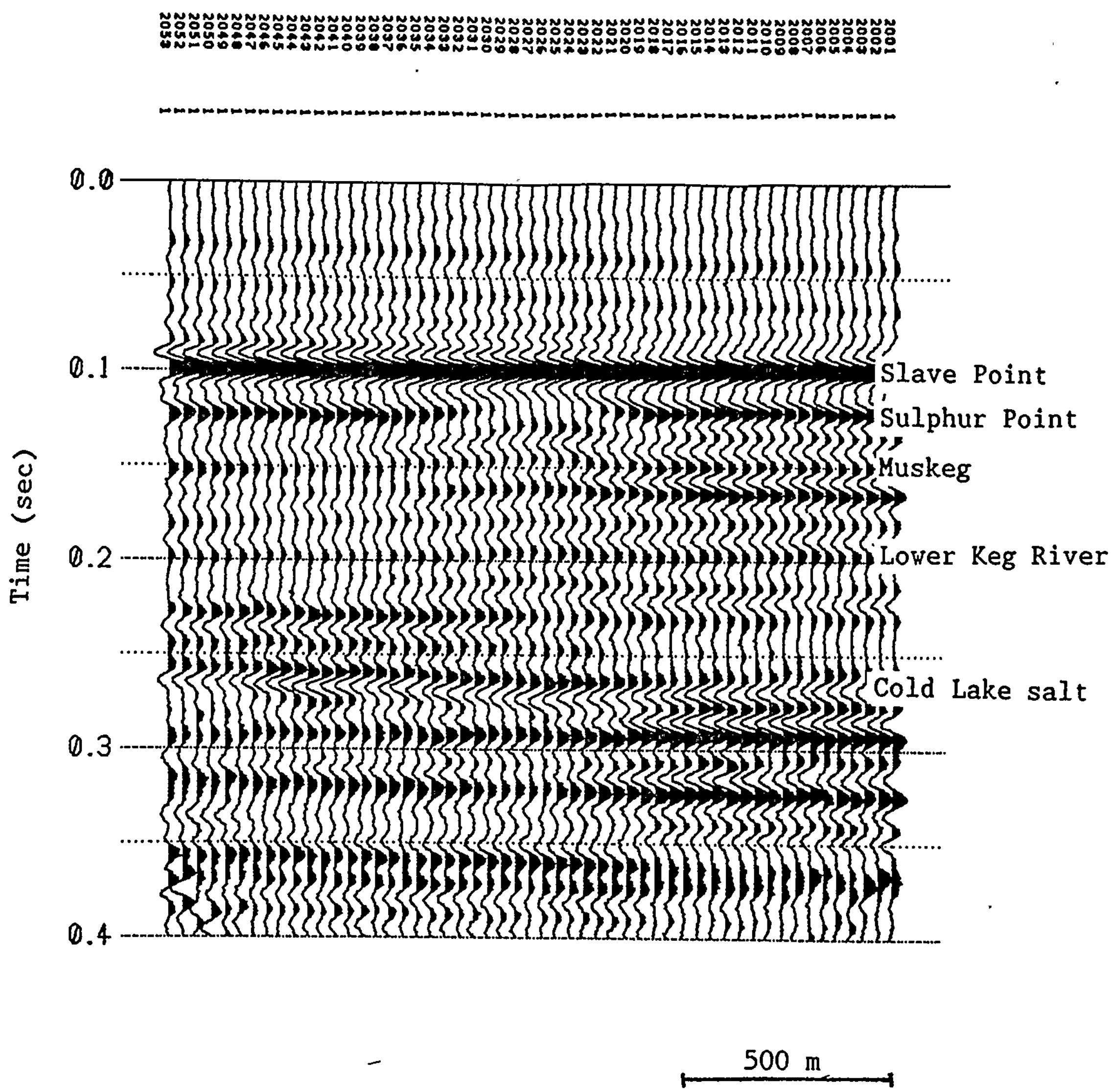

Figure 4.25 Zero-offset line over reef crest for Slave Point depth at 1680 m.

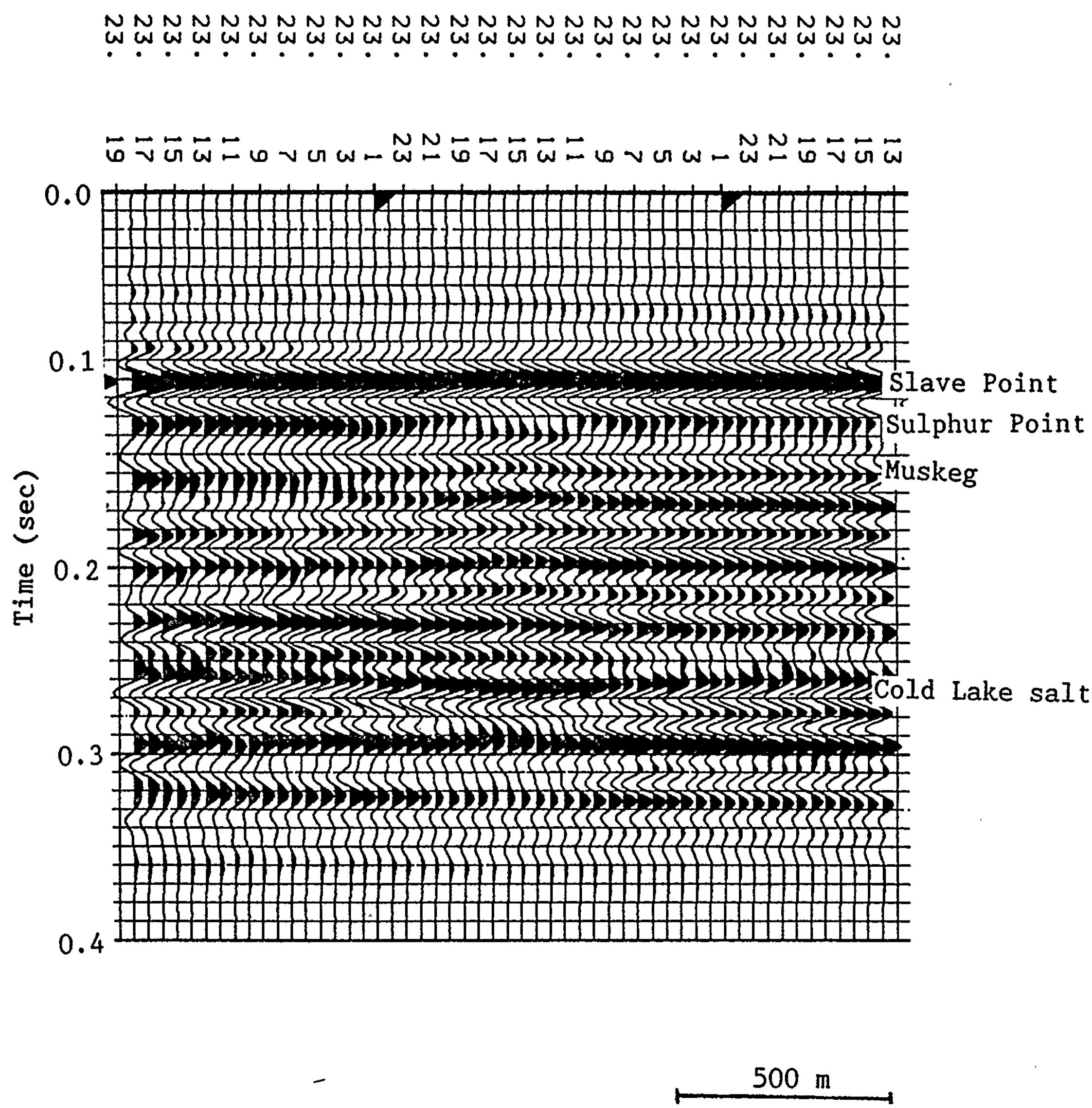

Figure 4.26 Migrated zero-offset line over reef crest for Slave Point depth at 1680 m.

the regional Muskeg reflection, which should not be present under the drape feature, is continuous and shows anticlinal character under the drape (see Figures 4.23, 4.24, 4.25). The anticlinal feature is not a velocity anomaly due to Muskeg drape since the difference in traveltime through 90 m of Sulphur Point versus 90 m of Muskeg is less than 1 ms. Both of these anomalous occurrences are attributed to the effects of the Fresnel zone and tuning of wave propagation.

Unfortunately, since the velocities are not exactly specified at each spatial location, time migration cannot compensate for this Fresnel zone effect (Figure 4.26). Depth migration, in which the velocities and geometry of the drape feature are specified, is required to resolve the Muskeg structure.

An isolated Keg River reef event is not apparent on any of these sections. However, a velocity "push-down" anomaly under the low-velocity Keg River reef is visible on the Cold Lake salt event on all of the sections. The amount of "push-down", approximately 7 ms, is equal to the difference between travel time through 120 m of Upper Keg River versus 120 m of Muskeg. Examination of the Cold Lake salt event amplitudes reveals interesting focusing effects due to the convex/planar lens shape of the Keg River reef. As the depth of the model increases, the strongly focused energy was observed to appear successively earlier in the sections. This result matches the basic lens theory which states that image distance and object distance are inversely related (Hecht and Zajac, 1979).

Time slices of the zero-offset surveys were generated and examined before and after the two-pass migration procedure. To ensure comparable time slices, the datasets were flattened on the Slave Point reflection and time slices were selected with reference to this reflection. Figure 4.27 shows time slices taken at 30 ms below the Slave Point reflection for scaled Slave Point depths of 1090 m, 1260 m, and 1680 m. Referring to equation (4.8) in Section 4.4.2, the radii of the first Fresnel zones, approximately 90 m below the Slave Point, for each of the models are: 1090 m model, r_1 = 207 m; 1260m model, r_1 = 221 m; and 1680 m model, r_1 = 252 m. The discrepancies in the overall appearance of the time slices between different datasets is a result of the model having slight variation in tilt at the various depths. Before migration, the area of the reflection from the top of Muskeg drape increases in relation to the size of the Fresnel zone. After migration, the area of reflection is smaller and approximately equal for all three surveys. The reduction in the area of reflection after migration indicates an improvement in horizontal resolution.

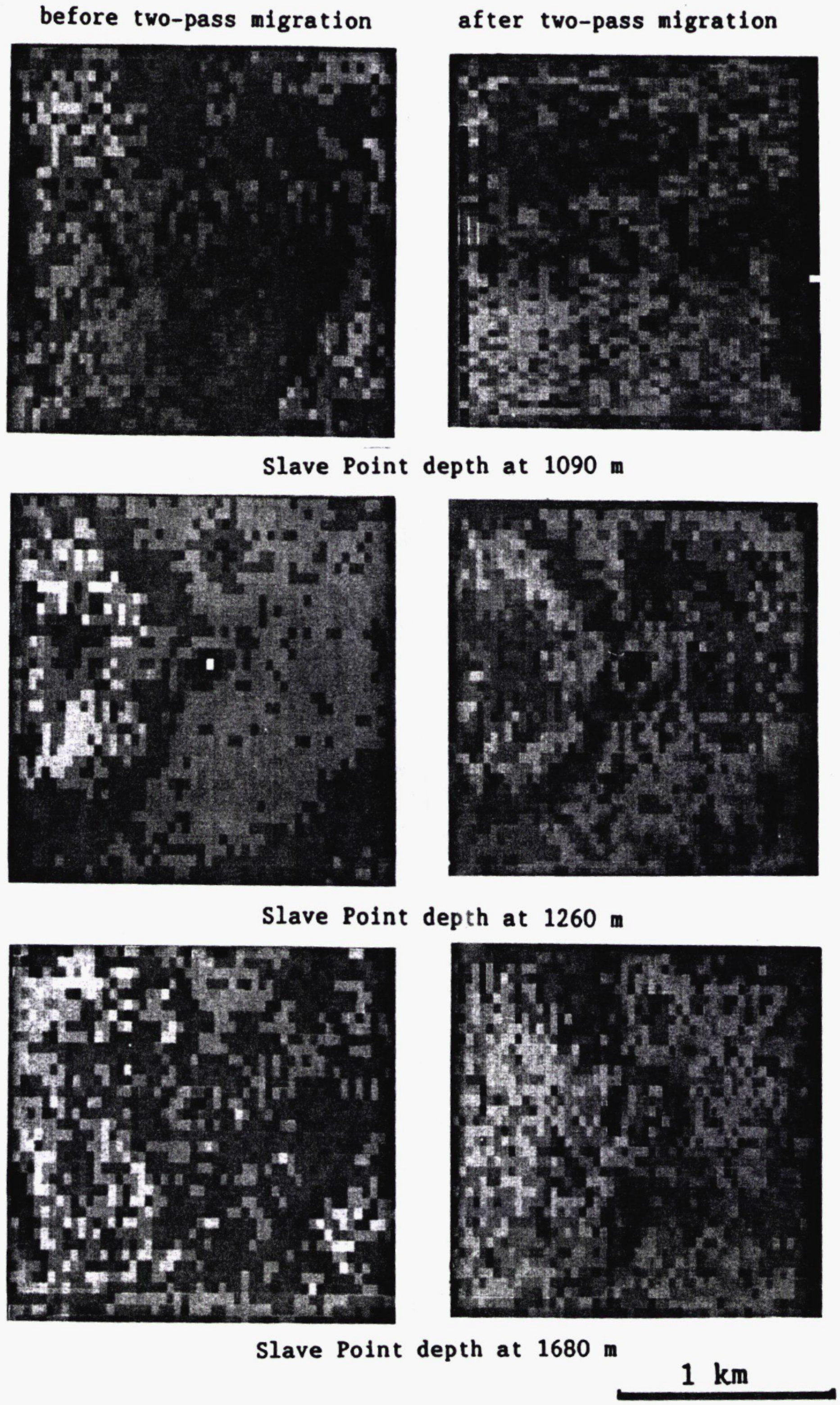

All time slices are taken 30 ms below the Slave Point reflector.

Figure 4.27 Time slices before and after two-pass migration.

4.5.3 Multi-offset 3-D Data

A multi-offset 3-D survey with acquisition parameters similar to the field data, was acquired over the physical model. A flattened, stacked section and the corresponding migrated section over the reef crest from the modelled 3-D survey were analyzed. The flattened stacked section and migrated section are shown on Figures 4.28 and 4.29 respectively.

The multi-offset, stacked data (Figure 4.28) are different in character from the corresponding zero-offset data (Figure 4.25). In general, the frequency content of the stacked multi-offset section appears lower, presumably due to NMO stretch and mis-stacking. However, the laterally coherent events on the stacked multi-offset data are all directly correlatable with reflecting interfaces in the model, whereas on the zero-offset data, many events are present where reflecting interfaces are not expected. These unexpected events on the zero-offset data have been identified as a combination of multiple reflections and direct arrival energy, both of which are attenuated in Figure 4.29 by the normal moveout correction and stacking procedures. The reflection from the top of the Muskeg drape feature appears to be degraded on the stacked data and there are variations on the stacked data in lateral continuity of the Sulphur Point and Muskeg events that are not apparent on the zero-offset data. These discrepancies

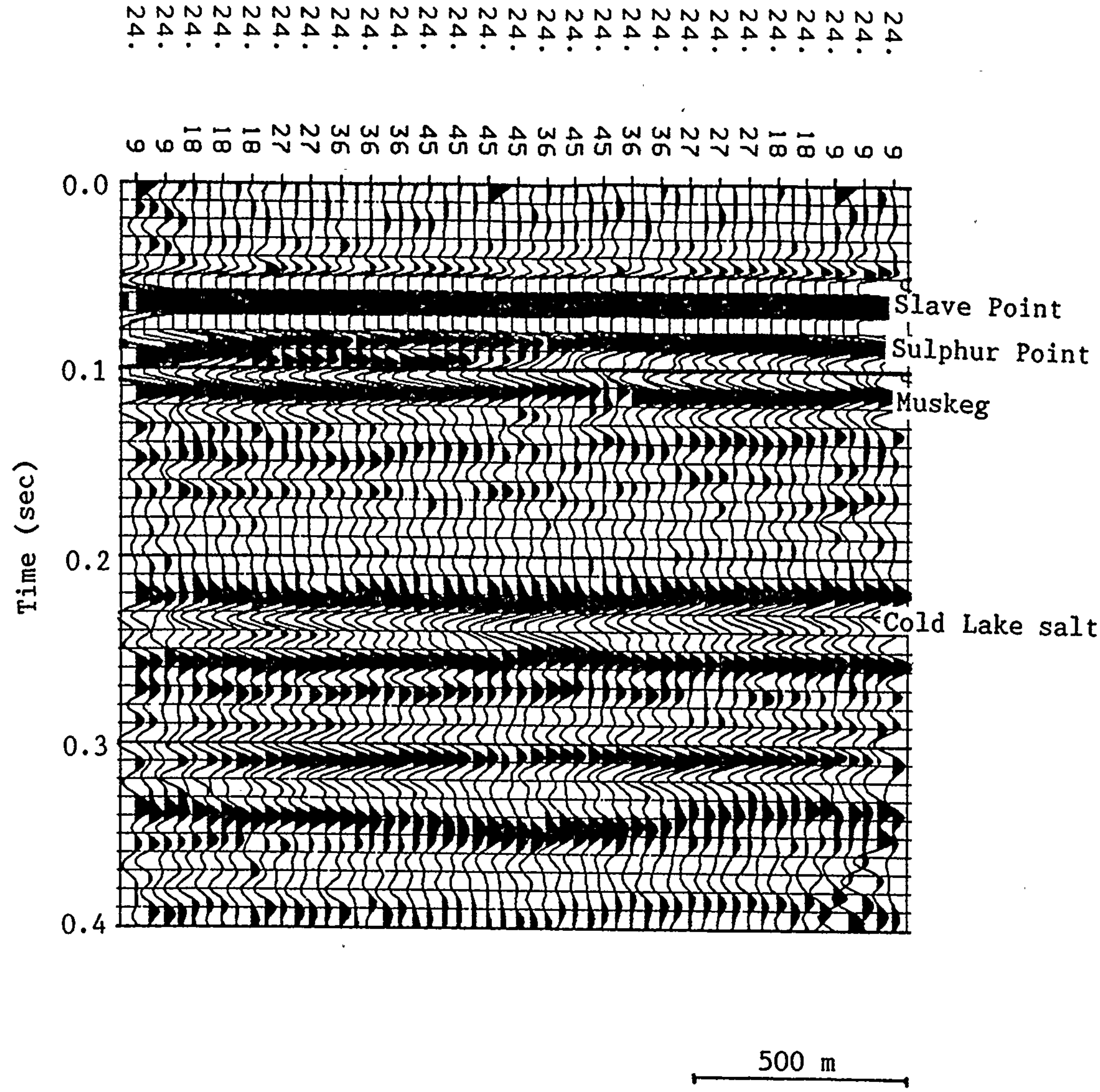

Figure 4.28 Physically modelled multi-offset stacked section.

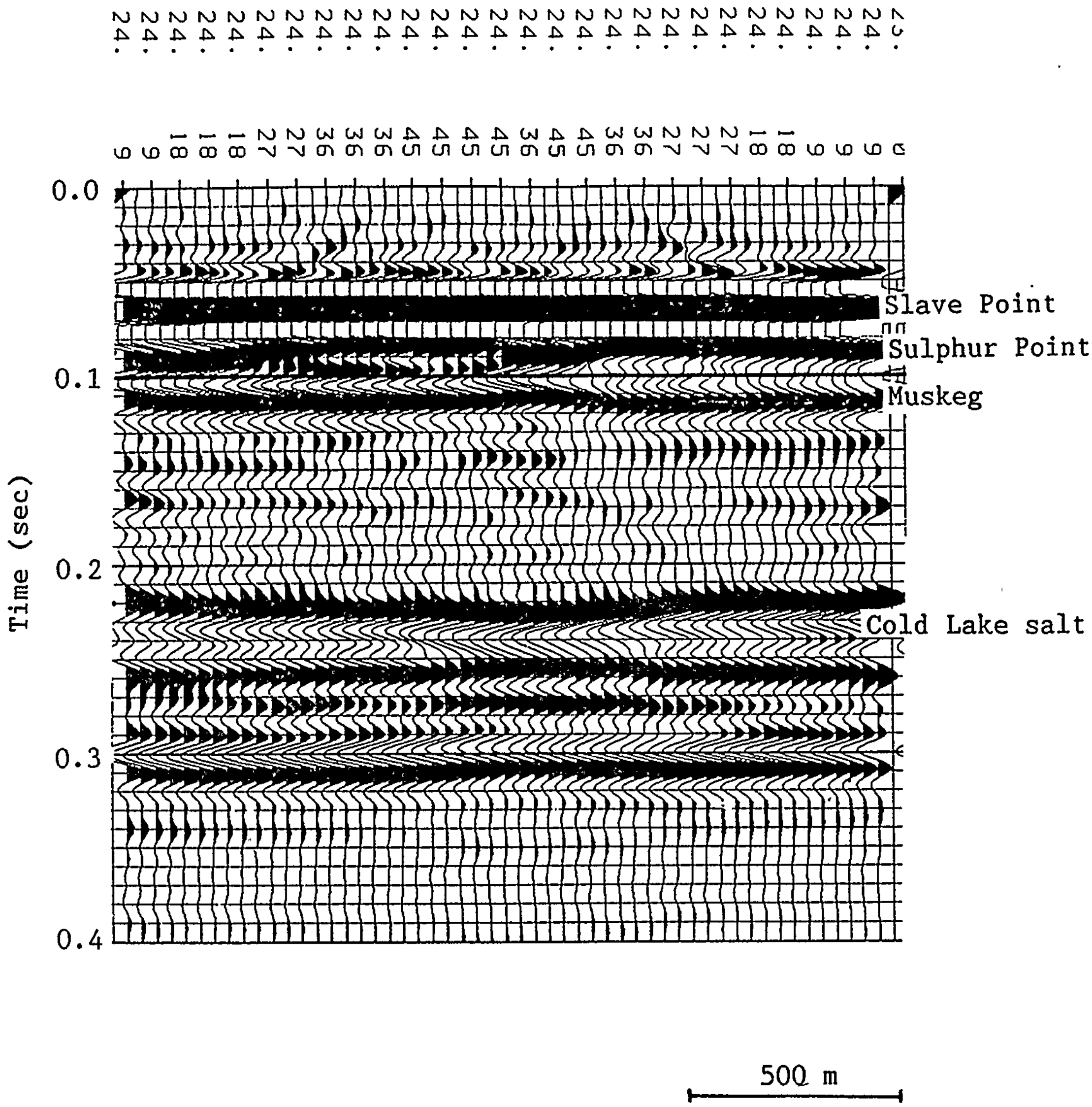

Figure 4.29 Physically modelled multi-offset migrated section.

are attributed to mis-stacking of these weaker events and contamination by random noise.

The migrated section (Figure 4.29) shows many improvements in image detail over the flattened stacked section (Figure 4.28). The migrated data appear to have a higher signal-to-noise ratio, with greater lateral reflection continuity, due to the mixing nature of the migration process. The migration procedure has also gathered energy from outside of the plane of the section as well as in the plane of the section to produce a significantly improved image of reflections caused by the low-velocity Keg River reef and has sharpened the image of the Muskeg "bump" over the reef.

4.6 Discussion

4.6.1 Comparison of Physically and Numerically Modelled Data

A zero-offset line over the crest of the reef from the physically modelled dataset (Figure 4.30) is compared to line 10a from the numerical modelling dataset (Figure 4.17). Both lines are positioned over the crest of the reef and have the same receiver station spacing. The major events, Slave Point, Sulphur Point, Muskeg, Upper and Lower Keg River, and Cold Lake salt, are marked on

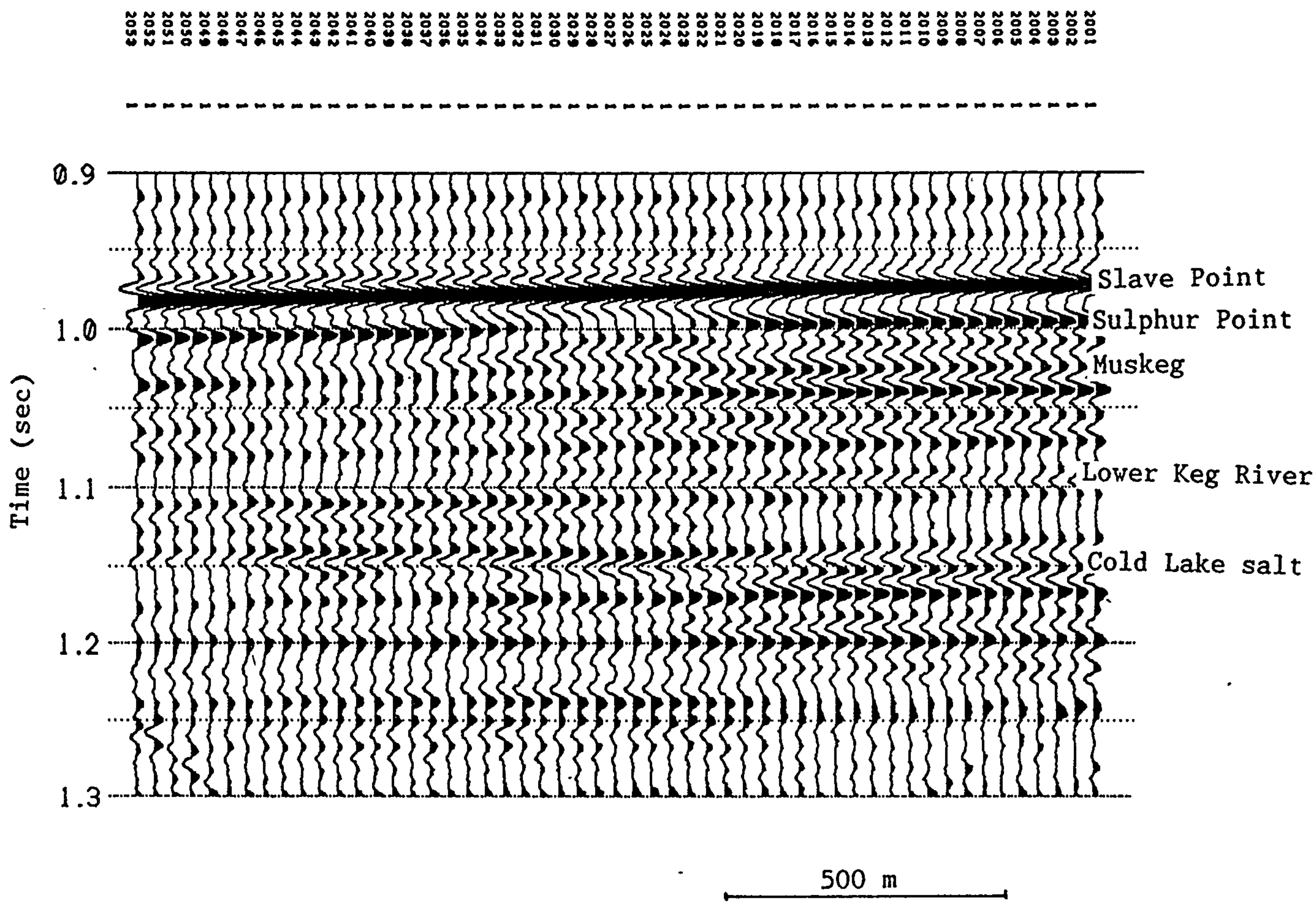

Figure 4.30 Physically modelled zero-offset line over reef crest.

Figures 4.30 and 4.17. The physical model section is slightly thicker than the numerical model because some of the thin, flat-lying units were made thicker than required during the model building process. In general, the physically modelled data appear noisier but the reflection events are more laterally continuous than the numerically modelled data, which have no noise added. The physical data have a number of unexpected events which are the result of direct arrival energy and/or multiple energy. Events on the two sections are similar in many respects but there are important differences.

Although considerable effort was made to ensure that all the factors involved in both physical modelling and numerical modelling were comparable, differences still existed. The variations which caused these discrepancies are grouped into two separate categories: procedural differences and conceptual differences.

Procedural differences are classified as differences in the specification of the model, in the positioning of the model, in the generation of the source wavelet, and in the way the source and receiver positions were specified. Many of the discrepancies between the numerical model section and the physical model section can be attributed to procedural differences. For example, the slight tilt in the physical model data is a result of uneven model positioning in the physical modelling tank. Differences in the specification of the model have produced some noticeable effects. The Watt Mountain/Sulphur Point event is less continuous on the physical model section because of differences between the construction of the physical model and the numerical model. In practice, with physical model building, it is difficult to produce perfectly uniform layers of arbitrary thickness, and the contact between layers and structures is not perfectly smooth. However, with numerical model specification, layers of the model can have perfectly uniform thickness and the contacts at the boundaries are smooth. Lateral changes in waveform of flat events on the physical model data are probably caused by small flaws in the construction of the model. Generation of the source wavelet, which in the physical modelling case results from the summation of three wave trains to give a close to zero-phase wavelet with some side lobe energy, has resulted in ringing of the physical modelling data compared to the numerical modelling data, which uses a perfect zero-phase Ricker wavelet. Size limitations of the transducers in the physical modelling system require that the source and receiver be separated by a minimum of 1 cm. This departure from zero-offset, while small, may produce minor effects due to mode conversions, change in amplitude with offset and directional anomalies related to source-receiver azimuth.

Conceptual differences are classified as differences in the way in which seismic energy theoretically interacts with the models. Some of the discrepancies between the physical data and the numerical data can be related to wavefront propagation, with associated Fresnel zone effects, versus raypath propagation. The increased lateral continuity of the Muskeg and Cold Lake salt events on the physical model dataset, compared to the numerical model data, is caused by reflection from an area so that abrupt changes tend to be smoothed out by contributions from the flat parts of those reflectors. The weaker appearance of reflections from the Keg River reef on the physical modelling data is again a Fresnel zone effect as energy from the very small reef is dispersed out of the plane of this section. The physical data are noisier than the numerical data. Sources of noise on the physical data include mechanical vibrations of the modelling tank apparatus, air currents and vibration of the building due to wind, settling or activity in the building. Finally, multiples generated between layers of the model were not included in numerical modelling and may be a source of noise on the physical modelling data.

4.6.2 Comparison of Physically Modelled Data and Field Data

A migrated, stacked section over the crest of the physical reef model (Figure 4.28) is compared to a similarly positioned field data section (Figure 4.1). The major reflectors are indicated on both sections. The seismic events on the physical modelling data appear more continuous and less noisy than the field data. The major events are quite similar on both sections and exhibit many of the same characteristics. Based on the similarity of reflection characteristics between the physically modelled data and the field data, the interpretation derived from the field data which was used to design the physical model was judged to be quite accurate. However, the major differences are identified and are discussed below.

Considerable effort was made to ensure that construction of the physical model, acquisition of the physically modelled data and processing of the model data would be as similar to the field data case as interpretational and practical limitations would permit. Discrepancies between the model data and the field data are broadly grouped into the procedural differences category.

In this case, procedural differences are classified as differences in the acquisition geometry, in processing, and most importantly, in the specification of the model. The field data were acquired with many different receivers recording the energy from each shot while with the physical model data, the same receivers recorded all of the data for every shot. Thus, in the field, every different receiver and shot is assumed to have the same response, whereas in the modelling tank, the source is assumed to have controlled repeatability. The consistency of the waveform coupled with the isolated nature of the modelling tank has contributed to the less noisy appearance of the physically modelled data compared to the field data. Positioning errors on near-offset traces caused by the finite size of the source and receiver transducers has introduced stacking errors in some of the data. An extra trim statics procedure was introduced into the processing flow to help correct these errors. Changes between the zero-offset data and the stacked model data are probably partly due to this problem. Reflection strength gain and flattening of the dataset to the Slave Point reflector were applied to the physical modelling data.

Many of the differences mentioned above between the sections are attributed to differences between the specification of the model and the actual field example. Differences, in this category, between events on the physical modelling data and the field data will be explained individually starting with the Slave Point event and continuing down to the Cold Lake salt event. The Slave Point reflector is much stronger in amplitude on the physical model data because of the artificially high reflection coefficient between water and modelling compounds. For this reason, drape on the Slave Point unit was not included on the model data whereas drape is present at this level in the subsurface. For the next reflection down from the Slave Point reflector, lateral changes in the Watt Mountain/Sulphur Point event on the model data are caused by difficulties in maintaining a uniform thickness of the thin Watt Mountain unit during model construction. The following Muskeg event is stronger on the model data, possibly due to the abruptness of transition between Sulphur Point and Muskeg compared to the field. Differences in the shape, size and distribution of porosity in the model Keg River reef compared to the actual reefal buildup may result in differences in Keg River reef reflections between the two surveys. Finally, the Cold Lake salt layer is probably not uniform in the subsurface which explains the lateral changes in the strength of this reflection on the field data.

Several of the model specification differences mentioned above have indirect effects on other reflection events. An absence of a velocity "push-down" anomaly below the reef mass is noted in the field data. Two factors can contribute to the absence of this feature. First, the presence of Slave Point drape in the field example produces a velocity "pull-up" anomaly which will tend to reduce any effect from the low-velocity reef. Referring to table 4.1 for the velocity values for the various earth layers. The velocity "pull-up" effect from 25 m of drape of Slave Point with V=5900 m/s replacing the overlying sediment with V = 3500 m/s is 6 ms which will almost counteract the 7 ms of "push-down" caused by the low-velocity reef. Second, the reef mass may have developed over a subtle structural high which will also tend to mask any velocity sag. Another indirect phenomenon, the focusing of energy under the reef, occurs at an earlier time on the field data than on the modelled data. This result indicates a different reef morphology between the two datasets, with a smaller radius of curvature either on the top or the bottom of the field reef.

Chapter 5: Conclusions and Recommendations

5.1 Introduction

In this thesis, seismic responses over and around models of two selected Devonian pinnacle reefs were generated using physical and numerical modelling. Seismic data acquired over these models were used to examine some of the three-dimensional effects of pinnacle reefs on reflection seismic data.

5.2 Physical Modelling System

5.2.1 Conclusions

The physical seismic modelling method was employed to study seismic responses of pinnacle reefs. The method records the natural interactions of the complicated parameters governing acoustic wave propagation. These interactions, if they can be predicted by current technology, may be very time consuming and expensive to reproduce with full wave-equation numerical modelling-schemes. Physical modelling can provide control data for known model and acquisition geometries. Once physical model construction is complete, the system is very flexible for acquiring data with various acquisition geometries. The system hardware and software was expanded as part of this project to accommodate 3-D seismic acquisition geometries.

5.2.2 Recommendations

The physical seismic modelling system at the University of Calgary has proven to be a useful tool for investigations into acoustic energy propagation and should continue to be utilized. However, several improvements to the system could be implemented. These improvements would lead to more flexibility in choosing the scale factors for the models and enable smoother experimental operations.

Several components of the physical modelling system could be upgraded:

1) An oscilloscope with greater storage capacity and variable sampling interval would allow more samples to be recorded in a trace and increase flexibility in choosing the time scale factor.
2) A selection of transducers that operate at different frequency ranges would also ease the restriction of the scaling factors.
3) The analogue pulse generator could be replaced by a digital pulse generator to enable specification of the source wavelet and would give more control over the

source wavelet used in the experiments.

4) Computer software should be modified to record source and receiver positions directly onto the trace header. Such information in the trace header would simplify the subsequent processing of the modelled data.

5.3 Golden Spike Reef Model

5.3.1 Conclusions

Experience with the Golden Spike reef model indicated several potential problems associated with detailed model construction and scale parameter selection. Present facilities in the physical modelling laboratory for mixing, pouring and curing large volumes of epoxy resin were found to be inadequate. Construction of the Golden Spike reef model was halted when a layer of epoxy resin, representing the Ireton Formation, failed to harden. However, useful results were obtained from data acquired over the model Leduc reef mass before the Ireton layer was added.

Many complex events were identified on the physical modelling data. Comparisons between the physical modelling data and two-dimensional numerical raytrace modelling data indicated many effects associated with the three-dimensional geometry of the reef:

1) Sideswipe reflections are identified on the physically modelled data and are a potential source of interpretational error.
2) The 3-D geometry of the reef, with reflection from an area, was attributed to be the cause of some unexpected losses in amplitude.
3) Sideswipe reflections were shown to result in a larger apparent reef size on unmigrated seismic data.

5.3.2 Recommendations

Difficulty was encountered in this part of the study with construction of the large model. In addition to problems with hardening of modelling materials, epoxy resin and PVC were found to deteriorate from being submerged in heavily chlorinated water for a prolonged period of time.

Experience with the Golden Spike reef model led to the following recommendations:

1) Covering the completed model with a thin coat of acrylic may help to prevent deterioration of the model.
2) Care should be taken to ensure that the final scaled temporal sampling rate is an integral number of milliseconds.
3) Investigation and testing of other suitable modelling

materials should be continued, offering a wider range of acoustic and physical properties.

5.4 Shekilie Reef Model

5.4.1 Conclusions

The acquisition design and analysis of data collected over the Shekilie pinnacle reef model were influenced by several factors. The detailed examination of many attributes led to the following conclusions:

1) Fresnel zone effects are significant and limit resolution of Muskeg drape and Upper Keg River structure.

2) Two-pass 3-D migration is an important and desirable processing step. Migration has been found to reduce the Fresnel zone and to increase lateral resolution. The migrated sections had a higher signal-to-noise ratio and are easier to correlate and interpret than unmigrated sections.

3) In the absence of Slave Point drape and with an even Cold Lake salt formation surface, a velocity "push-down" of the Cold Lake salt reflection event under the Upper Keg River reef is caused by longer traveltime through the low-velocity reef.

4) Focusing of events under the lens-shaped reef has

been identified. This phenomenon allows for ranking reefs of similar morphologies and depths of burial according to size; larger reefs focus events later in the section.

5) The numerical modelling data are not suitable for modelling the effects observed on the physical modelling data. The numerical data are inadequate because they do not account for Fresnel zone effects. Numerical modelling methods based on solutions to the wave equation should be better at reproducing effects observed on the physically modelled data.

6) Based on the similarity of the field and physically modelled datasets, the original interpretation of the field 3-D survey is believed to be quite accurate.

7) Slave Point drape has contributed to the absence of a velocity "push-down" anomaly of the Cold Lake salt horizon under the reef in the field data.

8) Differences between the Keg River reflections and the level at which focusing beneath the reef occurs on the field and physical modelling datasets are attributed to minor differences between the porosity distribution and morphology of the model reef and the field reef.

5.4.3 Recommendations

Analysis of the Shekilie pinnacle reef model data has led to the following recommendations:

1) The minimum offset for the recorded data should be larger than the size of the tranducers to eliminate physical contact between the source and receiver transducers.

2) Extra background traces, not over the model, should be collected for each zero offset line. Direct arrival trailing energy on the zero offset data (see Figure 4.23, section 4.5.2) could be attenuated by subtracting the background traces from the model data.

3) More work needs to be done on the choice of bin size and recording aperture, given the lack of precision in the velocity function for the migration process. Data should be recorded over the model with different bin sizes and the results compared. Recording aperture can be investigated by processing smaller subsets of data centered over the reef and noting when differences begin to occur.

4) More advanced processing procedures, such as pre-stack migration, should be applied to the physical modelling dataset to improve the image of dipping interfaces.

5) Full wave-equation numerical modelling techniques should be employed to model this feature and the results compared with the physical modelling data.

REFERENCES

Anderson, N.L., 1986, An Integrated Geophysical/Geological Analysis of the Seismic Signatures of Some Western Canadian Devonian Reefs: Ph.D. Thesis, University of Calgary, Alberta.

Anderson, N.L., and Brown, R.J., 1987, The Seismic Signatures of Some Western Canadian Devonian Reefs: Journal of The Canadian Journal of Exploration Geophysicists, vol. 23, no. 1, p7-26.

Belyea, H.R., and the Committee on Slave Point and Beaverhill Lake Formations, 1964, Upper Devonian: in McCrossan, R.G., and Glaister, R.P., (editors), Geological History of Western Canada, Calgary, Alberta, Society of Petroleum Goelogists, p60-88.

Berkhout, A.J., 1984, Handbook of Geophysical Exploration, Section 1: Seismic Exploration, vol. 12: Seismic Resolution: Geophysical Press, London, U.K.

Barss, D.L., Copland, A.B., and Ritchie, W.D., 1970, Geology of Middle Devonian Reefs, Rainbow Area, Alberta, Canada: in Halbouty, M.T., (editor), Geology of Giant Petroleum Fields, Bulletin of American Association Petroleum Geologists, Mem. no. 14, p19-49.

Buckingham, E., 1914, On Physically Similar Systems; Illustrations of the Use of Dimensional Equations: Physical Review, vol. 4, p345-376.

Burg, J.P., 1964, Three-dimensional Filtering with an Array of Seismometers: Geophysics, vol. 29, p693-713.

Claerbout, J.F., 1985, Imaging the Earth's Interior: Blackwell Scientific Publications, Palo Alto, Ca.

Cheadle, S.P., 1988, Applicatons of Physical Modeling and Localized Slant Stacking To a Seismic Study of Subsea Permafrost: Ph.D. Thesis, University of Calgary, Alberta.

Cheadle, S.P., Bertram, M.B., and Lawton, D.C., 1985, Development of a Physical Seismic Modeling System, University of Calgary: Current Research, Part A, Geological Survey of Canada, Paper 85-1A, p499-504.

Cooper, H.W., and Cook, R.E., 1984, Seismic Data Gathering: Proceedings of the IEEE, vol. 72, no. 10, p1266-1275.

Cotton, R.W., 1988, The Acquisition of Seismic Reflection Data in 3 Dimensions: Society of Exploration Geophysicists Education Department SEGED88.

ERCB 1987 Correlation Chart. Energy Resources Conservation Board.

ERCB 1988, Alberta's Reserve of Crude Oil, Oil Sands, Gas, Natural Gas Liquid, and Sulphur, Energy Resources Conservation Board. Paper ERCBST88-18.

French, W.S., 1974, Two-dimensional and Three-dimensional Migration of Model-experiment Reflection Profiles: Geophysics, vol. 39, p265-277.

French, W.S., 1975, Computer Migration of Oblique Seismic Reflection Profiles: Geophysics, vol. 40, p961-980.

Gardner, G.H.F., Gardner, L.W., and Gregory, A.R., 1974, Formation Velocity and Density - The Diagnostic Basics of Stratigraphic Traps: Geophysics, vol. 39, p770-780.

Hecht, E., and Zajac, A., 1979, Optics: Addison - Wesley Publishing Company, Inc.

Hilterman, F.J., 1970, Three-dimensional Seismic Modeling: Geophysics, vol. 35, p1020-1037.

Hilterman, F.J., 1982, Interpretative Lessons from Three-dimensional Modeling: Geophysics, vol. 47, p784-808.

Hospers, J., 1985, Sideswipe Reflections and Other External and Internal Reflections from Salt Plugs in the Norwegian-Danish Basin: Geophysical Prospecting vol. 33, p53-71.

Hriskevich, M.E., 1970, Middle Devonian Reef Production Rainbow Area, Alberta, Canada: Bulletin of American Association of Petroleum Geologists, vol. 54, no. 12, p2260-2281.

Kotcher, J.S., Gardner, G.H.F., and McDonald, J.A., 1984, Modeling the Effect of Static Errors in Areal Seismic Data Caused by Glacial Erosion over Carbonate Reefs: Geophysics, vol. 49, p1-16.

Langton, J.R., and Chin, G.E., 1968, Rainbow Member Facies and Related Reservoir Properties, Rainbow Lake, Alberta: Bulletin of Canadian Petroleum Geology, vol. 16, no. 1, p104-143.

Lyatsky, H., 1988, Reflection Seismic Study of a Shallow

Coal Field in Central Alberta: M.Sc. Thesis, University of Calgary, Alberta.

May, B.T., and Hron, F., 1978, Synthetic Seismic Sections of Typical Petroleum Traps: Geophysics, vol. 43, p1119-11147.

McCamis, J.G., and Griffith, L.S., 1967, Middle Devonian Facies Relationships, Zama Area, Alberta: Bulletin of Canadian Petroleum Geology, vol. 15, p434-467.

McDonald, J.A., Gardner, G.H.F., and Hilterman, F.J., (editors), 1983, Seismic Studies in Physical Modeling: IHRDC, Boston, MA.

McGillivray, J.G., and Mountjoy, E.W., 1975, Facies and Related Reservoir Characteristics Golden Spike Reef Complex, Alberta: Bulletin of Canadian Petroleum Geology, vol. 23, p753-809.

Mountjoy, E.W., 1980, Some Questions about the Development of Upper Devonian Carbonate Buildups (Reefs), Western Canada: Bulletin of Canadian Petroleum Geology, vol. 28, p315-344.

Newman, P., 1980, 3-D Acoustic Model Experiments: Paper presented at 50th annual international meeting, SEG.

O'Connor, M.J., and Gretener, P.E., 1974, Differential Compaction within the Woodbend Group of Central Alberta: Bulletin of Canadian Petroleum Geology, vol. 22, p269-304.

Prodruski, J.A., Barclay, J.E., Hamblin, A.P., Lee, P.J., Osadetz, K.G., Procter, R.M., and Taylor, G.C., 1988, Conventional Oil Resources of Western Canada (Light and Medium) Part 1: Resource Endowment, Geological Survey of Canada, Paper 87-26.

Sierra Geophysics Exploration Software User Notes, 1983.

Sheriff, R.E., 1977, Limitations on Resolution of Seismic Reflections and Geologic Detail Derivable from Them: in Seismic Stratigraphy - Applications to Hydrocarbon Exploration, Bulletin of American Association Petroleum Geologists, Mem. no. 26, p3-14.

Sheriff, R.E., and Geldart, L.P., 1982, Exploration Seismology: Cambridge University Press, New York, N.Y.

Stoakes, F.A., 1980, Nature and Control of Shale Basin Fill and its Effect on Reef Growth and Termination: Upper Devonian Duvernay and Ireton Formations of

Alberta, Canada: Bulletin of Canadian Petroleum Geology, vol. 28, p345-410.

Trott, B.G., 1981, Gravity Study of Reefs in Central Alberta: M.Sc. Thesis, University of Calgary, Alberta.

White, J.E., 1965, Seismic Waves: Radiation, Transmission, and Attentuation: McGraw-Hill, New York, N. Y.